PHASE 2 INITIAL BOREHOLE DRILLING AND TESTING, SOUTH BRUCE AREA

WP10 – Geological Integration Report for Borehole SB_BH02

APM-REP-01332-0339 **May 2023**

Nuclear Waste Management Organization

nwmo
NUCLEAR WASTE MANAGEMENT ORGANIZATION
SOCIÉTÉ DE GESTION DES DÉCHETS NUCLÉAIRES

Nuclear Waste Management Organization
22 St. Clair Avenue East, 4th Floor
Toronto, Ontario
M4T 2S3
Canada

Tel: 416-934-9814
Web: www.nwmo.ca

Phase 2 Initial Borehole Drilling and Testing, South Bruce Area

WP10 – Integration Report for Borehole SB_BH02

APM-REP-01332-0339

May 2023

Nuclear Waste Management Organization

All copyright and intellectual property rights belong to NWMO.

Document History

Title:	Phase 2 Initial Borehole Drilling and Testing, South Bruce Area. WP10 – Integration Report for Borehole SB_BH02		
Report Number:	APM-REP-01332-0339		
Revision:	R0	Date:	
Author Company(s) Nuclear Waste Management Organization			
Authored by:	Alexandre Cachunjua, Aaron DesRoches, Andy Parmenter		
Verified by:	Terry Carter (Carter Geologic), Warwick Watt (NWMO)		
Accepted by:	Sarah Hirschorn		

Revision Summary		
Revision Number	**Date**	**Description of Changes/Improvements**
R0	May 2023	Initial issue

ABSTRACT

Title:	Phase 2 Initial Borehole Drilling and Testing, South Bruce Area. Single Borehole Integration Report for SB_BH02
Report No.:	APM-REP-01332-0339
Author(s):	Alexandre Cachunjua, Aaron DesRoches, Andy Parmenter
Company:	Nuclear Waste Management Organization
Date:	May 2023

The Initial Borehole Drilling and Testing project in the South Bruce Area, Ontario is part of Phase 2 Geoscientific Preliminary Field Investigations of the Nuclear Waste Management Organization's (NWMO) Adaptive Phased Management (APM) Site Selection Phase. This project involves the drilling and testing of the second of two vertical boreholes at the South Bruce Site. The second drilled borehole, SB_BH02, is located approximately 5.5 km northwest of the community of Teeswater, Ontario, and was drilled to 900.57 meters below ground surface (m BGS). SB_BH02 was drilled through the entire sedimentary bedrock sequence to approximately 14 m into the Precambrian basement. Access to the SB_BH02 drill site is via a gravel road off Concession Road 8 in Teeswater, Ontario. This Geological Integration Report serves as the primary reference of the geological findings from the borehole drilling and testing activities at SB_BH02.

The objective of the Geological Integration Report is to evaluate relevant core logging observations and geophysical well log data to provide an integrated analysis of the tops of stratigraphic formations, units and members intersected in SB_BH02. For each stratigraphic layer, this report will also explore the dominant lithological and geophysical well log characteristics, and summarize the relevant alteration and structural characteristics, as well as hydrocarbon occurrences. Initial stratigraphic tops were interpreted as part of the geological and geotechnical core logging activity based strictly on drill core observations.

Overall, the interpreted stratigraphic sequence encountered was comparable to that predicted to occur at the location of SB_BH02 based on a recently completed regional-scale 3D geological model (Carter et al., 2021). Additionally, formation thicknesses and distribution were very similar to that encountered at the Bruce Nuclear Site (Intera, 2011).

A total of 12 different types of rock were identified, dominated by limestone, shale and dolostone. Overall alteration was minor, and karstic pores/vugs in the Lucas and Amherstburg formations indicate that recent weathering was limited to the shallow stratigraphic sequence. Paleo-erosional surfaces have also experienced some degree of paleo-weathering, with extensive paleo-karstification in the Salina A-1 Unit Carbonate and Guelph Formation in particular. The types and distribution of hydrocarbon occurrences suggest that distinct hydrocarbon zones can be distinguished, consistent with the recognition that the shale units, in particular, represent cap (barrier) rocks that greatly inhibit cross-formational vertical connections.

The distribution and intensity of fracturing in SB_BH02 is as expected, being consistent with the results from the DGR Site Characterization Study completed by Intera (2011) at the Bruce Nuclear Site. An increased fracture intensity occurs in the shallow subsurface and down to the base of the Guelph Formation; these are attributed to shallow karstic conditions in the Devonian formations as well as paleokarst in the Salina A-1 Unit Carbonate and Guelph Formation. Below this formation, the fracture intensity decreases markedly through the entire Upper Ordovician succession. An increase in fracture intensity is again observed in the Precambrian bedrock intersected in the bottom of the borehole. Importantly, the very low intensity of fractures throughout the Upper Ordovician shales and limestones suggests the presence of unidentified deep-seated basement faults in close proximity to SB_BH02 is unlikely. However, due to the near vertical orientation of the borehole, it is extremely difficult to rule out steeply dipping or vertical faults. 3-D seismic interpretation is ongoing and will help ascertain the presence of faults at the South Bruce Site.

TABLE OF CONTENTS

ABSTRACT ..... **iii**

1 INTRODUCTION **10**

1.1 Technical Objectives and Scope of Report **10**

2 Background Information **11**

2.1 Geological Setting **11**

2.1.1 Lithostratigraphic Terminology 11

2.1.2 Paleozoic Geology 13

2.1.3 Tectonic History 16

2.1.4 Burial/Erosion and Thermal History, Diagenesis 16

2.1.5 Salt Dissolution 19

2.1.6 Karst and Paleokarst 19

2.2 Background and Overview of Borehole Drilling and Testing **20**

2.2.1 Drilling Site Description 20

2.3 Borehole Details for SB_BH02 ..... **21**

2.3.1 Borehole Construction 21

3 Integrated Geological Interpretation **23**

3.1 Data Used for Geological Interpretation **23**

3.2 Geological Results **25**

3.2.1 Stratigraphic Formation and Member Descriptions 25

3.2.1.1 Pleistocene Deposits 27

3.2.1.2 Devonian Rocks 27

3.2.1.3 Silurian Rocks 28

3.2.1.4 Upper Ordovician Rocks 32

3.2.1.5 Precambrian Rocks 35

3.2.1.6 Geophysical Characteristics for Stratigraphic Formations and Members 35

3.2.2 Lithological Characteristics 42

3.2.2.1 Geophysical Characteristics of Logged Rock Types 45

3.2.3 Rock Alteration and Hydrocarbon Occurrences 48

3.2.3.1 Rock Alteration, Weathering and Karst 50

3.2.3.2 Hydrocarbon Occurrences 50

3.2.4 Structural Terminology 50

3.2.5 Structural Summary 51
3.3 Discussion 54
3.3.1 Upper and Lower Silurian Formations/Units 55
3.3.2 Upper Ordovician Formations 60
3.3.3 Cambrian Sandstone 60

4 Summary of Findings and Uncertainties 61
4.1 Findings 61
4.2 Uncertainties 62

5 References 64

Appendix A: 71

Appendix B: 72

Appendix C: 73

LIST OF TABLES

Table 1: Summary of top, bottom and thickness of formations and members interpreted through and integrated analysis of core observation and geophysical well log data for SB_BH02. Presented depths represent position along the borehole. 25

Table 2: Summary of Logged Rock Types in SB_BH02..... 42

Table 3. Summary of Lockport Group tops from SB_BH02, T004881 and F012062. 59

Table 4. Summary of Salina Group tops from SB_BH02, T004881 and F012062 overlying the Lockport Group. 59

LIST OF FIGURES

Figure 1. Bedrock geology of southern Ontario, derived from Somers (2017), Carter et al. (2019, 2021) and Carter (2023). 12

Figure 2. Lithostratigraphy of southern Ontario, colour-coded by rock type. Adapted from Brunton et al. (2017) and Carter et al. (2017) as updated from Armstrong and Carter (2010). The central column is representative of the stratigraphic succession encountered in the South Bruce area. 14

Figure 3. Hypothetical burial history curves for locations within the Michigan. Interpretations are based on data collected from Upper Ordovician carbonate sedimentary rocks. Orange curve is from Coniglio and Williams-Jones (1992) after Cercone (1984) evidenced from sediment accumulation rates, regional dips and maturity of Pennsylvanian age coals. Black curve is from Wang et al. (1994) derived from fission-track ages measured for Carboniferous outcrop samples. (a) Indicates the present day burial depth of approximately 675 m for the middle of the Upper Ordovician sedimentary succession at the Bruce Nuclear Site. See text for further discussion. 16

Figure 4. Location Map showing boreholes SB_BH01 and SB_BH02 drilled as part of Geoscientific Preliminary Field Investigations by NWMO. 21

Figure 5. Geophysical well log showing natural gamma ray, spectral gamma (Potassium, Uranium and Thorium), long spaced neutron counts, mean gamma-gamma density, long spaced resistivity and compression P-wave velocity log. Formations and members are colour classified (colour legend is displayed in Table 1) and subdivided into age periods, Devonian, Silurian, Ordovician and Precambrian. The Salina formations are grouped into the Salina Group. Lithology is presented as relative proportions for each measured interval (colour legend is displayed in Table 2). Depth scale is 1:4000. See Appendix C presenting figure at 1:500 scale. 37

Figure 6. Natural Gamma (cps), Neutron LS (long spaced; cps), Density (g/cc), P-wave (m/s) and resistivity (Ohm*m) boxplots presenting distribution of values for each formation from the base of the casing to the bottom of the borehole. Boxplots present the statistical median, first and third quartiles (25% and 75%) and the minimum and maximum values (total range). The notch in the boxplot represents the 95% confidence interval..... 39

Figure 7. Grid of scatterplots presenting relationships and general trends between different geophysical logs (Gamma, Neutron, Vp, Density and Resistivity). Generalized trends are displayed as dashed lines. Data are colour classified by formation and member intervals shown in Table 1 and Figure 5. 40

Figure 8. Grid of scatter plots for the Upper Ordovician formations presenting relationships and trends between different geophysical logs (Gamma, Neutron, Vp, Density and Resistivity). Data are colour classified by formation and member intervals shown in Table 1 and Figure 5. 41

Figure 9. Correlation between P-wave velocity versus natural gamma. a) shows results for all formations logged in SB_BH02 with an R-squared coefficient of correlation of 0.610. b) presents results for Ordovician formations which significantly improving the correlation coefficient to 0.788..... 42

Figure 10: Summary of logged rock types for all formations and members in SB_BH02. The upper 36.94 m of the borehole was drilled using a cable tool rig resulting in bedrock chip samples. Rock types for the upper 36.94 m of the borehole were logged (separately) for the upper part of the Lucas Formation but not captured in acQuire, therefore, not showing in this figure. 44

Figure 11. Natural Gamma (cps), Neutron LS (long spaced; cps), Density (g/cc), P-wave velocity (m/s) and long spaced resistivity (Ohm*m) boxplots presenting distribution of values for each rock type logged from the base of the casing to the bottom of the borehole. Boxplots present the statistical median, first and third quartiles (25% and 75%) and the minimum and maximum values (total range). The notch in the boxplot represents the 95% confidence interval. Color legend for lithologies shown in Table 2 46

Figure 12. Grid of scatterplots presenting trends between different geophysical logs (Gamma, Neutron, Vp, Density and Resistivity) for the entire logged length of the borehole. Data points are colour classified using the dominant core logged rock types. 47

Figure 13. Grid of scatterplots presenting trends between different geophysical logs for the Ordovician Formations (Gamma, Neutron, Vp and Density and Resistivity). Data points are colour classified using the dominant core logged rock types. 48

Figure 14. Summary of Logged Alteration and Hydrocarbon Occurrences in SB_BH02 49

Figure 15: Summary of Logged Structures in SB_BH02, including fracture frequency and occurrence logs for joints (JN), veins (VN), vein zones (VNZ), intact fracture zones (IFZ), faults (FLT), broken core zones (BCZ) and lost core zones (LCZ). Geological aperture (total aperture), and fracture frequency logs are presented per 2 metre interval. 53

Figure 16 . Modified and adapted from Carter (2023). West to east cross-section immediately north of the South Bruce Site, constructed from a regional 3-D geological model (Carter et al. 2021) showing dissolution edge of the Salina B Salt with associated subsidence/collapse of the overlying Salina B, C, D, E, F, and G units, and thickening of the Bass Islands Formation. Younger strata appear to be unaffected, suggesting dissolution and subsidence occurred before deposition of the Bass Islands Formation. ... 56

Figure 17. Facies belts in the Lockport Group, modified from Sanford (1969), Bailey (1986) and Carter et al. (1994) showing thickened carbonate banks on a slowly subsiding carbonate platform in the east and a regional karst horizon, pinnacle belt and inter-pinnacle karst belt developed on a paleotopographic high in what is now the Michigan Basin in the west (Brintnell, 2012; Brunton et al. 2020), Carter (2023). Geographic regions are presented as counties. 57

Figure 18. Conceptual model of a Guelph pinnacle reef showing stratigraphic, lithological and structural relationships with regional strata of the Lockport Group and lower Salina Group, within the Pinnacle and Interpinnacle Karst Belt of southern Ontario. Modified and adapted from Brintnell (2012), Brunton and Brintnell (2020), Carter et al. (2021) and Carter (2023).

A-0 Unit Carbonate is interpreted to occur on flanks of reefs or in non reefal areas, which is supported by drill core findings from SB_BH02. 58

Figure 19. The shaded region represents the area of Southern Ontario in proximity to SB_BH01 and SB_BH02 underlain by Cambrian Sandstone as per the Carter et al. (2021) regional model..... 61

1 INTRODUCTION

Borehole drilling and testing project in South Bruce, Ontario is part of Phase 2 Geoscientific Preliminary Field Investigations of the Nuclear Waste Management Organization's (NWMO) Adaptive Phased Management (APM) Site Selection Phase. Following Phase 1 of Geoscientific Desktop Preliminary Assessment summarized by Geofirma (2014), an area located in South Bruce was selected by the NWMO for further investigation through an initial borehole drilling campaign involving drilling and testing of two deep boreholes SB_BH01 and SB_BH02 at the South Bruce Site (Figure 1).

Project fieldwork was carried out by a team led by Geofirma Engineering Ltd. on behalf of the NWMO. The overall program includes activities related to mobilization and set up of the borehole drilling site, the recovery and logging of the bedrock core, drilling water management and groundwater sampling, borehole geophysical and hydraulic testing, laboratory testing, and on-going monitoring activities at the borehole. All activities are documented in work package (WP) data reports that describe test methods, collected data, and calculations, where applicable. The full list of work packages and their associated data reports are included in Appendix A.

This report presents an integrated summary of geological and geophysical information collected primarily during the completion of three work packages, including Borehole Drilling and Coring (WP02: Geofirma, 2023a), Geological and Geotechnical Core Logging, Photography and Sampling (WP03: Geofirma, 2022a) and Geophysical Well Logging and Interpretation (WP05: Geofirma, 2023b).

1.1 Technical Objectives and Scope of Report

The main objective of this geological integration report is to evaluate relevant core logging observations and geophysical well log data to provide an integrated analysis of the tops of stratigraphic formations, units and members intersected in SB_BH02. Initial stratigraphic tops were interpreted as part of the core logging (WP03: Geofirma, 2022a) based strictly on drill core observations. However, formation tops can often be obscured by gradational lithological changes, and these changes can be better identified when integrated with an appropriate suite of geophysical well logs. Overall, the objective of this report is to define the depths to formation top picks in SB_BH02 using an approach that is consistent with the framework defined in Armstrong and Carter (2006, 2010), Intera (2011), and Carter et al. (2021). The outcome of this analysis has been incorporated into a 3-dimensional model for the update of the local stratigraphy (DesRoches et al. 2022).

For each stratigraphic layer, this report will also explore the dominant lithological and geophysical well log characteristics, and summarize the relevant alteration, hydrocarbon occurrences and structural characteristics. These rock characteristics will be important for describing each of the stratigraphic layers within the Descriptive Geosphere Site Model (DGSM) report. Additional information related to characterization of the petrophysical and transport properties of the bedrock in South Bruce, as well as the geomechanical, hydrogeological, litho- and hydrogeochemical, and thermal properties will be presented in separate data reports and also integrated into the DGSM report. The DGSM report will summarize the additional borehole- and laboratory-derived data related to these topics and will present this information including a geological model that integrates the WP10 results for each of the two deep boreholes drilled at the South Bruce Site.

2 BACKGROUND INFORMATION

2.1 Geological Setting

Southern Ontario is underlain by a thick Paleozoic sequence of undeformed sedimentary rocks, ranging in age from Cambrian to late Devonian, and Mississippian in some regions (Carter 2023). This sequence of sedimentary strata rests unconformably on an erosional surface of the Precambrian crystalline basement of the Grenville Province, a tectonic subdivision of the Canadian Shield (Figure 1).

As shown in Figure 1, southern Ontario is located between two major sedimentary basins, the Michigan Basin to the west and the Appalachian Basin to the southeast. The Michigan Basin is a roughly circular, carbonate-dominated intracratonic basin with evaporite deposits; and the Appalachian Basin is an elongate siliciclastic-dominated foreland basin. The basins were ideal settings for the accumulation and preservation of marine sediments deposited in epeiric seas that periodically flooded this part of eastern North America, punctuated by periods of uplift and erosion in response to vertical epeirogenic movements and horizontal tectonic forces (Leighton 1996, Howell and van der Pluijm 1999). These two basins are separated by a regional structural high known as the Algonquin Arch which extends northeast through southern Ontario with a southwestern extension into the United States called the Findlay Arch. The Algonquin and Findlay arches are separated by a partially fault-bounded structural depression known as the Chatham Sag. Figure 1 illustrates the relationship between the arches of the basins and how they are separated geographically. To the northeast of southern Ontario, the sedimentary strata thin and eventually pinch out on the southwestern side of the Frontenac Arch within the Grenville Province of the Canadian Shield.

The Paleozoic section underlying SB_BH02 at the South Bruce Site was deposited in the Michigan Basin. These same strata are largely overlain by unconsolidated sediments of mostly glacial origin. The unconsolidated sediments average tens of metres in thickness, locally reaching a maximum thickness of approximately 250 metres east of the Niagara Escarpment (Gao et al. 2006; Gao 2011).

2.1.1 Lithostratigraphic Terminology

The following section provides definitions for formal lithostratigraphic unit terms used for classification and naming of Paleozoic sedimentary bedrock units in southern Ontario. The terminology used is derived from The International Commission on Stratigraphy (ICS) (International Subcommission on Stratigraphic Classification, ISSC, 1999).

Lithostratigraphic unit - Lithostratigraphic units are bodies of rocks, bedded or unbedded, that are defined and characterized on the basis of their lithological properties, or combination of lithological properties and their stratigraphic relations. Lithostratigraphic units are the basic units of geological mapping in sedimentary/supracrustal rocks. The traditional formal lithostratigraphic terms (names) as applied to sedimentary rocks are group, formation, member, bed.

Group - A succession of two or more contiguous or associated formations with significant and diagnostic lithological properties in common.

Formation – The primary formal unit of lithostratigraphic classification. No formation is considered justifiable and useful that cannot be delineated at the scale of geological mapping practiced in the region. The thickness of formations may range from less than a meter to several thousand meters. A formation name normally consists of a geographic name followed by either a descriptive geological term (such as the predominant rock type) or by the word “formation”.

Member – A named lithologic subdivision of a formation which possesses lithological properties distinguishing it from adjacent parts of the formation. Some formations may be completely divided into members, may have only certain parts designated as members, or may not be subdivided.

Bed - The smallest formal unit in the hierarchy of sedimentary lithostratigraphic units, e.g. a single stratum lithologically distinguishable from other layers above and below.

The ISSC guidelines have been applied in Ontario in the naming of stratigraphic units in the Paleozoic bedrock, although not rigorously. Descriptions of the stratigraphic relations and distinguishing features of named lithostratigraphic units in southern Ontario are contained in Armstrong and Carter (2010). They also provide type sections with 17 regional subsurface stratigraphic cross-sections utilizing 63 reference wells, supplemented by 11 reference outcrop sections. The stratigraphic chart utilized in Armstrong and Carter (2010) has been updated by the Ontario Geological Survey (Brunton et al. 2017, Carter et al. 2017 – see Figure 2) and has been adopted by the Geological Survey of Canada in 3D models of the Paleozoic bedrock of southern Ontario (Carter et al. 2021). One naming convention utilized in Ontario that is not consistent with the ISSC is the use of the term “Unit” within the named formations of the Salina Group and is adopted from the original stratigraphic definitions utilized in Michigan.

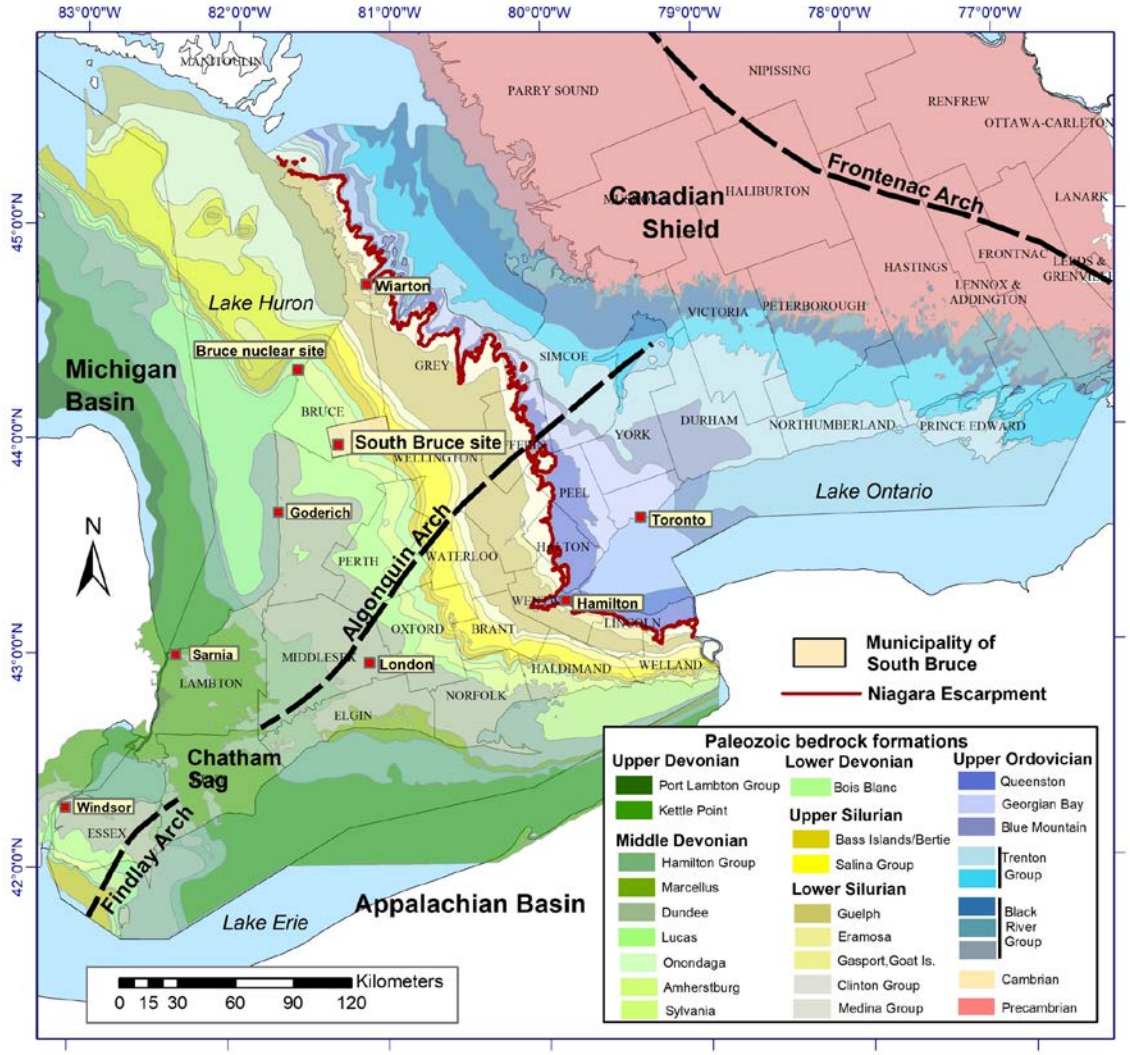


Figure 1. Bedrock geology of southern Ontario, derived from Somers (2017), Carter et al. (2019, 2021) and Carter (2023).

2.1.2 Paleozoic Geology

A relatively undeformed succession of marine sedimentary rocks overlies the Grenvillian (Precambrian) basement of southern Ontario. Rock types include limestone, dolostone, sandstone, shale, siltstone, anhydrite and beds of halite (Armstrong and Carter 2010) deposited in a shallow epeiric sea that periodically covered this part of eastern North America during the Paleozoic Era from approximately 501 to 250 million years ago. In general, the stratigraphy in South Bruce is predominantly composed of carbonates (limestone, dolostone) with some beds of anhydrite/gypsum and shale layers. The central column of Figure 2 is representative of the stratigraphic succession encountered in the South Bruce area.

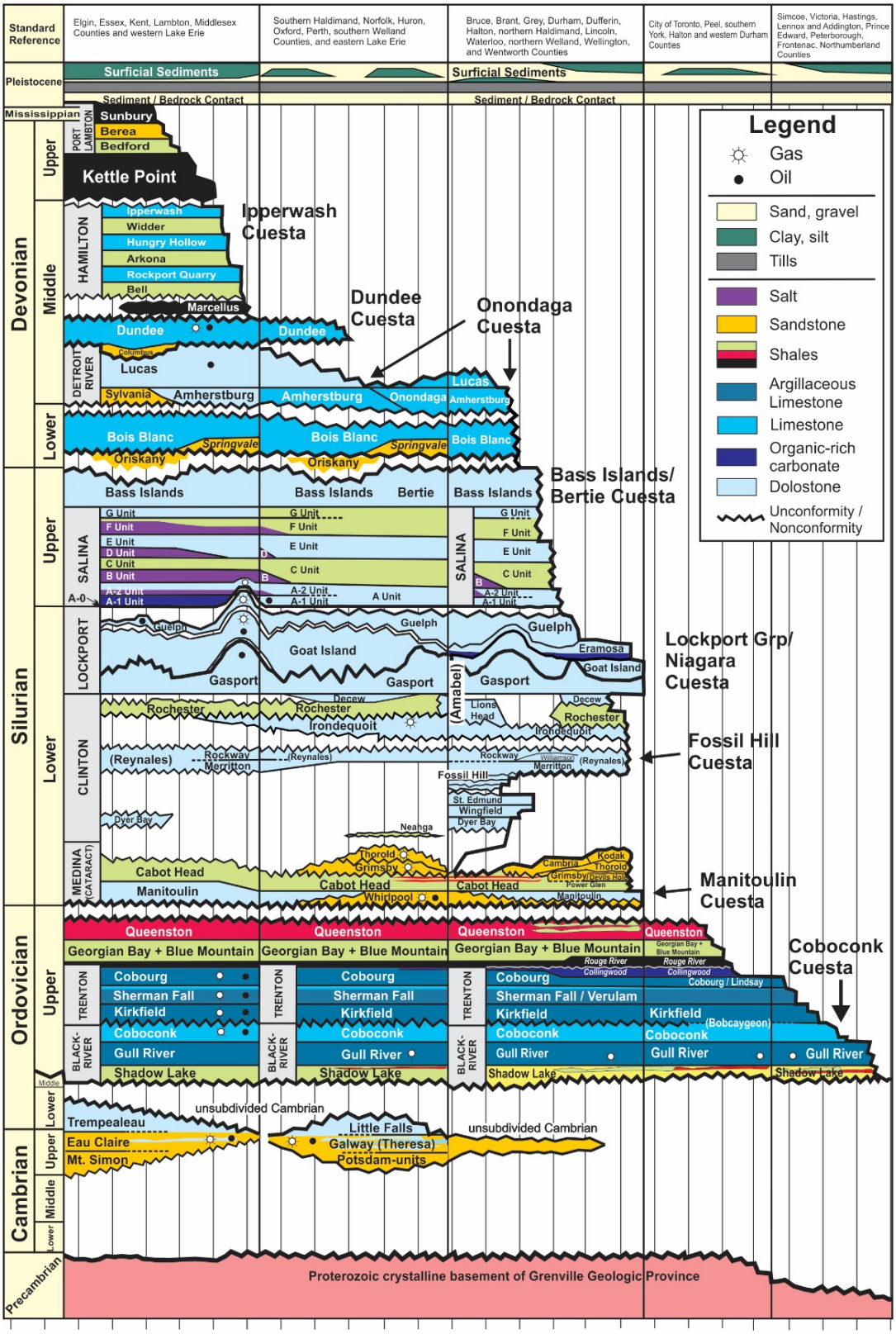


Figure 2. Lithostratigraphy of southern Ontario, colour-coded by rock type. Adapted from Brunton et al. (2017) and Carter et al. (2017) as updated from Armstrong and Carter (2010). The central column is representative of the stratigraphic succession encountered in the South Bruce area.

The maximum preserved thickness of Paleozoic rocks is approximately 4800 m in the Michigan Basin and 7000 m in the Appalachian Basin to the southeast (Armstrong and Carter 2010). In southern Ontario, the maximum preserved thickness of Paleozoic strata is approximately 1300 metres in the onshore portion of the Chatham Sag, thickening to 1450 metres beneath west-central Lake Erie and over 1500 metres beneath southern Lake Huron, thinning over the Algonquin Arch and towards the Frontenac Arch to the northeast. The Precambrian rocks that underlie southern Ontario are part of the Grenville Province comprising 2,690 to 990 million year old metamorphic rocks deformed during several orogenic events, the latest of which occurred 1,210 to 970 million years ago (Percival and Easton, 2007; White et al., 2000). Older tectonic events, including the 2.7 Ga Kenoran Orogeny, and the 2.0 - 1.7 Ga Trans-Hudson/Penokean Orogeny, built the Laurentian (proto-North American) craton upon which Grenville deformation was imprinted. In South Bruce, the basement gneiss is overlain by approximately 900 metres of Paleozoic sedimentary rocks.

The Paleozoic strata dip shallowly at 3.5 to 12 m/km (≤ 1°) down the flanks of the arches westwards into the Michigan Basin and southwards into the Appalachian Basin, steepening with depth and distance from the arches. Regional dip is 3 to 6 m/km along the crests of the arches into the Chatham Sag (Armstrong and Carter 2010).

The Devonian rocks, occurring at the South Bruce Site directly beneath the Pleistocene surficial sediments, consist of limestones, dolostones and cherty dolostones. The formations in the Devonian are named Lucas, Amherstburg and Bois Blanc in descending order. These are all carbonate-dominated sedimentary rocks deposited in shallow seas. The Bois Blanc Formation unconformably overlies the Upper Silurian Bass Islands Formation.

The Silurian rocks are subdivided into 4 major groups, named Salina, Lockport, Clinton and Medina groups in descending order. The Bass Islands Formation is the uppermost formation of the Silurian and has not been formally classified into any of the Silurian groups. The Upper Silurian Salina Group is characterized by a succession of evaporites and carbonates deposited in a hypersaline, restricted marine environment (Armstrong and Carter 2010). The Lower Silurian Lockport Group is characterized by widespread carbonate deposition consisting regionally of reefal carbonates of the Guelph Formation capped by the Salina Group (Johnson et al.1992). The Lower Silurian Clinton and Medina groups consist of alternating intervals of shale and limestone at the South Bruce Site. More detailed descriptions of Silurian strata are presented in subsequent chapters and in a regional geology summary report (Carter 2023).

The Upper Ordovician rocks are characterized by an upper sequence of predominantly shale formations with subordinate carbonate interbeds comprising the Queenston, Georgian Bay and Blue Mountain formations in descending order. Beneath these shales are the carbonates of the Trenton and Black River groups (youngest to oldest). The Trenton Group consists of the Collingwood Member of the Cobourg Formation, the lower Cobourg Formation, the Sherman Fall Formation and the Kirkfield Formation from youngest to oldest. The Black River Group consists of the Coboconk, Gull River and Shadow Lake formations. With the exception of the Shadow Lake Formation, the Trenton and Black River groups form a thick succession of limestones underlying all of southern Ontario. The Shadow Lake Formation is the base of the Upper Ordovician, and consists of glauconitic siltstone and sandstone with minor sandy shales uncomfortably overlying Cambrian Sandstone or the Precambrian when the Cambrian Sandstone is absent.

The Cambrian bedrock in onshore portions of southern Ontario is dominated by white to grey quartz sandstone unconformably overlying the Precambrian basement. Regional lithological variations include fine- to medium-grained crystalline dolostone, sandy dolostone and argillaceous dolostone to fine- to coarse-grained quartz sandstone (Hamblin, 1999). The Cambrian unit has been removed by erosion over the crest of the Algonquin Arch (Bailey Geological Services Ltd. and Cochrane, 1984a), and thus is expected to be absent beneath the eastern and central parts of the Area of the Five Communities identified in Phase 1 of Geoscientific Desktop Preliminary

Assessment (see Geofirma 2014). The Precambrian in southwestern Ontario is part of the Central Gneiss Belt of the Precambrian Grenville Province. This basement complex consists of a variety of metamorphic rock types ranging from felsic gneiss to mafic metavolcanic rock to marble (Armstrong and Carter 2010).

2.1.3 Tectonic History

The Paleozoic bedrock succession of southern Ontario resulted from a complex interplay of regional tectonic forces that caused vertical and sometimes lateral movements of tectonic units, such as faulting, subsidence and uplift, and siliciclastic sedimentation associated with orogenic activity and eustatic/global sea level fluctuation (Johnson et al. 1992; Sanford 1993b). Subsidence in the Michigan Basin started by late Cambrian time and was followed by on and off periods of subsidence and uplift, continuing through to the Late Jurassic (Sloss 1988; Leighton 1996; Howell and van der Pluijm 1999; Brunton and Brintnell 2020). The cause of subsidence in intracratonic basins, and in this case the Michigan Basin, is still poorly understood but it has been variously ascribed to a hypothetical mantle plume, cooling of stretched mantle lithosphere, densification of underlying lithosphere due to phase changes and/or to a response to compressional effects of Appalachian collisional tectonics (Brunton and Brintnell 2020). The Appalachian foreland basin formed in response to major continental collision events related to plate tectonic processes that resulted in four major orogenies: the Taconic (Ordovician), Salinic (Silurian), Acadian (Devonian), and Alleghanian (Pennsylvanian to Permian) orogenies (Johnson et al. 1992; Ettensohn 2008).

2.1.4 Burial/Erosion and Thermal History, Diagenesis

Figure 3 shows maximum burial-erosion curves for carbonate rocks of Upper Ordovician age from two different locations within the Michigan Basin. The orange curve in Figure 3 was included in a study of Ordovician diagenesis (Coniglio and Williams-Jones 1992, Geosynthesis 2011) and was drawn primarily based on stratigraphic information and data from Cercone (1984).

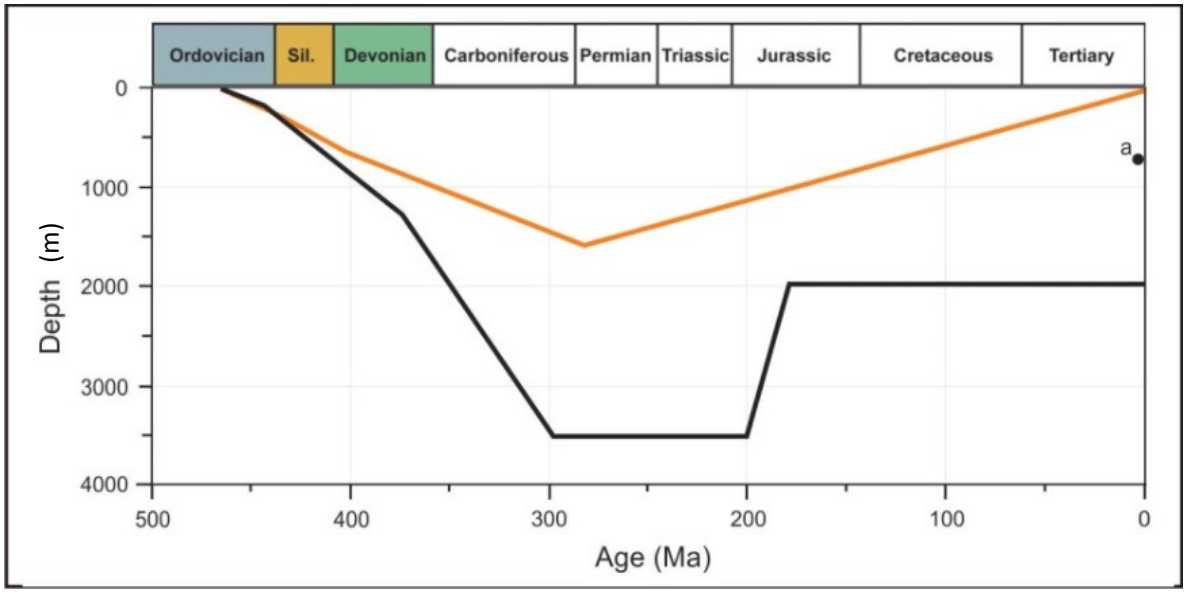


Figure 3. Hypothetical burial history curves for locations within the Michigan. Interpretations are based on data collected from Upper Ordovician carbonate sedimentary rocks. Orange curve is from Coniglio and Williams-Jones (1992) after Cercone (1984) evidenced from sediment accumulation rates, regional dips and maturity of Pennsylvanian age coals. Black curve is from Wang et al. (1994) derived from fission-track ages measured for

Carboniferous outcrop samples. (a) Indicates the present day burial depth of approximately 675 m for the middle of the Upper Ordovician sedimentary succession at the Bruce Nuclear Site. See text for further discussion.

Coniglio and Williams-Jones (1992) estimate that a minimum of 1500 m of compacted Paleozoic sediment has been eroded from the Manitoulin Island region (NW corner of Figure 1) since Permo-Carboniferous peak burial (Geosynthesis ,2011). An analysis of regional apatite fission track dates from around the south-central portion of the Michigan Basin, focused more directly on understanding the complete burial-erosion history (black line in Figure 3), was completed by Wang et al. (1994). Wang et al. (1994) studied apatite fission tracks within Carboniferous sediments and documented a similar late Carboniferous to early Permian timing for peak burial of ~3500 m of sediment at this south-central location within the basin, and determined that a maximum of 1500 m of sediments had been eroded. Given that the top of the Upper Ordovician succession exposed at Manitoulin Island is encountered at 450 mBGS beneath the Bruce Nuclear Site (Intera 2011), and the Bruce Nuclear Site is located slightly closer to the basin centre, it is reasonably estimated that a maximum of approximately 1000 m of sediment has been eroded from above the existing Paleozoic succession at the site and the surrounding area.

Based on the above discussion, an approximate peak burial in situ temperature for the top of the Trenton Group limestones, at the top of the Collingwood Member of the Cobourg Formation (~650 mBGS), has been calculated (assuming no other factors are involved). Ziegler et al. (1977) and Morel and Irving (1978) both define a position for southwestern Ontario at around 10°-15° south of the Equator during the Ordovician which allows for a mean annual surface temperature of 25°C at this time. Geothermal gradients of 20-30°C/km (Legall et al. 1981) and ~23°C/km (Hogarth and Sibley 1985) are suggested for the central and northern parts of the basin, respectively. An additional 1000 m of sediment at the Bruce Nuclear Site would have placed the Trenton Group (Collingwood Member) top at approximately 1650 mBGS resulting in an in situ temperature of 63.0°C using a 23°C/km estimate, 66.3°C using a 25°C/km estimate, and 74.5°C using a 30°C/km estimate, respectively, for the geothermal gradient. Therefore 70°C is considered a reasonable conservative maximum in situ burial temperature for the top of the Trenton Group beneath the Bruce Nuclear Site.

The resulting in situ temperatures, and therefore the maximum burial estimates in Figure 3, are consistent with results from Legall et al. (1981) which characterize two thermal alteration facies in the Paleozoic strata of southern Ontario using primarily a conodont alteration index (CAI). The first, from the top of the Paleozoic to the mid-Ordovician Trenton Group limestones, represents an organically immature to marginally mature facies that attained a maximum temperature of approximately 60°C. The second facies extends from the mid-Ordovician downwards to the base of the Paleozoic sequence (Shadow Lake Formation). This group would comprise predominantly the Black River Group in the South Bruce and surrounding areas where the Cambrian is very thin or nonexistent. These rocks attained maximum burial temperatures of 60-90°C (Legall et al. 1981). Samples taken approximately 80 km east of the formerly proposed Deep Geological Repository (DGR) indicate a CAI of 1.5, representing Ordovician burial temperatures of approximately 75-85°C (Legall et al. 1981). Legall et al. (1981) also designate a third maturation facies in eastern Ontario and southern Quebec. Paleozoic sediments in this region attained much higher maximum burial temperatures of 90-120°C as a result of proximity to the path of the Great Meteor Hotspot (Heaman and Kjarsgaard 2000).

The regional CAI estimate of 1.5 (Legall) represents a burial temperature of around 75°C with a possible error range of approximately ±15°C. This large error could potentially mask any localized low-level heating by hydrothermal fluids, which could have migrated into the region from the basin centre. Occurrences of thin planar dolomite horizons are found within the Ordovician shales beneath the Bruce Nuclear Site (Intera 2011) and may represent the results of percolation and horizontal migration of warm fluids from deeper in the basin.

Powell et al. (1984) suggest that the alteration facies designation devised by Legall et al. (1981) would indicate a very limited potential for in situ petroleum generation in rocks as deep as the Upper Ordovician Trenton Group in southern Ontario in general. Importantly, this interpretation is consistent with the observation that the same rocks beneath the Bruce Nuclear Site only barely reached the oil window in terms of thermal hydrocarbon maturation (Intera 2011). This is consistent with the observed transition from immature to mature hydrocarbons across the Georgian Bay – Blue Mountain sequence beneath the Bruce Nuclear Site (Intera 2011). A more recent study by Engelder (2011) concluded that limited hydrocarbon maturation at the Bruce Nuclear Site is a result of subsidence that reached a total burial depth of approximately 1.5-2 km, creating temperatures that only marginally crossed the oil generation window (60°C). This lack of thermal maturity in combination with low organic content has resulted in the generation of a very limited occurrence of commercially unexploitable hydrocarbons at the Bruce Nuclear Site. The peak temperature estimates addressed in the previous section suggest that any addition of a hydrothermal fluid component within the Ordovician sediments beneath the site was (in the absence of additional data) indiscernible from the temperature effects of burial.

The two burial curves in Figure 3 are considered to be suitable for constraining maximum peak burial conditions for rocks within the South Bruce and surrounding area, including the Bruce Nuclear Site. They vary, however, in their interpretation of the timing and rate of erosion. While the orange curve depicts a constant erosion rate since peak burial until the present day, the black curve indicates a non-constant erosion rate where much of the 1500 m was removed prior to the Middle Jurassic. This timing constraint is justified by the observation of a regional unconformity that separates Middle Jurassic sandstones from Pennsylvanian sandstones within the centre of the basin (Wang et al. 1994, Dickinson et al. 2010). Given that this unconformable relationship is regional in scale (e.g., Sloss 1963), and that the Bruce Nuclear Site shares a common geological history with the Michigan Basin, it is reasonable to suggest that much of the missing 1000 m of Paleozoic rocks at the Bruce Nuclear Site were eroded during the same (pre-Mid Jurassic) time interval. A late Paleozoic to early Mesozoic timing for the majority of the erosion at the Bruce Nuclear Site therefore coincides with the waning of the Alleghenian stage of the Appalachian Orogeny, the break-up of Pangaea and opening of the Atlantic Ocean.

Paleozoic rocks of southern Ontario have generally been altered through their deposition and post-depositional lifecycle by diagenetic processes. The most significant of these is dolomitization whereby calcite or aragonite is converted to dolomite by the replacement of calcium ions by magnesium ions, and is interpreted to have occurred in response to tectonically driven fluid migration associated with Paleozoic orogenic events (Coniglio and Williams-Jones 1992). The timing of dolomitization events ranged from during or shortly after marine carbonate deposition during the Ordovician to the Late Paleozoic/Early Mesozoic, and/or corresponding to maximum burial compaction. Hydrothermal dolomitization selectively altered the Paleozoic rocks along and adjacent to discrete fracture systems (possibly faults) in response to tectonic events during the Paleozoic and Early Mesozoic. The conditions that led to dolomitization within the South Bruce area of the Michigan Basin (i.e., basinal groundwater flow, fracture-related tectonically driven flow, and hydrothermal dolomitization) have not existed for the last approximately 200-250 Ma (e.g., Coniglio and Williams-Jones 1992).

Coniglio and Williams-Jones (1992) argue that hydrothermal dolomitization may have involved percolation of fluids much warmer (ca. 100 to 200°C) than would be expected due to burial alone. In some cases, this mechanism of dolomitization was associated with the development of large hydrocarbon deposits, generally where a structural control also dominated, for example the fault-related Albion-Scipio hydrocarbon field in southern Michigan described by several authors (e.g., Prouty 1988, Hurley and Budros 1990, Davies and Smith 2006). Several studies indicate that when hydrothermal fluids are included as a component of the system, widely ranging peak temperature conditions are likely to prevail at the basin scale (e.g., Hurley and Budros 1990, Coniglio and

Williams-Jones 1992, Davies and Smith 2006). In turn, this suggests that the extent or volume of hydrothermal dolomitization can also vary along with its morphology. Instances of dolomitization, formed both in situ due to compaction under ambient conditions of burial, and/or hydrothermal due to percolation of hot fluids, appear to have developed at all scales in the Michigan Basin. Regional studies (e.g., Legall et al. 1981) suggest that low burial temperatures prevailed throughout much of the South Bruce area.

The key post-dolomitization diagenetic phases are all volumetrically minor including late-stage calcite cements, Mississippi Valley Type (MVT) mineralization, and late-stage anhydrite and gypsum (Budai and Wilson 1991, Coniglio et al. 1994). These phases do not include those related to modern surface exposure in the near-surface rocks of the Michigan Basin, which are not discussed here. Other diagenetic events include salt dissolution and subsequent subsidence/collapse features (Upper Silurian and Devonian stratigraphy), clay alteration at the Precambrian-Paleozoic boundary, and hydrocarbon migration and emplacement. More recent insights on dolomitization and diagenesis are provided in Al-Aasm and Crowe (2018), Al-Aasm et al. (2021), Diamond et al. (2015), Haeri-Ardakani et al. (2013a, b, c), Petts et al. (2017), Tortola (2019) and Tortola et al. (2020). The hydrochronology of these diagenetic events is addressed in Davis 2013, 2016; Davis et al. 2020 and Sutcliffe et al. 2020), and pyrite diagenesis in Jautzy et al. 2020. See discussion in Carter (2023).

2.1.5 Salt Dissolution

Dissolution of halite beds of the Salina Group has occurred at the margin of the Michigan Basin in a zone extending from the Bruce Peninsula south along Lake Huron and into southwestern Ontario. This process occurred primarily during the late Silurian phase of the Salinic Orogeny. A second major salt dissolution event occurred during the Devonian Acadian Orogeny (Sanford et al. 1985). Dissolution was by downdip infiltration of unsaturated surface water and shallow groundwater, beginning immediately after deposition and occurring until at least late Devonian time (Sanford 1969, Armstrong and Carter 2010, Carter 2023). Salt dissolution is also interpreted to have occurred via fluid migration through regional fractures (Sanford et al. 1985) and above pinnacle structures in the underlying Guelph Formation. Removal of salt from the subsurface is interpreted to have created subsidence/collapse features (e.g., breccia) and initiated fracturing within the overlying Upper Silurian and Devonian strata. The zones affected by this dissolution are brecciated and characterized by veins and joints completely filled with evaporite (mainly gypsum) cement enclosing dolostone and anhydrite clasts. The pervasive cementation and fracture infilling has resulted in very low measured hydraulic conductivities in the Silurian rocks (Intera 2011).

2.1.6 Karst and Paleokarst

Karstic dissolution of carbonate and evaporite rocks can greatly enhance porosity and permeability. Karst and paleokarst horizons are the principal control on groundwater movement and the location of all significant aquifers in the Paleozoic bedrock of southern Ontario (Carter et al. 2021). Carbonate and evaporite rocks are widespread in southern Ontario, particularly on the Michigan Basin side of the Algonquin Arch. Where these rocks are exposed at the present-day surface or subcrop beneath thin unconsolidated overburden, they are subject to dissolution by acidic meteoric water or shallow groundwater, most of which has occurred since the last phase of the Pleistocene glaciations (Carter 2023). This greatly increases the porosity and permeability of the rock forming a dual-porosity aquifer with water storage in the rock matrix and most flow through high-permeability interconnected dissolution conduits. Groundwater flow velocities through these conduits are enhanced in comparison to an equivalent porous medium or fractured rock. Karstification is most pronounced in shallow freshwater zones with low concentrations of dissolved solids (Worthington 2011).

Paleokarst refers to karst that formed in the geological past during periods of subaerial exposure of carbonate and evaporite bedrock at major disconformities, and which has subsequently been

buried, cemented, and preserved beneath younger rocks in the subsurface. Numerous disconformities occur in the Paleozoic bedrock of southern Ontario, some of regional extent while others are of local or undocumented geographic extent (Figure 2). Where these disconformities have affected carbonate rocks, paleokarst intervals of enhanced porosity and permeability have been formed. Enhanced porosity and permeability associated with paleokarst development occurs immediately below disconformities at the top of the Lucas Formation (Uyeno et al. 1982; Birchard 1990; Birchard et al. 2004), the Bass Islands Formation (Kobluk et al. 1977; Armstrong 2017, 2018; Sun 2018), the Guelph Formation (Kahle 1988; Smith 1990; Brunton et al. 2012; Brunton and Brintnell 2020; Carter et al. 1994) and the unsubdivided Cambrian (Coogan and Maki 1987; Desrochers and James 1988; Mussman et al. 1986, 1988). Carter (2023) and Carter et al. (2021) provide a more detailed review of the distribution of karst and paleokarst in southern Ontario.

2.2 Background and Overview of Borehole Drilling and Testing

2.2.1 Drilling Site Description

Borehole SB_BH02, is located approximately 5.5 km northwest of the community of Teeswater, Ontario. Access to the SB_BH02 drill site is via Bruce Road 4 and West on Concession 8 (Figure 4). SB_BH02 was drilled vertically to a total depth of approximately 900m. Further details on the final borehole construction are presented in Geofirma (2023a) and briefly summarized in Section 2.3 of this report. SB_BH02 is located approximately 2.5 km west of SB_BH01.

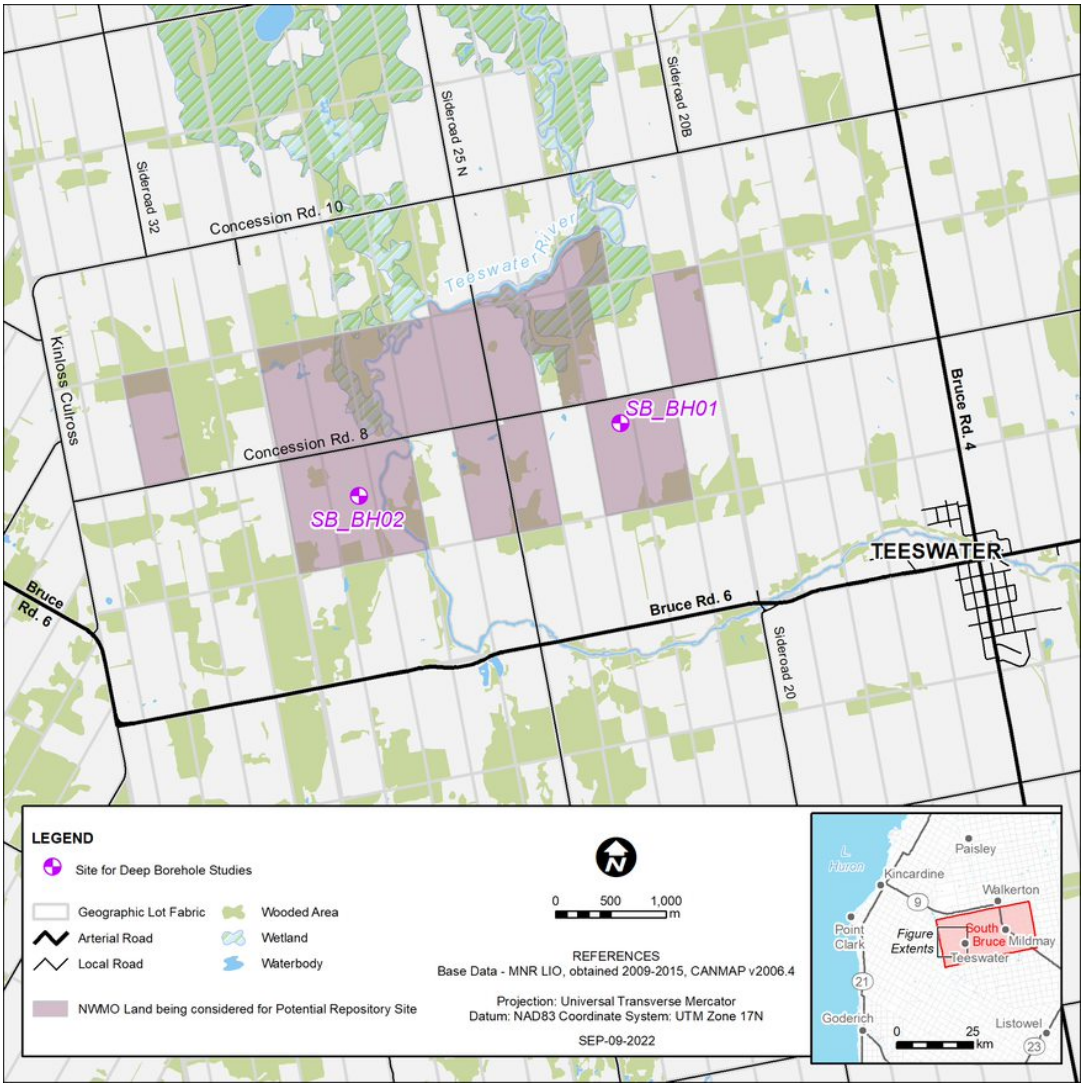


Figure 4. Location Map showing boreholes SB_BH01 and SB_BH02 drilled as part of Geoscientific Preliminary Field Investigations by NWMO.

2.3 Borehole Details for SB_BH02

2.3.1 Borehole Construction

In order to meet the casing requirements of the Provincial Operating Standards of the Oil, Gas and Salt Resources Act, multiple telescoped-casing installations were necessary to provide a permanent seal between various known aquifers within the unconsolidated overburden and Devonian and Silurian bedrock formations and to provide suitable blow-out prevention (BOP) in the event of drilling through a gas-pressurized zone. To accommodate this, SB_BH02 was drilled in the following five distinct stages:

Stage 1: Conductor Borehole and Casing Installation (0 to 34.6 meters below ground surface-mBGS)
Drill through overburden material using cable tool rig while advancing conductor casing (406.4 mm OD) to produce ~406 mm diameter borehole from ground surface to top of bedrock.

Stage 2: Surface Borehole and Casing Installation (34.6 to 49.88 mBGS)

Continue drilling through shallow weathered bedrock using cable tool rig to produce a borehole with a minimum diameter of 375 mm (14 ¾”). Install and cement 298 mm ± (11 3/4”) OD diameter Surface Casing to seal off overburden sediment and groundwater in the shallow bedrock from the borehole and deeper formations.

Stage 3: Intermediate Borehole and Intermediate Casing #1 Installation (49.88 to 78.82 mBGS)

Continuously core using Class A (rotary) annular BOP with freshwater drilling fluid and PQ3 wireline equipment from bottom of cement to 78.82 mBGS. Enlarge borehole to 273 mm +/- (10 3/4”) and install and cement 219 mm +/- (8 5/8”) OD Intermediate Casing #1 to seal off any potential salty water below this depth from cross connecting with any shallow fresh water aquifer(s) used by nearby residences as a potable water supply source.

Stage 4: Intermediate Borehole to Salina Fm F-Unit shale and Intermediate Casing #2 (main BOP string/steel casing) (78.82 to 204.95 mBGS)

Continuously core using Class B (rotary) full stack BOP with freshwater drilling fluid and PQ3 wireline equipment from bottom of cement to tentatively 5 m into the Salina F Unit shale. Complete borehole geophysical logging (natural gamma ray and spectral gamma from 0 m to 204.95) of the upper bedrock. Enlarge borehole to 196 mm +/- (7 3/4”) and install and cement 139.7 mm +/- (5 ½”) OD Intermediate Casing #2 (main BOP string) to allow P-size coring (123 mm) below Salina F Unit shale and seal off any shallow freshwater aquifer(s) for drilling with brine.

Stage 5: Main Borehole to Precambrian Basement (204.95 to 900.57 mBGS)

Continuously core using Class B (rotary) full stack BOP with brine drilling fluid and PQ3 wireline equipment to produce a 123 mm +/- (4 7/8”) open borehole from the Salina F Unit shale to total depth approximately 14 m into Precambrian basement.

The borehole was planned to be drilled vertically at an inclination of -90° without any azimuth. While the target is to keep the borehole as straight and vertical as possible, variations of inclination and azimuth while drilling vertical boreholes are common. No corrections were made for deviation during drilling operations, however reasonable care was taken in selection of drilling rates using weight on bit and selection of downhole stabilizers to keep the inclination close to vertical.

Borehole orientation was measured using a north-seeking gyroscopic tool (Axis Champ Gyro) to measure the azimuth and plunge of the borehole as it advanced. A calibration check was completed at ground surface prior to lowering the tool into the rods on a wireline inside of the drill rods to the targeted depth. The Axis Champ Gyro provides azimuth readings to within +/- 0.75° and dip to within +/- 0.15°.

Single-shot borehole orientation measurements were collected every 50 m as drilling progressed. The maximum reported borehole inclination over the entire borehole during any one measurement was 3.19 degrees at ~177 mBGS and the maximum reported inclination below the deepest casing installation (~205 mBGS) was 3.06 degrees at ~757 mBGS. The inclination near the bottom of the borehole was 2.79 degrees from vertical.

A final borehole orientation survey was conducted using the same Axis Champ Gyro on March 23, 2022 following the completion of drilling BH02. The final borehole survey was completed taking measurements at every 10 m; and was comparable to the single shot measurements every 50 m. The final borehole orientation survey resulted in an average inclination over the entire borehole length of -87.30° degrees and an average azimuth of 54°. The total deviation from the original collar location was calculated as approximately 42 m at the bottom of the borehole. A copy of all borehole orientation survey data collected with gyroscopic tool is presented in Appendix C of the WP02 Data Report for SB_BH02 (Geofirma, 2023a).

3 INTEGRATED GEOLOGICAL INTERPRETATION

3.1 Data Used for Geological Interpretation

A comprehensive suite of geological and geophysical data was incorporated in this study to provide an updated interpretation of stratigraphic tops (formations, units and members) intersected within SB_BH02. Initial stratigraphic tops were interpreted as part of the core logging (WP03: Geofirma, 2022a) based strictly on drill core observations. Important data sets derived from the core logging include bedrock lithology, alteration, weathering, hydrocarbon occurrences, structural features, regionally significant key marker beds, fossil types and grain size observations. Lithologies were delineated primarily based on mineralogy as well as sedimentary structures, bedding thickness, grain size and sorting attributes, and were logged using a minimum thickness of 5 cm, except for marker beds which have a unique geological significance (e.g. volcanic ash bed). Alteration was logged based on any observable change to the mineralogical composition of a rock brought about by hydrothermal processes (e.g. silicification). The presence of hydrocarbons was recorded only when visually observed, and classified based on presence of natural gas, visible oil, petroliferous odour, or UV visible oil. High-resolution core imagery was evaluated in this study to allow for detailed lithological review and comparison with results from geophysical well logs.

An appropriate set of geophysical well logs (Geofirma, 2023b), useful for distinguishing mineralogical and lithological characteristics of the bedrock, are incorporated in this study to assist with the interpretation of stratigraphic tops in SB_BH02. The natural gamma and spectral gamma logs (K, U, Th) provide a measure of the naturally occurring radioactivity from the bedrock and can help differentiate between lithology and mineralogy across stratigraphic boundaries. Increased natural radioactivity is mainly attributed to the abundance of shales and clay minerals in the bedrock and is used as a measure of variations in shale content along the borehole. Distinctive patterns in the variation of shale content can be used to identify formation tops in the Paleozoic bedrock of southern Ontario with considerable accuracy (see Armstrong and Carter 2010).

Bedrock resistivity is a measure of the rocks resistance to conducting an electrical current. Varying amounts of shale within a carbonate bedrock result in a highly variable resistivity. Shale-dominated rocks conduct electrical current easily resulting in a low measured resistivity. Since the resistivity log is also sensitive to the presence of shale, these log results tend to display an inverse relationship with the natural gamma log. In this analysis, the long-spaced normal resistivity log is used as it best represents the true electrical properties of the bedrock including the *in situ* porewater salinity.

Gamma-gamma density provides a measure of electron density, which is related to bulk density of the bedrock. The gamma-gamma density log is an active source that emits gamma rays that collide with electrons in the rock, resulting in a loss of energy recorded at a sensor. The recorded data provides a measure of bulk density of the bedrock and can be used to differentiate the lithology. As

a result, the bulk density log can be used to identify evaporite minerals and gas-bearing intervals. In addition, the gamma-gamma density is related to porosity of the bedrock and, consequently, may highlight boundaries between porous and non-porous rock, and the density of pore fluids. Low density spikes in the log may also correlate with zones of increasing borehole diameter (i.e. highly porous zones along the borehole wall). In this analysis, the long-spaced gamma-gamma density is used. as it best represents the true bulk properties of the bedrock. The neutron log provides a measure of the hydrogen ion content within the bedrock, including hydrogen in the pore space and bound hydrogen in the mineral structure. In shale-free rocks the neutron log measures liquid-filled (water, oil) porosity. Similar to gamma-gamma density, neutron logging relies on an active source that emits neutrons that collide with, and are absorbed by, hydrogen atoms in the bedrock and are measured at a sensor. The rate at which these neutrons are measured is proportional to the hydrogen concentration. Similar to the density log, the long-spaced neutron is used as it best represents the true bulk properties of the bedrock for this analysis. Although not completed for this analysis, the neutron log results recorded using a calibrated probe can be converted to a neutron porosity log providing a measure of bedrock pore volume. Despite this calculation being possible, there are challenges and uncertainties associated with calculating neutron porosity in shale units.

Lastly, the full waveform sonic log was used to derive bedrock P-wave and S-wave velocities. Interval transit times measure the speed at which a sonic wave travels through the bedrock, where these transit times can vary as a function of lithology and porosity. As a result, the derived bedrock velocity log provides a means to help differentiate transitions between different stratigraphic formations, units and members, as well as to help identify boundaries between porous and non-porous bedrock. Both the P-wave and S-wave velocities were incorporated for the analysis of the stratigraphic tops. However, only the compressional P-wave velocities were incorporated in the figures throughout this report. Sonic logs are also used to calibrate seismic data.

In addition to data acquired as part of the drilling and testing project, several key historical and more recent references are incorporated as part of this integrated analysis for the identification of tops of formations and members. Armstrong and Carter (2006; 2010) provide a guide to the subsurface Paleozoic stratigraphy of southern Ontario, including definitions and descriptions of sedimentary strata, consistent standards for picking of formation contacts in drill cuttings and geophysical logs, and their economic significance.

NWMO Bruce Nuclear Site Technical Reports on bedrock formations (Sterling, 2010; 2011; Wigston and Heagle, 2010; Sterling and Melaney, 2011) and the Descriptive Geosphere Site Model (Intera 2011) provide a summary compilation, description, assessment and interpretation of geoscientific data collected during scientific investigations at this site, which are described in a series of technical reports. They also summarize the current understanding of underground geological, hydrogeological and geomechanical conditions of the Bruce Nuclear Site, relevant to DGR repository engineering and safety assessment functions. Findings from the Bruce Nuclear Site studies provide a natural analogue to help characterize and understand the South Bruce Site due to their close proximity, same depositional (sedimentary) environments, tectonic history and, in particular, the transferability of geoscientific information for the Upper Ordovician succession.

The NWMO Phase 1 Geoscientific Desktop Preliminary Assessment Report on interpretation of borehole geophysical logs and 2D seismic data (Sterling and Schieck, 2014) presents the findings of an interpretation study looking at historical borehole geophysical well log data and historical 2D seismic data.

Recently, the Geological Survey of Canada completed a regional 3D lithostratigraphic model of the Paleozoic bedrock of southern Ontario (Carter et al., 2021), updating an earlier model Carter et al. 2019). This updated version encompasses the entire Phanerozoic succession of southcentral and southwestern Ontario including 53 model Paleozoic bedrock layers representing 70 formations, as well as the Precambrian basement and overlying unconsolidated sediment. Additionally, the model

provides a more representative/realistic lateral continuity of formations, and an updated stratigraphic chart.

3.2 Geological Results

This section presents the results from the integration of geological core logging (WP03) with the geophysical well logging (WP05) datasets to provide a robust interpretation of the depths to top of formations, members, and units within SB_BH02. The interpretation of these formations, members and units using core and geophysical logging data are consistent with criteria described in Armstrong and Carter (2010), and more recently modelled in a 3D stratigraphic model in Carter et al. (2021).

Through the process of data integration, a total of 34 Paleozoic lithostratigraphic units were identified for SB_BH02, in addition to the Pleistocene overburden deposits on top of the bedrock and the Precambrian basement (Table 1). A well log presenting the layers along with lithology and a suite of geophysical logs is presented showing their distribution along the length of the borehole (Figure 5).

Given the final stratigraphy in SB_BH02, each interval is analyzed to assess the dominant lithology and their geophysical well log characteristics. Structural characteristics, hydrocarbon occurrences and petrophysical property distributions are briefly summarized in this report but will be further explored in a separate study. Geophysical well log characteristics are explored using a series of boxplots and scatterplots (Figure 6, Figure 7, Figure 11 and Figure 12) to display the measurement variability for each stratigraphic interval as well as for each dominant lithology. Due to the steel casing being installed to a depth of 204.95m, P-wave velocity and normal resistivity logs measurements are only analyzed for the open portion of the borehole, from 204.95m to bottom of hole.

3.2.1 Stratigraphic Formation and Member Descriptions

This section describes the final interpretations of formation and member tops identified within SB_BH02. These final formation tops comprise an important update that takes into account the integration of rock core observations (WP03 – Geofirma 2022a) with variable response observed in geophysical well log data (WP05 – Geofirma 2023b). As a result, the outcome of the stratigraphic picks are consistent with the framework presented by Carter et al. (2021), and were picked following guidance from Armstrong and Carter (2006, 2010) as well as criteria described in previous detailed reports from the Bruce Deep Geological Repository study (Intera 2011). Although Armstrong and Carter (2010) provide more of a regional approach to formation descriptions and picking criteria of sedimentary strata in southern Ontario, the descriptions of formations and nature of contacts/tops in this report are based only on what was observed in core (WP03) and interpreted in geophysical logs (WP05). These observations and interpretations may slightly differ from regional literature because they are based on a single borehole (SB_BH02).

In total, 36 lithostratigraphic units (including overburden and Precambrian) were identified in SB_BH02 representing formations and members spanning from the Devonian Lucas Formation to the Precambrian basement rocks (see Table 1). The following subsections provide summary descriptions of all formations and members that were observed, as well as the rationale for the stratigraphic pick based on core observations and geophysical well log data. Representative photos for each formation and/or member are provided for reference in Appendix B with detailed features for each formation, which are consistent with the lithology summary below.

Table 1: Summary of top, bottom and thickness of formations and members interpreted through and integrated analysis of core observation and geophysical well log data for SB_BH02. Presented depths represent position along the borehole.

	Color Legend[3]	Formation and Member	Top Position along borehole (m)	Bottom Position along borehole (m)	Thickness along borehole (m)	Basis for Interpretation [2]
		Overburden/Surface	0	34.6	34.6	Drill Cuttings
Devonian		Lucas Formation	34.6	88.73	54.13	Drill Cuttings and Drill Core
		Amherstburg Formation [1]	88.73	130.5	41.77	Drill Core
		Bois Blanc Formation[1]	130.5	156.91	26.41	Drill Core
Upper Silurian		Bass Islands Formation	156.91	185.73	28.82	Drill Core
		Salina G Unit[1]	185.73	192.55	6.82	Drill Core, Geophysical Logs
		Salina F Unit	192.55	238.13	45.58	Drill Core, Geophysical Logs
		Salina E Unit	238.13	263.64	25.51	Drill Core, Geophysical Logs
		Salina D Unit	263.64	266.4	2.76	Drill Core, Geophysical Logs
		Salina C Unit[1]	266.4	283.07	16.67	Drill Core, Geophysical Logs
		Salina B Unit[1]	283.07	290.6	7.53	Drill Core, Geophysical Logs
		Salina B Unit Equivalent	290.6	304.99	14.39	Drill Core, Geophysical Logs
		Salina B Unit Anhydrite	304.99	306.97	1.98	Drill Core, Geophysical Logs
		Salina A-2 Unit Carbonate	306.97	332.24	25.27	Drill Core, Geophysical Logs
		Salina A-2 Unit Anhydrite[1]	332.24	337.58	5.34	Drill Core, Geophysical Logs
		Salina A-1 Unit Carbonate[1]	337.58	375.83	38.25	Drill Core, Geophysical Logs
		Salina A-1 Unit Evaporite[1]	376.1	383.18	7.08	Drill Core, Geophysical Logs
		Salina A-0 Unit Carbonate1	383.18	386.84	3.66	Drill Core, Geophysical Logs
Lower Silurian		Guelph Formation	386.84	391.86	5.02	Drill Core, Geophysical Logs
		Goat Island Formation	391.86	408.0	16.14	Drill Core, Geophysical Logs
		Gasport Formation	408.0	415.3	7.30	Drill Core, Geophysical Logs
		Lions Head Formation [1]	415.3	418.10	2.80	Drill Core, Geophysical Logs
		Fossil Hill Formation	418.10	419.28	1.18	Drill Core, Geophysical Logs
		Cabot Head Formation	419.28	440.10	20.82	Drill Core, Geophysical Logs
		Manitoulin Formation[1]	440.10	449.25	9.15	Drill Core, Geophysical Logs
Upper Ordovician[4]		Queenston Formation	449.25	534.70	85.45	Drill Core, Geophysical Logs
		Georgian Bay Formation [1]	534.70	620.86	86.16	Drill Core, Geophysical Logs
		Blue Mountain	620.86	669.69	48.83	Drill Core, Geophysical Logs
		Cobourg Formation / Collingwood Member	669.69	677.54	7.85	Drill Core, Geophysical Logs
		Cobourg Formation / Lower Member	677.54	716.37	38.83	Drill Core, Geophysical Logs
		Sherman Falls Formation	716.37	762.03	45.66	Drill Core, Geophysical Logs
		Kirkfield Formation	762.03	805.63	43.60	Drill Core, Geophysical Logs
		Coboconk Formation	805.63	826.71	21.08	Drill Core, Geophysical Logs
		Gull River Formation [1]	826.71	881.58	54.87	Drill Core, Geophysical Logs
		Shadow Lake Formation	881.58	886.93	5.35	Drill Core, Geophysical Logs
		Cambrian Sandstone	NA	NA	0	NA
		Precambrian	886.93	900.57	13.64	Drill Core, Geophysical Logs

Notes:

1. Formation top/bottom depths updated based on drill core observations integrated with geophysical well log data. Initial formation top/bottom depths are reported in WP03 report (Geofirma 2022a).

2. Detailed descriptions of the criteria for each individual formation and member top pick is included in Sections 3.2.1.2 to 3.2.1.5.

3. Color legend assigned to formations and members. Color template is consistent with Carter et al (2021) for the Southern Ontario regional lithostratigraphic model.

4. Paleozoic stratigraphic nomenclature has changed between Bruce site drilling (2011) and South Bruce Site (2022). Changes to Ordovician time scale resulted in moving the Middle-Upper Ordovician boundary lower such that all of the strata traditionally referred to as Middle Ordovician in Ontario are now considered Upper Ordovician.

3.2.1.1 Pleistocene Deposits

Based on drill cuttings from SB_BH02, the Pleistocene overburden deposits overlying the Lucas Formation are approximately 34.6 m thick. The upper 27 m of the overburden consists of an equal proportion of poorly sorted unconsolidated fine-grained sand and gravel, underlain by 1.5 m of calcareous mud (lime mud) with minor gravel (27-28.5 m). The remaining 6.1m of the overburden consists of subrounded to well rounded fine- to very coarse-grained sand. Bedrock starts at 34.6m. Refer to SB_BH02_WP03_DQC for detailed descriptions of the overburden.

3.2.1.2 Devonian Rocks

Lucas Formation: The Lucas Formation represents the uppermost formation of the Detroit River Group, conformably overlying the Amherstburg Formation in the South Bruce area, and regionally comprising limestone, dolostone and anhydritic beds with local sandy limestone (Armstrong and Carter, 2010). Within SB_BH02, the Lucas Formation consists of non-fossiliferous, laminated to thin- to medium-bedded finely crystalline, light brown/tan limestone and dolostone with needle-like porosity. Karstic vugular porosity is prominent from 48 to 88 m (into the Amherstburg Formation). The top of the Lucas Formation was picked at a depth of approximately 34.60 m using drill cuttings marked by the first occurrence of bedrock while drilling with cable tool rig. This top pick is supported by the presence of light brown/tan limestone drill cuttings with needle-like pores. The Lucas Formation was logged with a total thickness of 54.13 m, making the bottom formation contact pick at 88.73 m. Refer to photographs B-1 and B-2 of Appendix B for representative photographs of the Lucas Formation and its contact with the Amherstburg Formation.

Amherstburg Formation: The Middle Devonian Amherstburg Formation is also part of the Detroit River Group. Within SB_BH02, the Amherstburg Formation consists of fossiliferous, cherty, nodular, argillaceous dolomitic limestone with laminations. The uppermost few meters consist of stromatoporoid-dominated limestone, sparse corals and brachiopods, with karstic vugular porosity at 88.73-91.24 m. The lower part of the Amherstburg Formation consists of medium grey limestone with irregular pale/light grey chert nodules. The Amherstburg Formation top pick is based on core only and is characterized by a change from laminated non-fossiliferous mudstone of the Lucas (with occasional beds of anhydrite) to a very fossiliferous brown-grey limestone. Natural gamma and spectral gamma logs are uniform and unresponsive through the Amherstburg Formation into the overlying Lucas Formation. The Amherstburg Formation is located between 88.73 m (top) and 130.5 m (bottom) with a total thickness of 41.77 m. Refer to photographs B-3 and B-4 of Appendix B for representative photographs of the Amherstburg Formation and its contact with the Bois Blanc Formation.

Bois Blanc Formation: The Lower Devonian Bois Blanc Formation disconformably overlies the Upper Silurian Bass Islands Formation. In SB_BH02, the Bois Blanc Formation consists of fine- to medium-grained, brown-grey, mottled dolomitic limestone with abundant pale/light grey to white chert nodules. Moderately fossiliferous cherty limestone is the dominant lithology in this formation. Fossils are mostly to partially silicified and they include crinoids, bivalves, brachiopods and corals. Although chert nodules/cherty dolostone constitute more than 80% of the formation, argillaceous limestone beds with laminations and stylolites are also seen in core along with bituminous shale laminae and zones.

The Amherstburg and Bois Blanc Formation contact is completely gradational, making it an extremely difficult pick. The bituminous, slightly to moderately cherty and fossiliferous dolostones of

the lower Amherstburg Formation gradually change to a very cherty dolostone with depth. The top of the Bois Blanc Formation is marked where the basal slightly to moderately cherty limestone/dolostone of the Amherstburg Formation exhibits a gradual increase in chert content/nodules (>50% chert). The natural gamma log does not provide any support in interpreting the top of the Bois Blanc due to lack of a lithological contrast, and its response is typically undiagnostic. Overall, the Bois Blanc Formation is considered one of the most unreliable picks in the entire Paleozoic stratigraphy (Armstrong and Carter 2010). The Bois Blanc Formation is located between 130.5 m (top) and 156.91 m (bottom) with a total thickness of 26.41 m. Refer to photographs B-4 and B-5 of Appendix B for representative photographs of the Bois Blanc Formation and its contact with the Bass Islands Formation.

3.2.1.3 Silurian Rocks

Bass Islands Formation: The Bass Islands Formation is the uppermost Silurian aged strata where the top of the formation represents the Devonian – Silurian erosional unconformity. The Bass Islands Formation consists of finely crystalline, slightly brecciated, argillaceous, tan to grey, laminated dolostone with occasional blue-grey evaporite mineral molds. Occasional decimeter scale beds of grey, karstic/vuggy dolostones are also observed throughout the Bass Islands Formation. Bituminous layering is common, with occasional karstic vugs infilled by calcite, trace pyrite and a blue-grey mineral that is interpreted to be celestite. The top of the Bass Islands Formation is picked based on the presence of paleokarst breccia with glauconitic sand pebbles (erosional unconformity). Armstrong and Carter (2010) indicate this formation pick to be relatively consistent across boreholes and is marked where a chert-dominated carbonate of the Bois Blanc Formation rapidly transitions into a homogeneous, finely crystalline dolo-mudstone of the Bass Islands Formation. The gamma ray log is unresponsive through the Bass Islands Formation and across the transition into the overlying Bois Blanc Formation. As such, the formation pick is only identifiable in core. The Bass Island Formation is located between 156.91 m (top) and 185.17. m (bottom) with a total thickness of 28.2 m. Refer to photographs B-5 and B-6 of Appendix B for representative photographs of the Bass Islands Formation and its contact with the Salina G Unit.

Salina Group

Salina G Unit: The Salina G Unit is the uppermost formation of the Salina Group. Within SB_BH02, the G Unit predominantly consists of very fine-grained, grey argillaceous dolostone, and dolomitic shale with vugs and moderate-abundant white-grey anhydrite/gypsum veins and layers. Some tan-brown argillaceous dolostone layers are observed. The top of the Salina G Unit is a reliable pick (Armstrong and Carter 2010) and can be identified both in core and geophysical logs. In core, the top is picked at the upper contact of two uppermost layers of shaly dolostone/dolomitic shale separated by anhydritic dolostone, which corresponds to a slightly elevated response in the natural gamma log. Regionally, this pick is just under 7 metres above the top of the F Unit. The Salina G Unit is interpreted between 185.73 m (top) and 192.55 m (bottom) with a total thickness of 6.82 m. Refer to photographs B-6 and B-7 of Appendix B for representative photographs of the Salina G Unit and its contact with the Salina F Unit.

Salina F Unit: The Salina F Unit consists predominantly of nodular and anhydritic, dark green dolomitic shale with subordinate slightly bituminous tan-brown dolostones with red staining and cm thick gypsum layers and veins. Anhydrite nodules are pink/orange in color and range from 1-10 cm in diameter. The top of F Unit can be picked in both core and geophysical logs. In core, the top is placed at a sharp transition from tan-brown dolomitic shale to grey-green dolomitic shale with increasing anhydrite nodules/gypsum veins, consistent with the criteria identified in Armstrong and Carter (2010). In geophysical logs, the top of the F Unit is picked at the corresponding increase in natural gamma intensity reflecting a higher shale content in the rock. The Salina F Unit is the

thickest unit (45.58 m) within the Salina Group in BH02 extending from 192.55 m (top) to 238.13 m (bottom). Refer to photographs B-8 and B-9 of Appendix B for representative photographs of the Salina F Unit and its contact with the Salina E Unit.

Salina E Unit: The Salina E Unit consists of interbedded, laminated to massive tan dolostone, light/pale grey-green argillaceous dolostone to dark green laminated to massive dolomitic shale with white anhydrite/gypsum veins that transitions with depth to brecciated dolostone with anhydrite. Minor bituminous layering is also observed in the upper 10 meters of the E Unit. The top of the E Unit can be picked in core and geophysical logs. In geophysical logs, the top is picked at the sharp increase in the natural gamma intensity at the contact. In core, this is reflected by sharp contact of tan/brown dolostone with underlying greenish-grey shaly dolostone immediately below a 5 cm thick gypsum layer. The Salina E Unit is interpreted between 238.31 m (top) to 263.64 m (bottom) with a total thickness of 25.51 m. Refer to photographs B-9 and B-10 of Appendix B for representative photographs of the Salina E Unit and its contact with the Salina D Unit.

Salina D Unit: The Salina D Unit consists of tan-grey slightly brecciated/fragmented, shaly dolostone with abundant gypsum layers/ veins throughout and a bluish anhydrite matrix (anhydritic dolostone). Brecciated beds have pebble size angular to sub-rounded dolostone clasts. The top of the Salina D is picked in both core and geophysical logs. In core, the top is picked at the downward gradational change from dolostone to blue grey anhydritic dolostone. In geophysical logs, the top is picked at the decrease in the gamma log, coinciding with an increase in the neutron and density logs. Based on the formation picks, the Salina D Unit occurs between 263.64 m (top) and 266.4 m (bottom) with a thickness of 2.76 m. Refer to photographs B-10 and B-11 of Appendix B for representative photographs of the Salina D Unit and its contact with the Salina C Unit.

Salina C Unit: The Salina C Unit consists of an upper bed of stained red and green dolomitic shale, with anhydrite and gypsum nodules/veins, and a lower bed of grey-blue anhydritic, dolomitic shale with minor blue brecciated anhydrite clasts. The Salina C Unit can be readily picked in core and geophysical logs. In core, the top of the C Unit is a gradational transition from blue-grey to brown anhydritic dolostone of the overlying D Unit to grey shale. In geophysical logs, the top is picked at the increase of natural gamma reflecting an increase in shale content. Based on the formation picks, the Salina C Unit occurs between 266.4 m (top) and 283.07m (bottom) for a thickness of 16.67 m. Refer to photographs B-11 and B-12 of Appendix B for representative photographs of the Salina C Unit and its contact with the Salina B Unit.

Salina B Unit: The Salina B Unit consists of argillaceous dolostone grading downwards to dolostone near base of unit. Dolomitic shale is grey-green with abundant gypsum/anhydrite veins, layers and nodules. It is locally brecciated with dolostone clasts. Dolostone is tan-brown with gypsum nodules and dark brown bituminous shale laminae. The B Unit pick is supported in both core and geophysical logs. In core, the top is confidently placed at the start of the thin, brown, brecciated anhydritic dolostone layer (1.1 m B Unit Marker Bed) and brecciated dolostone below red-green shale as B Salt is absent due to dissolution. In geophysical logs, this pick is partially supportive and occurs at a decrease in gamma ray intensity corresponding to the transition from shale of the C Unit to the anhydritic brecciated dolostone of the Marker Bed. The Salina B Unit occurs from 283.07 m (top) and 290.6 m (bottom) resulting in a thickness of 7.53 m. Refer to photographs B-12 and B-13 of Appendix B for representative photographs of the Salina B Unit and its contact with the Salina B Equivalent Unit.

Salina B Equivalent Unit: The B Equivalent Unit is an informal unit that consists of brecciated brown to grey-green argillaceous dolostone with white anhydrite/gypsum veins, patches and nodules. It is interpreted to be debris from sub-surface dissolution of halite of the B Salt. In the absence of the salt beds, a definitive pick separating the Salina B Unit from B Equivalent is nearly impossible both in drill core and geophysical logs. In SB_BH02, the top of the Salina B Equivalent is placed at approximately 6 m below the top of the Salina B Unit. This is based on expected

thicknesses from other boreholes in the study area (including SB_BH01). The Salina B Equivalent occurs from 290.6 m (top) to 304.99 m (bottom) resulting in a thickness of 14.53 m. Refer to photographs B-13 to B-15 of Appendix B for representative photographs of the Salina B Equivalent Unit and its contact with the Salina B Anhydrite Unit.

Salina B Anhydrite Unit: The Salina B Anhydrite Unit consists of interbedded dark green, grey-blue, brown, anhydritic dolomitic shale with abundant gypsum veins and thin layers/stringers and pure anhydrite. The unit has an anhydritic/gypsum matrix. The top is picked in both core and geophysical logs. In core, the top is picked at the change from dolostone to thinly interbedded anhydrite and dolostone. In geophysical logs, the top is picked at the lowest natural gamma response following a gradual decline in gamma ray intensity, with coincident increase in neutron and density log response. The Salina B Anhydrite occurs from 304.99 m (top) and 306.97 m (bottom) resulting in a thickness of 1.98 m. Refer to photographs B-15 and B-16 of Appendix B for representative photographs of the Salina B Anhydrite Unit and its contact with the Salina A-2 Carbonate Unit.

Salina A-2 Unit Carbonate: The Salina A-2 Unit Carbonate consists of wavy laminated argillaceous dolostone and grey limestone and dolostone. Dolostone is tan to grey, very fine- to fine-grained, laminated to massive, locally with dark brown to black bituminous laminae with strong sulphur odour in places. Argillaceous dolostone is grey-brown with trace of anhydrite/gypsum and has sulphurous odour when broken for sampling. Dolomitic shale is brown to dark grey, and locally contains dolostone clasts and distorted bedding. This contact is easily picked in geophysical logs and core. In geophysical logs, the top is picked at the slight increase in natural gamma compared to the overlying Salina B. In core, it has a sharp contact at the change from anhydrite of the B Anhydrite to brown tan laminated dolostones of the A-2 Carbonate. The A-2 Carbonate occurs from 306.97 m (top) and 332.24 m (bottom) resulting in a thickness of 25.27 m. Refer to photographs B-16 and B-17 of Appendix B for representative photographs of the Salina A-2 Carbonate Unit and its contact with the underlying Salina A-2 Anhydrite Unit.

Salina A-2 Unit Anhydrite: The Salina A-2 Unit Anhydrite consists of a light/pale grey-blue, very fine- grained, thinly bedded to laminated anhydrite and anhydritic dolostone and nodular anhydrite. Laminations are planar to wavy laminated. Much of the bedding occurs as pure anhydrite. The Salina A-2 Anhydrite can be picked in core and geophysical logs. In core, the contact is placed at the semi-gradational change from dark-grey dolostone of the A-2 Unit Carbonate with underlying thinly interlaminated blue-grey anhydrite and brown dolostone. In geophysical logs, the contact is placed at an increase in neutron response (typical of anhydrite beds) and a decrease in the natural gamma. The A-2 Anhydrite occurs from 332.24 m (top) and 337.58 m (bottom) resulting in a thickness of 5.54 m. Refer to photographs B-17 and B-18 of Appendix B for representative photographs of the Salina A-2 Anhydrite and its contact with the Salina A-1 Unit Carbonate.

Salina A-1 Unit Carbonate: The Salina A-1 Unit Carbonate consists of grey to tan-brown, slightly fossiliferous (crinoids and corals), very porous, karstic, argillaceous dolostone and limestone with some abundant dark grey, petroliferous shale laminae. Millimetre to centimetre-scale vugs increase in frequency with depth and are associated with moldic porosity. The A-1 Unit Carbonate contact is picked in core and geophysical logs. In core, the top is placed at the sharp transition from anhydrite to laminated dolostone. In geophysical logs, the contact is placed at the downward increase in gamma log and increase in neutron and density logs. The A-1 Carbonate is defined from 337.58 m (top) and 376.1 m (bottom) resulting in a thickness of 38.52 m. Refer to photographs B-18 and B-19 of Appendix B for representative photographs of the Salina A-1 Unit Carbonate and contact with the Salina A-1 Unit Evaporite.

Salina A-1 Unit Evaporite: The Salina A-1 Unit Evaporite consists of wavy to planar laminated blue-grey to tan anhydrite with minor dolomite content. The A-1 Evaporite contact is picked in geophysical logs and core. In geophysical logs, the contact is placed at the inflection point on the

downward decrease in the natural gamma curve marking the lithological change from dolostone of the A-1 Unit Carbonate to anhydrite of the A-1 Unit Evaporite. In core, this contact is gradational and coincides with a colour change from green- grey dolostone (A-1 Carbonate) to blue-grey anhydrite (A-1 Evaporite) The interpreted thickness of the A-1 Evaporite is 7.08m, starting from 376.1m to 383.18m. Refer to photographs B-19 and B-20 of Appendix B for representative photographs of the Salina A-1 Unit Evaporite and contact with the Salina A-0 Unit Carbonate

Salina A-0 Unit Carbonate: The Salina A-0 Unit Carbonate is the lowermost formation of the Salina Group and consists of very fine-grained, thinly laminated, petroliferous dolostone with black bituminous laminae. The A-0 Unit Carbonate contact is gradational in nature and can be picked both in core and geophysical logs. In core, the contact is picked at the transition from dominantly anhydrite of the Salina A-1 Unit Evaporite to tan-brown, laminated dolostone of the Salina A-0 Carbonate. In geophysical logs, this contact is reflected by a slight downward increase in the natural gamma from anhydrite to dolostone. The Salina A-0 Unit Carbonate has an interpreted thickness of 3.66m, with its top at 383.18m and its base at 386.84. Refer to photographs B-20 and B-21 of Appendix B for representative photographs of the Salina A-0 Unit Carbonate and contact with the Guelph Formation.

Guelph Formation: The Guelph Formation in SB_BH02 consists of brown-grey brecciated, karstic/vuggy medium-grained dolostone rubble with sucrosic texture. A wavy laminated, dark grey dolostone bed (marker bed) occurs in the middle of the formation. In core, the top of the Guelph Formation is placed at a sharp transition from laminated brown/tan dolostone to brown vuggy and sucrosic dolostone rubble. In geophysical logs, the top of the Guelph Formation is marked as a minor decrease in the natural gamma log and minor increase in the neutron log, reflecting decreased shale content and increased porosity. The Guelph Formation has full thickness of 5.02m, with its top starting at 386.84 m and the bottom at 391.86 m. Refer to photographs B-21 to B-22 of Appendix B for representative photographs of the Guelph Formation and its contact with the Goat Island Formation.

Goat Island Formation: The Goat Island Formation consists of a light-medium grey, very fine-grained, mottled to speckled, massive, hard, argillaceous dolostone with stylolites, and locally with abundant chert and some dark grey, irregular, bituminous laminae and trace pyrite. In core, the top is picked at the sharp transition from vuggy brown porous dolostone to very fine-grained, light/pale grey argillaceous dolostone. In geophysical logs, the top of the Goat Island Formation is picked at the inflection point of a strong downward increase in natural gamma ray response. The Goat Island Formation occurs between 391.86m (top) to 408 m (bottom) with a total thickness of 16.14 m. Refer to photographs B-22 to B-24 of Appendix B for representative photographs of the Goat Island Formation and its contact with the Gasport Formation.

Gasport Formation: The Gasport Formation consists of a mottled grey tan, blue-grey, sparsely fossiliferous dolostone with minor laminations, sparse stylolites and pinhole porosity. In core, the top of the Gasport Formation was placed at a gradational change to a lighter grey, coarser-grained, more porous dolostone compared to that in the Goat Island Formation. In geophysical logs, the contact is picked at the subtle decrease in natural gamma, which displays as consistent low gamma response below the higher natural gamma response of the Goat Island Formation, coincident with increases in neutron and density logs. The Gasport Formation is interpreted between 408 m (top) and 415.3 m (bottom) with a total thickness of 7.3 m. Refer to photographs B-24 and B-25 of Appendix B for representative photographs of the Guelph Formation and its contact with the Lions Head Formation.

Lions Head Formation: The Lions Head Formation consists of a mottled light tan to grey-brown, fine-grained, wavy laminated, argillaceous limestone. Limestone of the Lions Head Formation is sparsely fossiliferous with trace shale and siltstone clasts, and rare stylolites. The top of the Lions Head Formation has been identified in geophysical logs by an increase in argillaceous content

represented by a gradational downward increase in natural gamma response of massive grey dolo-wackestone with shaly partings. In core, the top of the Lions Head Formation was placed at a sharp increase in brown-grey shale content associated with a finer grain size and a decrease in fossil abundance, and the base of a thin interval of large angular clasts of dolostone. The Lions Head Formation occurs between 415.3 m (top) to 418.1 m (bottom) with a total thickness of 2.8 m. Refer to photographs B-25 and B-26 of Appendix B for representative photographs of the Lions Head Formation and its contact with the Goat Fossil Hill Formation.

Fossil Hill Formation: The Fossil Hill Formation consists of a grey to tan, fossiliferous, dolomitic limestone (packstone and grainstone) with common shale partings and weak wispy stylolites. The top of the Fossil Hill Formation is gradational. It is placed at the start of massive grey dolo-wackestone with shaley partings. This is supported in geophysical logs by a small and gradational decrease in the gamma log corresponding to an inflection point of increase in the neutron log. The Fossil Hill Formation occurs between 418.1. m (top) to 419.28 m (bottom) with a total thickness of 1.18 m. Refer to photographs B-26 and B-27 of Appendix B for representative photographs of the Fossil Hill Formation and its contact with the Cabot Head Formation.

Cabot Head Formation: The Cabot Head Formation consists of mottled to uniform, red and dark green calcareous shale with occasional staining. There are moderate to abundant brachiopods and trace amounts of trilobites. It grades with depth to interbedded shale and limestone. The shale beds sometimes have mud cracks and the limestone beds are mostly grey, coarse-grained dolomitic wacke to packstones with limestone clasts. The Cabot Head Formation top can be readily picked in core and geophysical logs. In core, the contact is picked at the change from grey dolo-wackestone of the Fossil Hill Formation to a massive grey-green shale. In geophysical logs, this contact is marked by a sharp increase in the gamma ray intensity and a sharp decrease in the neutron intensity. The Cabot Head Formation occurs between 419.28 m (top) to 440.1 m (bottom) with a total thickness of 20.82 m. Refer to photographs B-27 to B-28 of Appendix B for representative photographs of the Cabot Head Formation and its contact with the Manitoulin Formation.

Manitoulin Formation: The Manitoulin Formation consists of mottled, grey to brown, argillaceous, fossiliferous, cherty dolostones, with minor limestones and calcareous green shale interbeds. Fossils consist predominantly of shell fragments with trace to moderate amounts of coral. This is a gradational contact easily picked in core and in geophysical logs. In core, the contact occurs at the base of lowermost significant (> 10 cm) green shale bed in the Cabot Head Formation changing to grey cherty dolostone. In geophysical logs, the top is picked at the drop in natural gamma and increase in neutron log. The Manitoulin Formation ranges from 440.1 m to 449.25 m giving it an interpreted thickness of 9.15 m. Refer to photographs B-28 to B-29 of Appendix B for representative photographs of the Manitoulin Formation and its contact with the Queenston Formation.

3.2.1.4 Upper Ordovician Rocks

Queenston Formation: The Queenston Formation is the uppermost formation of the Upper Ordovician. The Queenston Formation consists of red to maroon, calcareous to non-calcareous shale, with subordinate amounts of grey-green shale and grey to brown dolostone, limestone and siltstone. Gypsum and anhydrite nodules are locally common. From the top through the middle of the formation, the red to maroon calcareous shale is interbedded with the grey-green shale beds. The latter have grey-green limestone interbeds within them. The Queenston Formation top is an erosional unconformity with the overlying Silurian strata and can be consistently picked in Ontario using drill core and geophysical logs (Armstrong and Carter 2010). In core, the top is picked at a sharp change from grey cherty dolostone to red-green interbedded shale. In geophysical logs, this change is reflected by a sharp increase in natural gamma and a sharp decrease in neutron. The

interpreted thickness of the Queenston Formation is 85.45 meters from 449.25-534.7 m depth. Refer to photographs B-29 to B-31 of Appendix B for representative photographs of the Queenston Formation and its contact with the Georgian Bay Formation.

Georgian Bay Formation: The Georgian Bay Formation consists of fissile, greenish to blue-grey shale with subordinate interbeds of fossiliferous limestone, and grey calcareous siltstone and sandstone beds. It contains trace anhydrite and gypsum nodules. Fossiliferous limestone beds decrease in abundance with depth from moderate to trace. Fossils include brachiopods, bivalves, crinoids and cephalopods. Pyritized fossil fragments were also observed in core. Petroliferous and sulphurous odour occurs towards the bottom of the formation with minor oil staining. The top of the Georgian Bay Formation is reliably identified in geophysical logs and supported by drill core observations. In core, the top of the Georgian Bay is picked at the base of the lowermost significant low-porosity limestone/siltstone bed. In geophysical logs, the top is picked at the inflection point of the increase in the natural gamma response and decrease in the neutron log. The interpreted thickness of the Georgian Bay Formation is 86.16 meters ranging from 534.7-620.86 m. Refer to photographs B-31 to B-33 of Appendix B for representative photographs of the Georgian Bay Formation and its contact with the Blue Mountain Formation.

Blue Mountain Formation: The Blue Mountain Formation consists of fissile, blue-grey, non-calcareous shale interbedded with minor cm-thick grey siltstone and limestone beds. The shale transitions to a grey to very dark grey variety with depth. Crinoids, brachiopods, shell fragments and trace fossils are abundant. The shale has petroliferous odour. Calcite-infilled fractures with pyrite mineralization are observed throughout. The top of the Blue Mountain Formation is gradational and is very difficult to identify reliably in core. The contact is placed at the bottom of the last significant (>10 cm) calcareous limestone bed near a subtle increase in core disking. In geophysical logs, this change is reflected as the last significant dip/decrease in gamma preceding less variable gamma log due to thinner and less frequent limestone beds of the Blue Mountain Formation. The interpreted thickness of the Blue Mountain Formation is 48.83 meters ranging from 620.86-669.69 m Refer to photographs B-33 to B-35 of Appendix B for representative photographs of the Blue Mountain Formation and its contact with the Cobourg Formation (Collingwood member).

Cobourg Formation (Collingwood Member): The Collingwood Member of the Cobourg Formation consists of dark brown-grey to black, calcareous shale interbedded with grey fossiliferous limestone. The Collingwood Member is much harder than the overlying Blue Mountain Formation and is less prone to core disking. Fossils include cephalopods, gastropods and corals. The abundance of fossiliferous limestone beds increases with depth. The contact is sharp and can be picked in both core and geophysical logs. In core, the top is picked at the start of the brownish grey limestone beds. In geophysical logs, it is picked at a sharp decrease in natural gamma intensity and an increase in the neutron response. The Cobourg Formation (Collingwood Member) has an interpreted thickness of 7.85 m ranging from 669.69-677.54 m. Refer to photographs B-35 to B-37 of Appendix B for representative photographs of the Collingwood member and its contact with the lower member of the Cobourg Formation.

Cobourg Formation (lower member): The lower portion of the Cobourg Formation consists of mottled, wavy laminated light/pale to dark grey to brownish grey, very fine- to coarse-grained argillaceous limestone deposited as packstones and grainstones. Fossils include brachiopods, crinoids and shell fragments. This lower member has petroliferous odour with traces of crude oil seeping from hairline fractures in the rock. In core, the top of the lower Cobourg Formation was sharp and was placed at the base of the lowermost significant (>10cm) dark grey-black shale bed of the Collingwood Member. This is reflected in the geophysical logs by a slight decrease in natural gamma and slight increase in neutron. Natural gamma response in the lower Cobourg is flatter compared to spikey/higher gamma response of the Collingwood Member. The lower Cobourg has an interpreted thickness of 38.83 m ranging from 677.54-716.37 m depth. Refer to photographs B-

37 and B-38 of Appendix B for representative photographs of the lower member of the Cobourg Formation and its contact with the Sherman Fall Formation.

Sherman Fall Formation: The Sherman Fall Formation consists of pale/light to medium grey, medium- to coarse-grained transitional to medium-grained with depth, argillaceous limestone. Coarse-grained beds are bioclastic and intraclastic grainstones. Fossils include brachiopods and other shell fragments. Grey-green, irregular shale laminae and beds are interbedded and interlaminated with the limestone beds, and increase in abundance with depth. The Sherman Fall Formation is locally mottled with depth and has intense petroliferous odour in the upper 5 meters. In core, the top is placed at the sharp contact between nodular argillaceous limestone and medium- to coarse-grained laminated and cross-bedded limestones. The upper part of the Sherman Fall Formation has lower gamma values than the lower Cobourg Formation. In geophysical logs, the contact is picked at the sharp decrease in the natural gamma. The Sherman Fall Formation has a thickness of 45.66 m from 716.37-762.03 m depth. Refer to photographs B-38 to B-40 of Appendix B for representative photographs of the Sherman Fall Formation and its contact with the Kirkfield Formation.

Kirkfield Formation: The Kirkfield Formation consists of grey to blue grey, fine- to medium-grained argillaceous, fossiliferous limestone interbedded with dark grey-green irregular to planar-bedded shale and limestone fragments/clasts. Fossils consist mainly of shell fragments including brachiopods, bivalves and crinoids with moderate petroliferous odour throughout. The Kirkfield Formation contact is readily picked in core and geophysical logs (Armstrong and Carter 2010). In core, the contact was placed at the top of a 0.35 m thick bioclastic limestone bed, below which a gradual decrease in shale content was observed. In geophysical logs, this contact is supported/reflected by a subtle decrease in the natural gamma response. The Kirkfield Formation has a thickness of 43.6 m ranging from 762.03-805.63 m depth. Refer to photographs B-40 to B-42 of Appendix B for representative photographs of the Kirkfield Formation and its contact with the Coboconk Formation.

Coboconk Formation: The Coboconk Formation consists of a grey to brown, fine-grained, fossiliferous and bioturbated limestone with irregular bituminous shale laminations. The Coboconk Formation has visible oil weeping from porous intervals and a trace to strong petroliferous odour. Two thin dark green clay (volcanic ash) marker beds are observed in the Coboconk Formation. The first marker bed is 0.08m thick and is found approximately one meter from the top of the Coboconk; the second volcanic ash layer (marker bed), is 0.05 m thick and is found approximately 5 meters into the Coboconk Formation. The top of the Coboconk can be readily picked in core and geophysical logs. In core, the top of the Coboconk Formation has been picked as a sharp transition from interbedded bluish-grey limestone and shale of the Kirkfield Formation to cleaner, light/pale grey bioturbated limestone of the Coboconk Formation. In geophysical logs, the contact is picked at a decrease in natural gamma and increase in neutron response reflecting a decrease in shale content in the Coboconk Formation. The Coboconk Formation has a thickness of 21.08 m ranging from 805.63-826.71 m depth. Refer to photographs B-42 to B-44 of Appendix B for representative photographs of the Coboconk Formation and its contact with the Gull River Formation.

Gull River Formation: The Gull River Formation consists of grey-blue, fine- to medium-grained, locally bioturbated and fossiliferous limestone, with brown to black bituminous shale laminae and beds. The Gull River Formation is petroliferous, with visible oil weeping from porous intervals and a trace to strong petroliferous odour. The formation top is readily picked in core and geophysical logs. In core, top of the Gull River Formation was picked at a sharp basal contact of grainstone bed with underlying very argillaceous limestone. In geophysical logs, the Gull River Formation is picked at the top of a downward increase in the natural gamma response with corresponding upward decrease in gamma ray intensity compared to the logs in the overlying Coboconk Formation. The Gull River Formation has a thickness of 54.87 m ranging from 826.71-881.58 m depth. Refer to

photographs B-44 to B-46 of Appendix B for representative photographs of the Gull River Formation and its contact with the underlying Shadow Lake Formation.

Shadow Lake Formation: The Shadow Lake Formation consists of an interbedded grey to light/pale green to grey-brown glauconitic siltstone and sandstone with minor grey-green sandy shale and trace pyrite mineralization. A few thick, fining-upward, immature “dirty” clasts are observed (moderately sorted with occasional feldspar pebbles). Sandstone beds comprise the basal portion of this formation, above the unconformity with the Precambrian basement. The top of the Shadow Lake Formation is readily identified in geophysical logs and in drill core. In geophysical logs, the Shadow Lake Formation is picked at the top of a large increase in natural gamma and decrease in neutron coinciding with the change from carbonates (Gull River Formation) to more porous glauconitic silty/sandstone (Shadow Lake Formation), as visible in core. The Shadow Lake Formation has an interpreted thickness of 5.35 m ranging from 881.58-886.93 m depth. Refer to photographs B-49 to B-47 of Appendix B for representative photographs of the Shadow Lake Formation and its contact with the Precambrian basement.

3.2.1.5 Precambrian Rocks

Precambrian basement: The Precambrian basement unconformably underlies the Paleozoic succession of southwestern Ontario. In SB_BH02, the Precambrian rocks consist of a medium- to coarse-grained, syenitic to granitic gneiss with minor schist. The pink to white felsic banding is commonly potassium feldspar-dominated with plagioclase, biotite and quartz. Darker mafic bands are dominated by biotite and amphibole. There is a strong foliation (gneissosity) throughout. The Precambrian top is easily picked in both geophysical logs and drill core. However, the contact may be difficult to pick consistently in geophysical logs due to the presence of weathered fragments of the Precambrian and the presence of secondary minerals (such as glauconite) in the overlying sedimentary strata, making a drill core pick more reliable (Armstrong and Carter 2010). The Precambrian basement’s top is picked at the sharp unconformable contact between sedimentary and metamorphic crystalline rock. In core, this contact is reflected by the change in character from glauconitic silty/sandstone of the Shadow Lake Formation to pink and banded gneiss (Precambrian). In geophysical logs, the top is picked at the large increase in the K-40 gamma response and increase in neutron log. The drilled portion of the Precambrian basement in SB_BH02 is 20.51 m ranging in depth from 886.93-900.57 m marking the end of the borehole. Refer to photographs B-47 and B-48 of Appendix B for representative photographs of the Precambrian basement.

3.2.1.6 Geophysical Characteristics for Stratigraphic Formations and Members

The following section summarizes the geophysical characteristics for each of the stratigraphic formations and members interpreted in SB_BH02. For this analysis, geophysical log data acquired by Geofirma (2023a) were each resampled along the length of the borehole at 5 cm increments. Because the natural gamma ray log is reported in counts per second, the range of counts can vary from borehole to borehole based on the logging speed, differences in calibration and well conditions (Shier, 2004). To account for variability between boreholes intersecting the same formations, normalization is applied to the natural gamma ray logs to rescale the values over a consistent range. For SB_BH02, the 5^{th} percentile and the 95^{th} percentile of the gamma ray values are scaled between the range of 10 and 100 cps. The use of the percentiles ensures that any outlier values do not impact the normalization. Lastly, z-score outlier removal was applied to all geophysical log data to filter erroneous data where values exceed 3 standard deviations from the mean value. Erroneous data can result from measurement error (e.g. tool and sensor issues) or from borehole conditions (e.g. washouts). It is important to remove such large outliers from the data as they influence statistical analyses.

Figure 5 presents a group of geophysical well logs showing the variability in log responses along the length of SB_BH02 relative to the position of the interpreted formations and members. P-wave velocity and normal resistivity logs in the upper ~200 m of SB_BH02 were clipped as they were measured through multiple layers of steel casing. The remaining logs were recorded before casings were installed. As a result, analysis of the neutron and density log responses for each formation presented below does not include the upper 80 m of the Devonian formations.

The natural gamma and spectral gamma ray logs show significant variability throughout the length of the borehole. Natural gamma values range from a few counts per second (cps) with the 95th percentile of 100 cps. The upper Ordovician Queenston, Georgian Bay and Blue Mountain formations display a uniformly high gamma ray response attributed to these formations being predominantly shale. Similarly, the potassium (K%), uranium (ppm) and thorium (ppm) logs show similar high response within these formations mainly attributed to the variable concentrations of the three dominant radioisotopes.

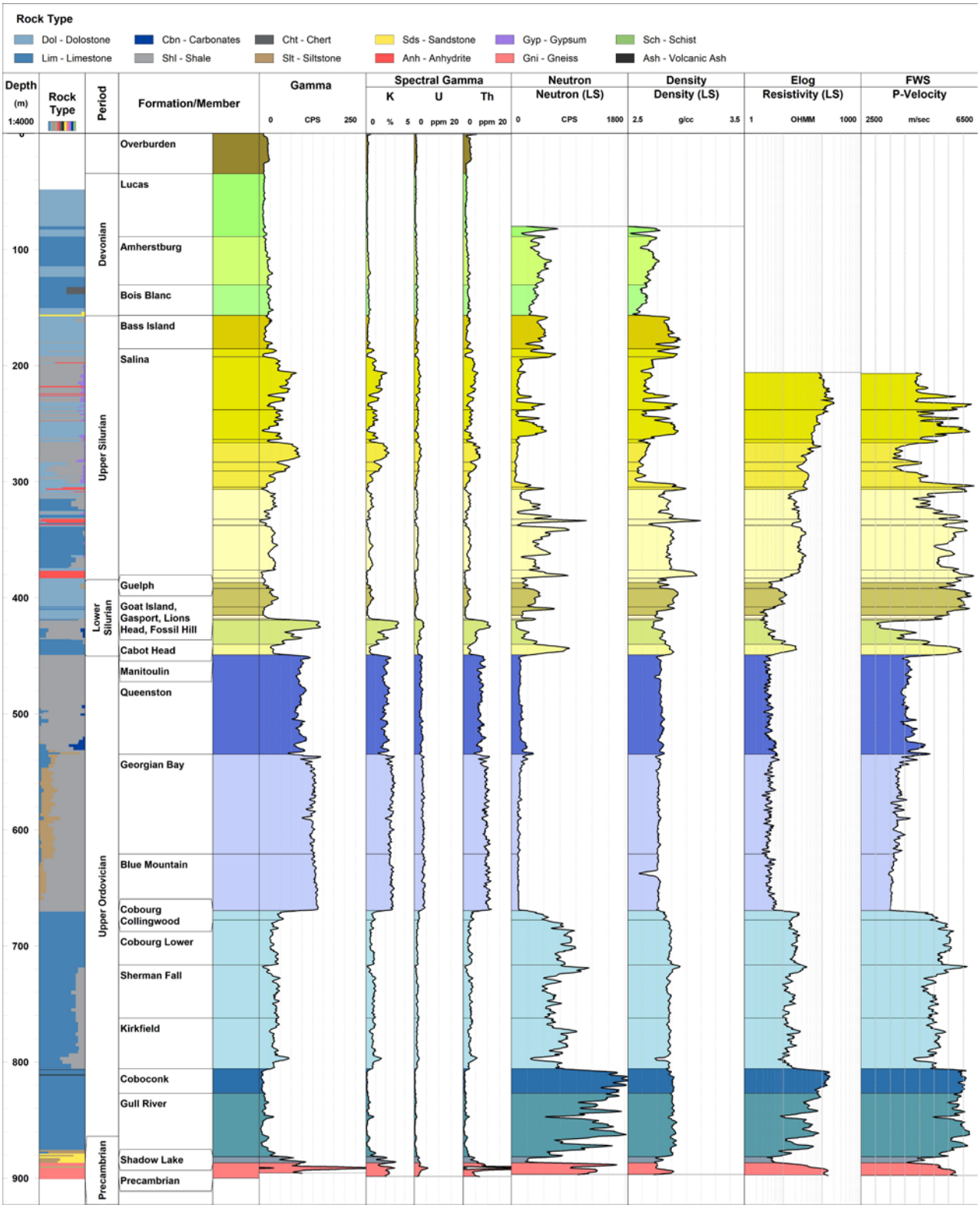


Figure 5. Geophysical well log showing natural gamma ray, spectral gamma (Potassium, Uranium and Thorium), long spaced neutron counts, mean gamma-gamma density, long spaced resistivity and compression P-wave velocity log. Formations and members are colour classified (colour legend is displayed in Table 1) and subdivided into age periods, Devonian, Silurian, Ordovician and Precambrian. The Salina formations are grouped

into the Salina Group. Lithology is presented as relative proportions for each measured interval (colour legend is displayed in Table 2). Depth scale is 1:4000. See Appendix C presenting figure at 1:500 scale.

It is apparent that the variability of natural gamma signature through the borehole is directly related to the variability in the shaliness qualitatively recorded through core logging. The sharp reduction in the gamma response at the base of the Blue Mountain Formation marks the sharp transition into the Cobourg (Collingwood member) which is predominantly limestone. The Cobourg Formation through to the Kirkfield Formation is relatively uniform in the natural gamma signature, as well as the neutron, density, resistivity and velocity logs. However, there are local variations in these log responses that can be attributed to variability in the amount of shale logged. The Coboconk and Gull River formations record among the lowest natural gamma response in the Upper Ordovician. These formations are dominated by fine-grained, fossiliferous and bioturbated limestones, and have very little shale present. The transition into the Shadow Lake Formation is marked by a sharp increase in natural gamma and a slight reduction in neutron, density, resistivity and velocity values. The increase in natural gamma is related to a change from Gull River Formation carbonates to more porous glauconitic siltstones and sandstones in the Shadow Lake Formation. Lastly, the Precambrian unit at the bottom of the borehole is marked by an increase in natural gamma, as well as an increase in neutron, density, velocity and resistivity making the sum of these geophysical signatures unique.

Boxplots presented in Figure 6 shows the distribution of geophysical log values for each formation or member from the base of the casing to the bottom of the borehole. Due to the installation of steel casing during drilling, geophysical log data is only presented up to the base of the steel casing. Each graph shows distribution of log values for the defined interval as the median value, bounded by the first and third quartiles (25% and 75%) and the minimum and maximum values (total range) for natural gamma (cps), neutron LS (long spaced; cps), rock density (g/cc), P-wave velocity (m/s) and resistivity (Ohm*m). The notch within the box represents the 95% confidence interval.

Lithology from the Salina Group is overall dominated by evaporites (carbonates+ anhydrite+ gypsum) but typically become more shale-rich in the upper Salina Group units (Armstrong and Carter 2010). This change in shale content can be observed in Figure 5 and Figure 6 where the natural gamma values show wide variability of counts through the Salina F Unit to the Salina B Unit. Figure 5 also presents the spectral analysis of the gamma rays and as a result are subdivided into the relative components of Potassium (%), Thorium (ppm) and Uranium (ppm) distributions along the borehole. From the Salina B Unit Equivalent to the Salina A-1 Evaporite Unit, and including the Guelph Formation, low magnitude natural gamma values are unresponsive with limited variability demonstrated by the narrow interquartile range. Low natural gamma counts are to be expected in a fully evaporitic and pure carbonate environment with limited shale content. The Goat Island Formation through to the Fossil Hill Formations present increasing natural gamma values and increasing variability within the Fossil Hill Formation itself. The Cabot Head Formation produces a strong increase in the natural gamma ray response as a result of a gradational increase in shale interbedded with limestones with depth.

Despite the weak natural gamma ray signature and general unresponsiveness in the Salina Group formations, the neutron, density and velocity logs (Vp) typically show a wide range of variability through these units, in some cases reflecting subtle changes in lithology as well as changes in borehole diameter. Into the Upper Ordovician succession, the Queenston, Georgian Bay and Blue Mountain formations show relatively stable and uniform neutron, density and velocity values reflecting their shale-dominated composition. There is an apparent correlation between the geophysical log response and the core observed lithology proportions as presented in Figure 5. In particular, the presence of sandstone and hard carbonate interbeds (upwards of 30% of the lithology over the logged interval) at the top and middle of the Georgian Bay Formation shows discrete inflections in the neutron, density and velocity signatures. The Cobourg, Sherman Fall and

Kirkfield formations similarly present uniform neutron, density and velocity signatures with an abrupt transition in these logs marked at the top boundary of the Cobourg Formation. The neutron log, and the Vp profiles and boxplots show a significant increase in their values at this boundary into the Cobourg, Sherman Fall and Kirkfield formations. Bulk density of the rock also increases in value moving from shales of the Blue Mountain Formation into the deeper formations dominated by argillaceous limestone.

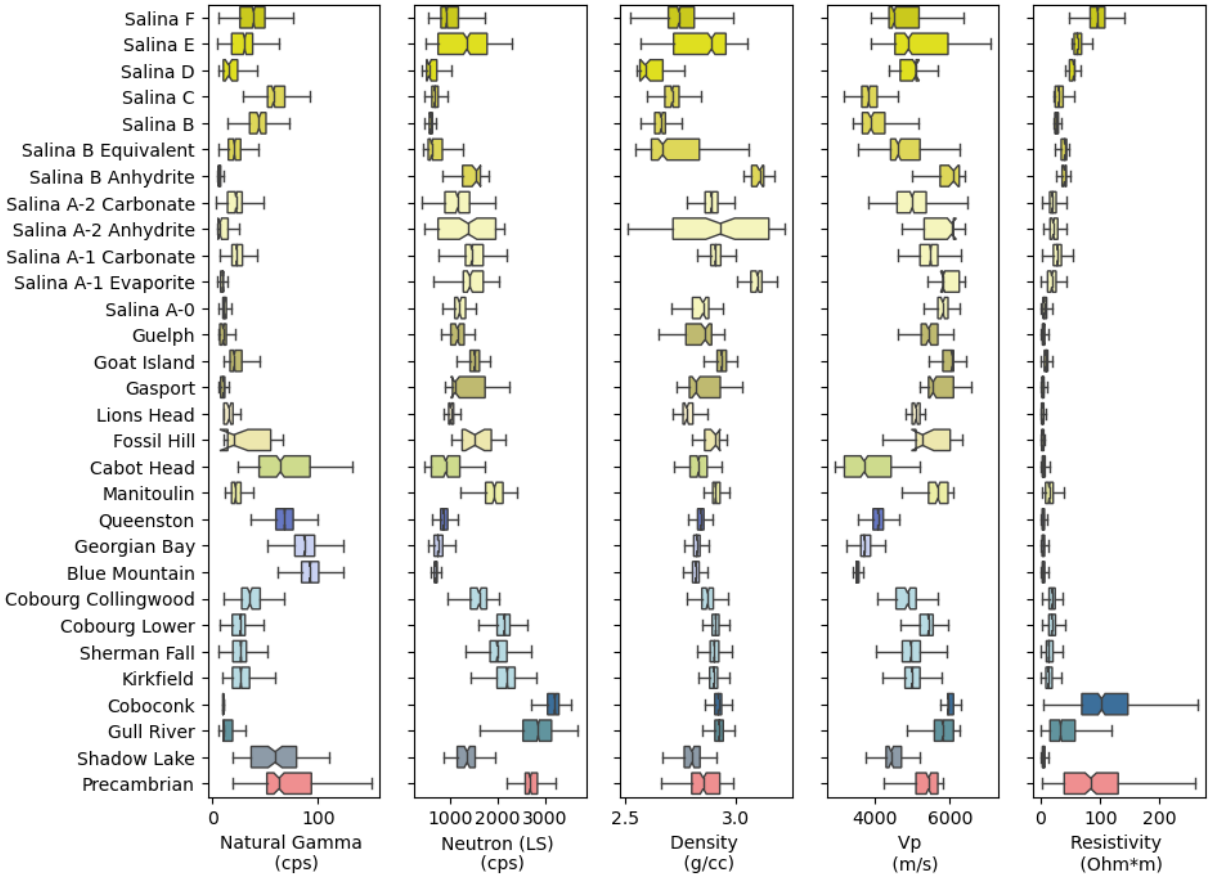


Figure 6. Natural Gamma (cps), Neutron LS (long spaced; cps), Density (g/cc), P-wave (m/s) and resistivity (Ohm*m) boxplots presenting distribution of values for each formation from the base of the casing to the bottom of the borehole. Boxplots present the statistical median, first and third quartiles (25% and 75%) and the minimum and maximum values (total range). The notch in the boxplot represents the 95% confidence interval.

Figure 7 presents a matrix scatterplot to explore relationships between the geophysical well log variables, such as natural gamma, neutron, Vp density and resistivity. Such a plot enables a large data set to be visualized on a single figure, and allows relationships to be visually identified and further explored through additional analysis. Data points are colour classified by formation or member using the colour scheme outlined in Table 1. Histograms are presented at the top of each column showing the distribution of log values recorded in each formation or member.

A few relationships become apparent upon visual inspection of Figure 7. First, the geophysical log values associated with Precambrian basement rock shows a distinct pattern that differs from the Paleozoic rocks. This is particularly evident in plots presenting gamma versus neutron, density versus neutron, as well as gamma versus P-wave velocity where the Precambrian values are separated from the Paleozoic data. There are also clear data anomalies presented in the plots as discrete peaks in the data set that trend away from the majority of the data points. These anomalies are clearest in the density versus gamma plot where there are anomalously low-density

values throughout the range of gamma values. These low densities, such at the middle and the base of the Blue Mountain Formation, and near the base of the Kirkfield Formation, are attributed to discrete zones of the borehole that co-locate with larger borehole diameter readings from collapses due to drilling. Despite these anomalies, it is apparent that log values of the Ordovician rocks (from the Queenston Formation to the Shadow Lake Formation) display strong trends between each of the variable pairs. These relationships and trends are further highlighted in Figure 8.

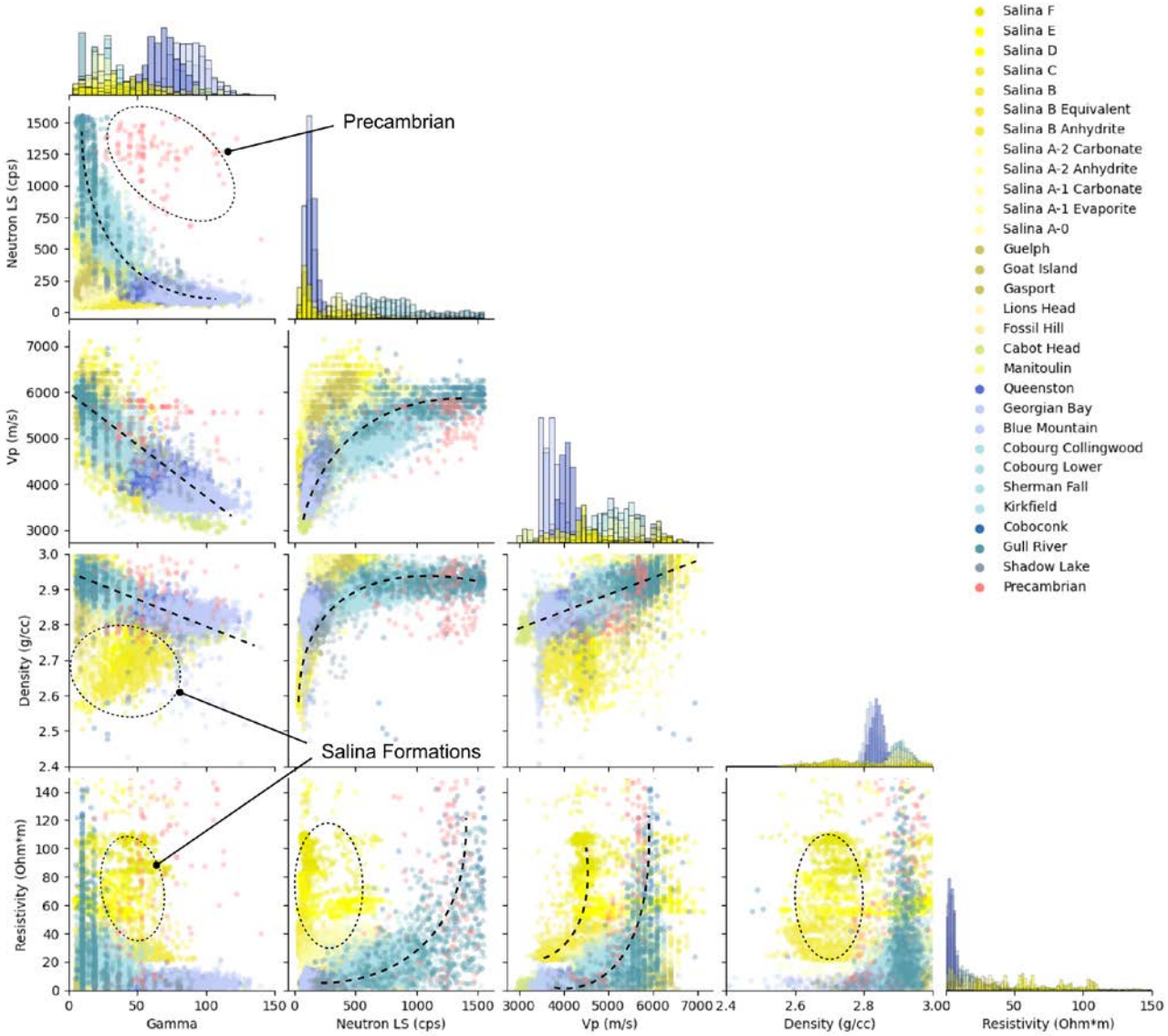


Figure 7. Grid of scatterplots presenting relationships and general trends between different geophysical logs (Gamma, Neutron, Vp, Density and Resistivity). Generalized trends are displayed as dashed lines. Data are colour classified by formation and member intervals shown in Table 1 and Figure 5.

The Upper Ordovician formations presented in Figure 8, dominated by shales and argillaceous limestones, show strong trends between the geophysical log variables comprising a mix of linear and non-linear correlations. The neutron log displays a non-linear correlation with each of the remaining log variables, with the neutron and gamma showing the tightest trend. As the natural gamma counts decrease, the neutron counts increase exponentially. However, as the neutron counts increase, the Vp values increase asymptotically to a maximum value of approximately 6000 m/s. The relationship between the gamma and Vp appears to be well-correlated, where a decrease

in the velocity of the rock results in an increase in natural gamma counts. Geologically, this trend is related to an increase in the shaliness of the bedrock. Similarly, when examining the distribution of colour classified data points along this trend, values transition from the higher velocity (and higher density) limestones to lower velocity shales of the Queenston, Georgian Bay and Blue Mountain formations. A similar trend can also be seen in the density versus velocity plot, which makes sense, as higher density rocks tend to also have higher velocities.

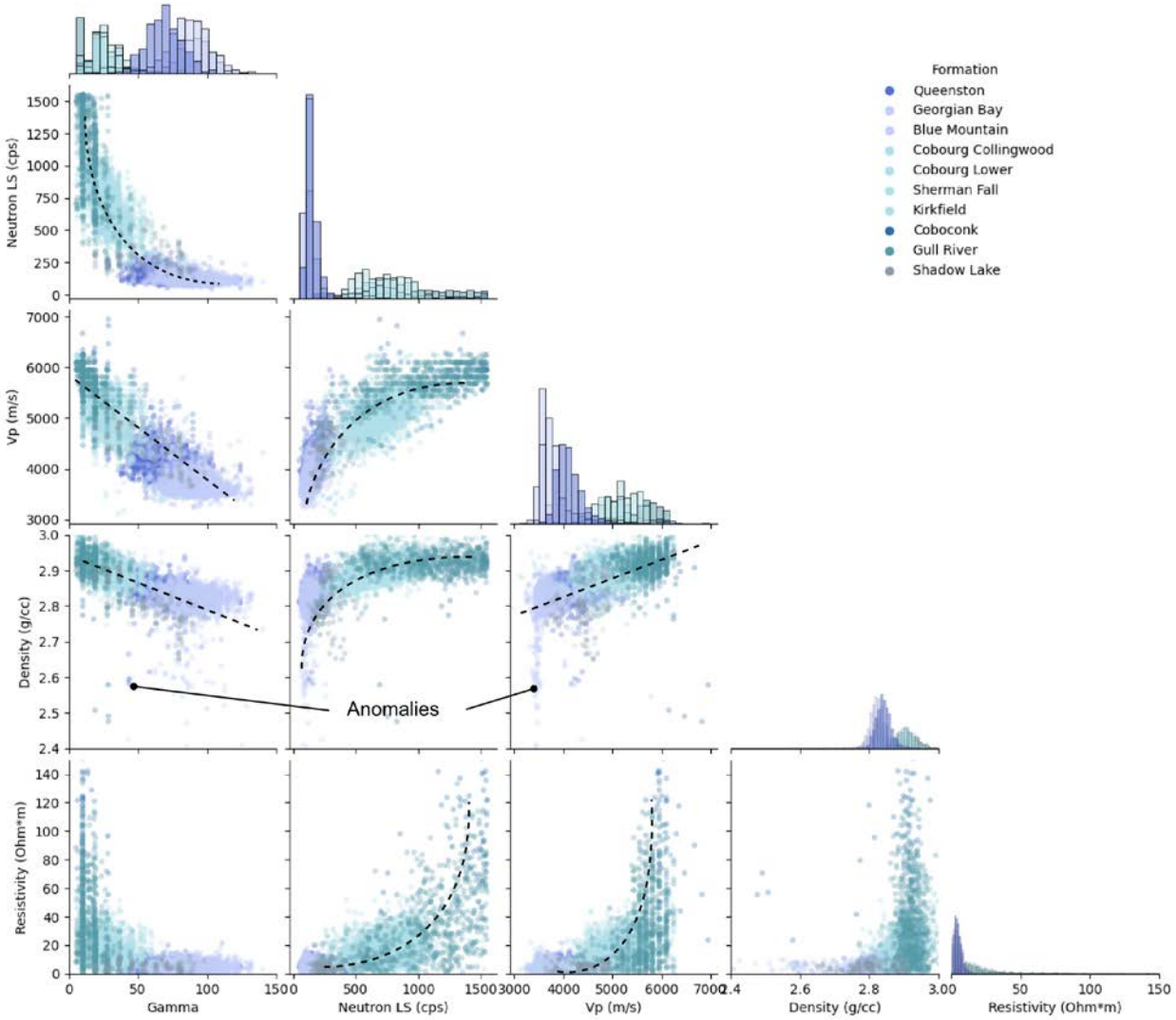


Figure 8. Grid of scatter plots for the Upper Ordovician formations presenting relationships and trends between different geophysical logs (Gamma, Neutron, Vp, Density and Resistivity). Data are colour classified by formation and member intervals shown in Table 1 and Figure 5.

Trends presented in Figure 7 and Figure 8 provide insight into how these log variables behave for the lithologies logged within the Paleozoic stratigraphy. Information in the OGSRL database from previously drilled boreholes in the region located around borehole SB_BH02 typically include a limited suite of geophysical logs, and, in some cases, only include natural gamma logs. As such, velocity, density, resistivity and neutron logs were not always recorded. Because the nearby boreholes are drilled through the same laterally continuous stratigraphic succession, it is assumed that these trends and correlations can be applied to predict log values in these regional boreholes. As an example, exploration of trends such as Vp versus gamma as shown in Figure 9 provides a

means to predict P-wave velocity in other regional boreholes where velocity logs are absent. However, it is apparent that some units and formations of the Silurian and Precambrian bedrock deviate from the linear trend line (see Figure 9a). Despite the deviation, the linear correlation model is well fitted with a correlation coefficient of 0.61 through the entire Paleozoic stratigraphy in SB_BH02. However, exploring the correlations strictly for the Ordovician Formations results in a more robust linear model with an R-squared correlation coefficient of 0.788 (see Figure 9b). Such inferences may be useful in the development of the 3D geological model for the region. The geophysical log trends and correlations are further explored in Section 3.2.2.1 in the context of the core logged lithologies in SB_BH02.



Figure 9. Correlation between P-wave velocity versus natural gamma. a) shows results for all formations logged in SB_BH02 with an R-squared coefficient of correlation of 0.610. b) presents results for Ordovician formations which significantly improving the correlation coefficient to 0.788.

3.2.2 Lithological Characteristics

Table 2 provides a summary of the rock types that were logged in SB_BH02 (Geofirma 2022a). A total of 12 rock types were logged, with the three most common rock types, limestone (36.7%), shale (35.0%) and dolostone (18.7%) comprising 90.4% of the cored interval. Other logged rock types generally only occurred as secondary components (e.g. chert, gypsum, siltstone), or were constrained to thin localized intervals of the borehole, such as sandstone in the Shadow Lake Formation and gneiss in the Precambrian basement rock. Thin ash layers logged in the Coboconk Formation are recognized as an occurrence of a regionally-persistent bentonite-rich marker beds deposited throughout the Appalachian and Michigan basins during episodic volcanic activity associated with the end of the Taconic Orogeny on the southeastern margin of Laurentia, approximately 454 million years ago (e.g. Huff et al. 1992, Kolata et al. 1998).

Table 2: Summary of Logged Rock Types in SB_BH02

Colour Legend	Rock Type[2]	Length Logged (m)[1]	Percent Core Logged (%)
	Limestone (Lim)	312.68	36.70%
	Shale (Shl)	298.64	35.00%

	Dolostone (Dol)	159.24	18.70%
	Siltstone (Slt)	32.27	3.80%
	Anhydrite (Anh)	14.44	1.70%
	Gneiss (Gni)	13.26	1.60%
	Gypsum (Gyp)	5.72	0.70%
	Sandstone (Sds)	4.77	0.60%
	Carbonate (Cbn) (undifferentiated)	3.31	0.40%
	Chert (Cht)	2.40	0.30%
	Schist (Sch)	0.38	<0.10%
	Volcanic Ash (Ash)	0.13	<0.1%

1. where multiple rock types were logged, the length of each rock type for that interval was calculated by multiplying the rock type percentage by the interval length
2. standard three-letter acronyms used for rock types

The distribution of the logged rock types along the length of SB_BH02 is presented in Figure 10. Detailed descriptions of the stratigraphic units, including lithology and formation top pick criteria, are provided in Section 3.2.1.

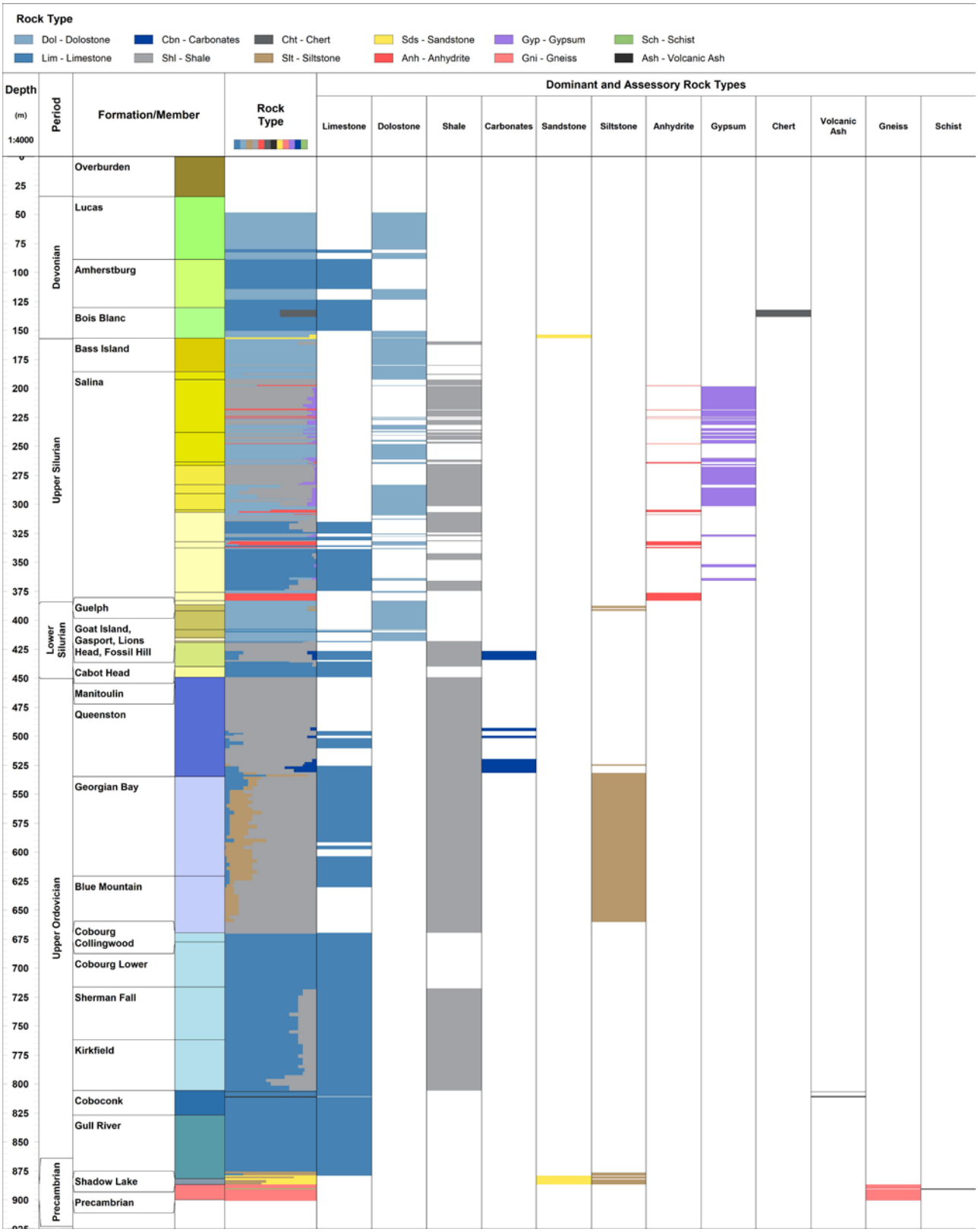


Figure 10: Summary of logged rock types for all formations and members in SB_BH02. The upper 36.94 m of the borehole was drilled using a cable tool rig resulting in bedrock chip samples. Rock types for the upper 36.94 m of the borehole were logged (separately) for the upper part of the Lucas Formation but not captured in acQuire, therefore, not showing in this figure.

3.2.2.1 Geophysical Characteristics of Logged Rock Types

This sub-section highlights how the geophysical well log values are related to the dominant core logged rock types. Boxplots presented in Figure 11 show the distribution of geophysical log values for the dominant rock types logged as primary lithology and recorded in SB_BH02 from the base of the casing to the bottom of the borehole. Similar to Section 3.2.1.6, due to the installation of steel casing during drilling, geophysical log data is only presented up to the base of the steel casing. Each graph shows the distribution of log values for the defined rock type as the median value, bounded by the first and third quartiles (25% and 75%) and the minimum and maximum values (total range) for natural gamma (cps), neutron LS (long spaced; cps), rock density (g/cc), P-wave velocity (m/s) and resistivity. The notch within the box represents the 95% confidence interval.

Results in Figure 11 show range in median values from different rock types for each geophysical log variable. The natural gamma shows that the shales (Shl) are elevated in magnitude relative to the other logged rock types. Although these shales have a high median value, they also present a wide interquartile range indicating significant variability in their response. This result is likely caused by the shales sometimes being interbedded with other rock types with a lower radiometric count rate, such as limestone and dolostone in the upper Salina formations. Conversely, the shales present low counts on the neutron log with low variability. Since low neutron counts are typically linked to the presence of hydrogen (water), it is assumed that this response is correlated to the presence of water in the bedrock as predominantly bound hydrogen in the mineral structure. The Vp log presents the shales with the lowest velocities relative to the other logged rock types. The majority of the other logged rock types, including dolostone (Dol) and limestone (Lim), show Vp values of low median values with a narrow standard deviation. The limestones and dolostones tend to show amongst the highest rock density and velocities compared to the other logged rock types. The main differentiation between these two rock types is based on the neutron counts which show the dolostones are depleted in neutron counts compared to the limestones.

The sandstones (Sds) are represented by a high median gamma value, and a moderate value for neutron, density and velocity. Each geophysical log distribution for the sandstones shows a high interquartile range, which can be attributed to this rock type being interbedded with shales of the Georgian Bay or Shadow Lake formations. In particular, the Shadow Lake Formation sandstones have higher gamma values due to secondary minerals (glauconite) and occasional feldspar pebbles from the underlying Precambrian basement rocks. This mixing of rock types tends to skew the geophysical log values away from what is expected for sandstones.

Gneiss and schist are logged over a few metres at the bottom of the borehole in the Precambrian bedrock. Although the gneiss is not part of the Paleozoic sequence, it does have a natural gamma signature that is comparable to the median values of the sandstones and shales. Schist, although only 0.38 m in SB_BH02, has natural gamma signatures that is greater that the median values of gneiss, sandstones and shales. Their natural gamma counts are high based mainly on the elevated potassium concentration, with relatively low levels of uranium and thorium concentrations observed from the spectral gamma logs (Figure 5).

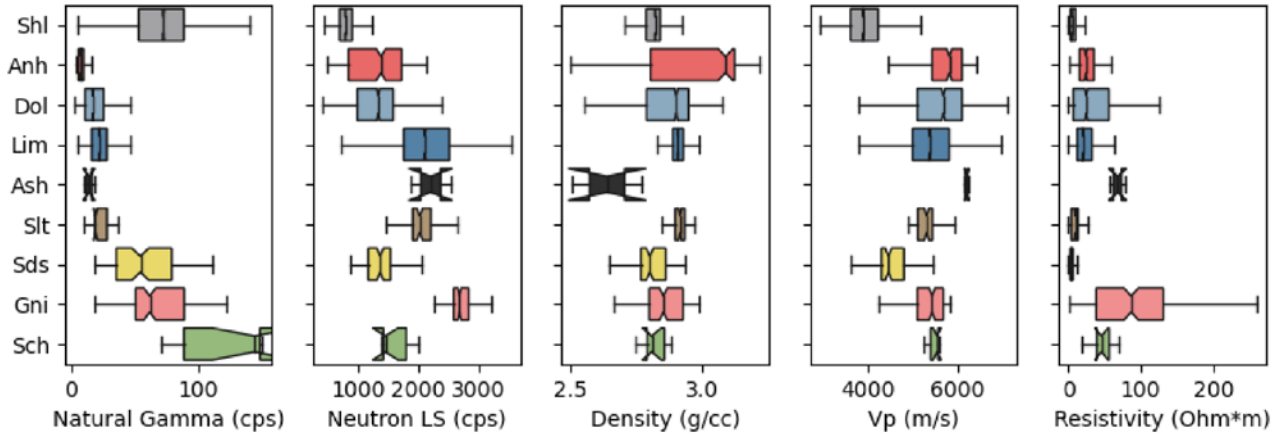


Figure 11. Natural Gamma (cps), Neutron LS (long spaced; cps), Density (g/cc), P-wave velocity (m/s) and long spaced resistivity (Ohm*m) boxplots presenting distribution of values for each rock type logged from the base of the casing to the bottom of the borehole. Boxplots present the statistical median, first and third quartiles (25% and 75%) and the minimum and maximum values (total range). The notch in the boxplot represents the 95% confidence interval. Color legend for lithologies shown in Table 2

To further explore geophysical characteristics of each logged rock type in SB_BH02, Figures 12 and 13 present matrix scatterplots highlighting the geophysical well logs for the entire logged section of the borehole and for the Ordovician formations, respectively. These plots are similar to those presented in Figure 7 and Figure 8, but here the data points are colour classified by the dominant rock type that was logged from drill core (colour legend is presented in Table 2). The diagonal component of matrix presents the histogram distribution of log values recorded in each rock type. As mentioned in Section 3.2.2, the combination of dolostone, limestone and shale represent 90.4% of the rock types logged, by total logged length, within SB_BH02.

As shown in Figures 12 and 13, it is clear that these three dominant rock types exhibit distinct geophysical characteristics that are useful in differentiating between them. It is apparent in most scatterplots that rock types typically grade from one to another along either linear or non-linear trends. The limestones and dolostones, for example, are separated from the shales mainly in scatterplots by the natural gamma counts where the shales are plotted on the right side and the limestones and dolostones are on the left. Its nearly impossible to differentiate between limestone and dolostone using borehole geophysical data alone. Although limited in occurrence in the borehole, the sandstones tend to spread across the full range of the trends which make their distinction challenging. On the other hand, geophysical relationships of the Precambrian basement rock show a distinct pattern that differs from all the Paleozoic rock types.

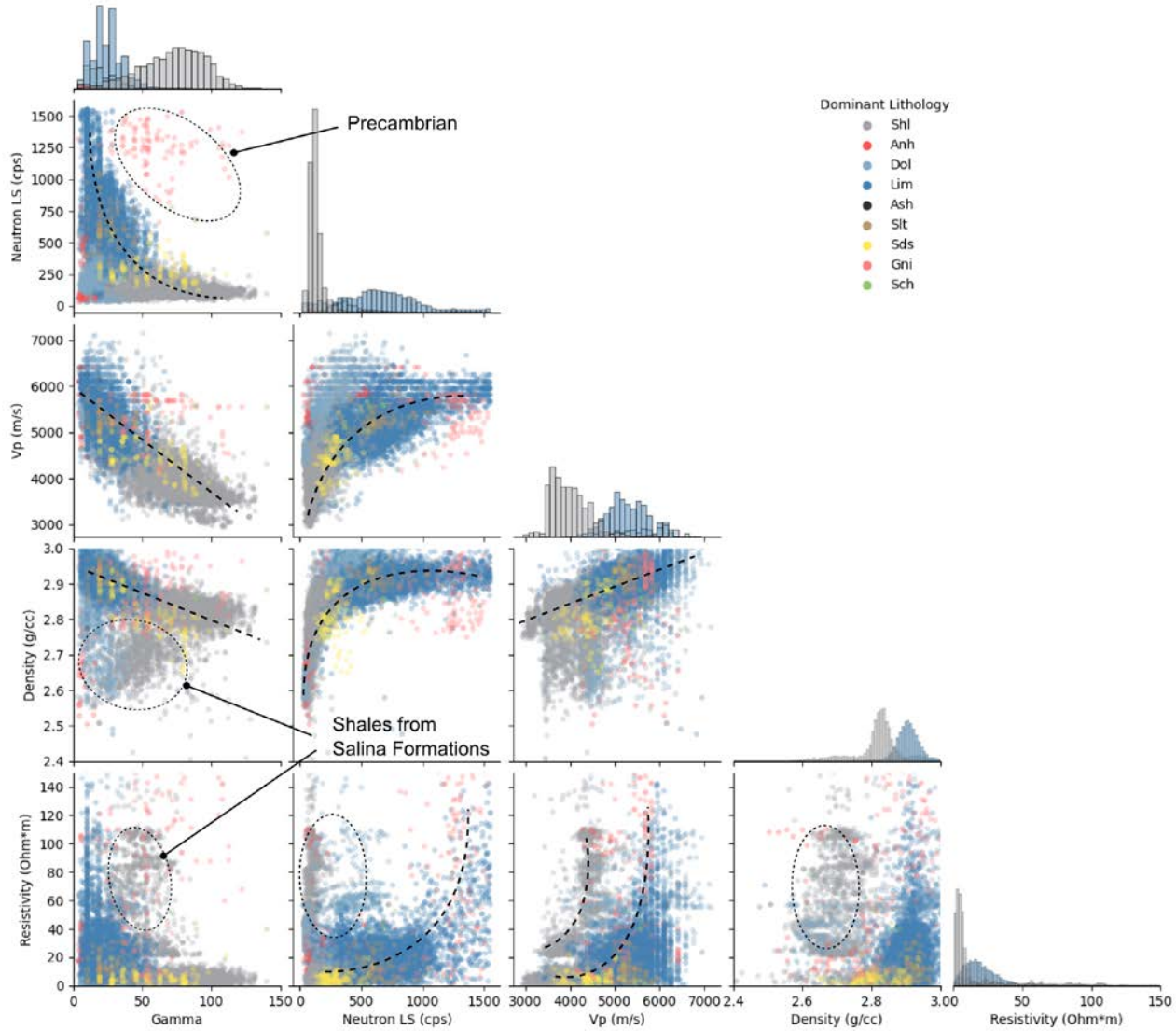


Figure 12. Grid of scatterplots presenting trends between different geophysical logs (Gamma, Neutron, Vp, Density and Resistivity) for the entire logged length of the borehole. Data points are colour classified using the dominant core logged rock types.

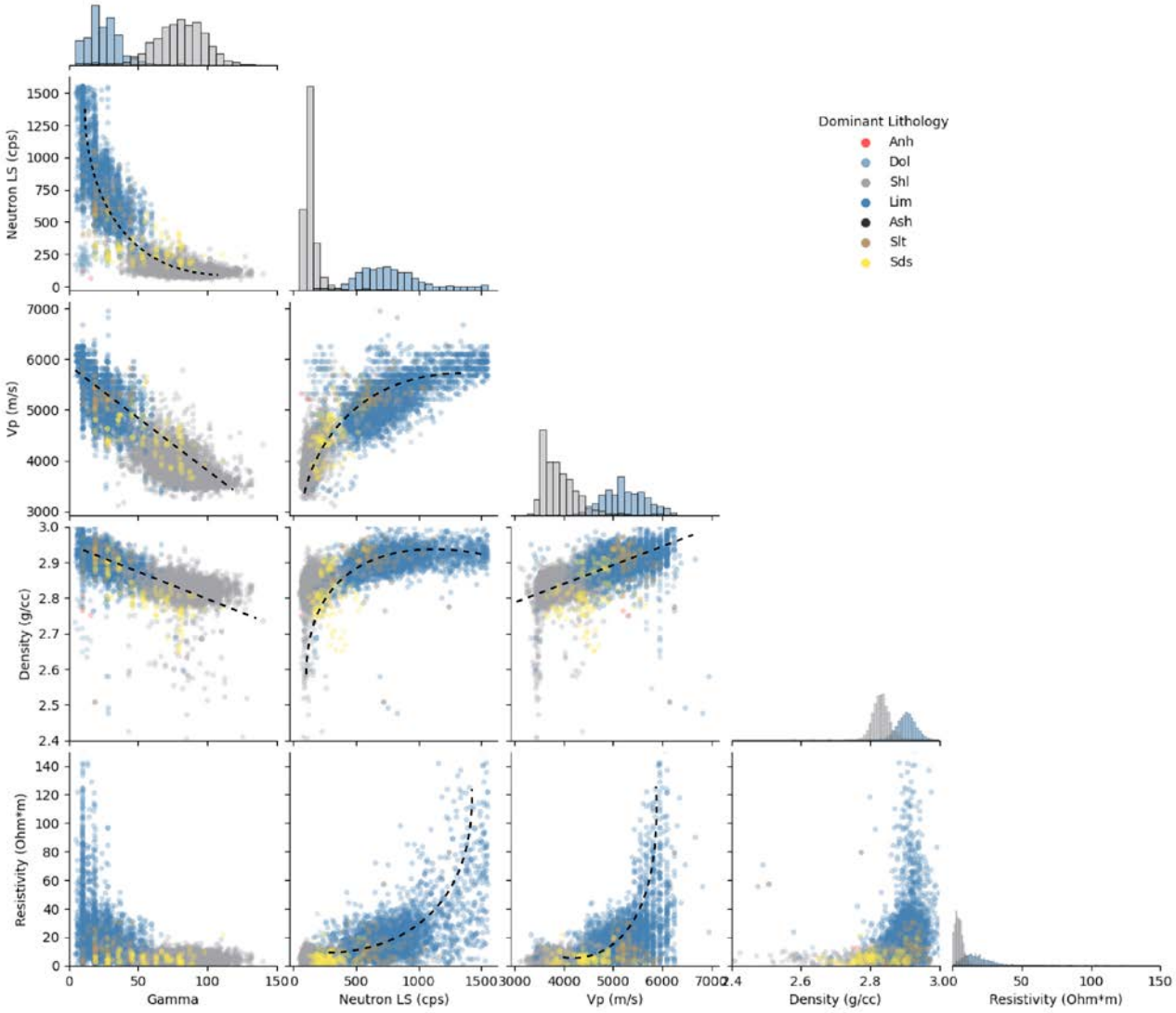


Figure 13. Grid of scatterplots presenting trends between different geophysical logs for the Ordovician Formations (Gamma, Neutron, Vp and Density and Resistivity). Data points are colour classified using the dominant core logged rock types.

3.2.3 Rock Alteration and Hydrocarbon Occurrences

Analysis of the core during geological and geotechnical logging (Geofirma, 2022a) included cataloguing the distribution of hydrothermal alteration and weathering features, and hydrocarbon occurrences along the length of SB_BH02. The presence of these features and occurrences are illustrated in Figure 14 and summarized in the sub-section below. Laboratory analyses are on-going and additional information (e.g., total organic carbon concentrations and information on the maturity of organic matter) will be integrated with this data set as they become available and reported in full in the South Bruce DGSM report.

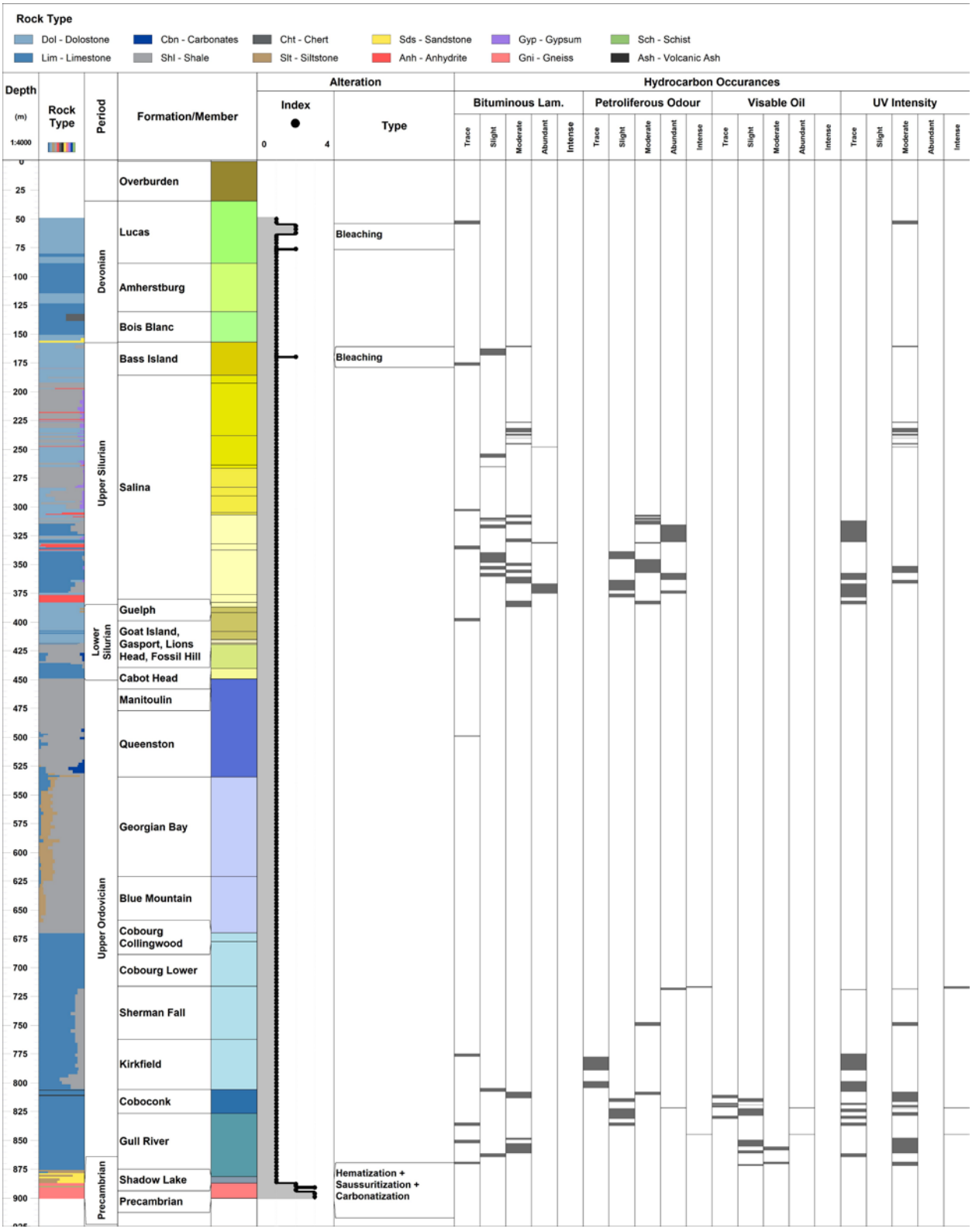


Figure 14. Summary of Logged Alteration and Hydrocarbon Occurrences in SB_BH02

3.2.3.1 Rock Alteration, Weathering and Karst

Logged alteration in SB_BH02 is shown in Figure 14. Rocks logged in SB_BH02 were generally unaltered, with some slight alteration noted as bleaching in the Lucas and Bass Islands formations. Slight to moderate saussuritization, carbonization and hematization of wall rock and along fractures was observed in the Precambrian gneissic basement. Dolomitization of limestone was not logged/characterized as alteration.

For purposes of this project, geological weathering was considered as a destructive process by which rock, on exposure to atmospheric water or processes, is changed in colour, texture, composition or form. Geological weathering was logged as karstic/porous vugs throughout the sedimentary strata as described in the lithological characteristic section above (3.2.2). Devonian formations (Lucas and Amherstburg) are altered by near surface/shallow karstification. Deeper in stratigraphic section the A-1 Unit Carbonate and Guelph Formation show evidence of paleokarst.

3.2.3.2 Hydrocarbon Occurrences

Logged hydrocarbon occurrences in SB_BH02 are shown in Figure 14. Discrete hydrocarbon occurrences were logged as thin bituminous laminations, indirectly as a petroliferous odour, and as minor localized visible seeping or oozing of oil from vugs or hairline fractures. In addition, an ultra-violet (UV) flashlight was used to scan the core for UV visible oil products.

Bituminous laminations are present in the Lucas Formation but are primarily concentrated in Silurian rocks, as well as a trace occurrence in the Upper Ordovician Queenston Formation and trace to moderate occurrences within the Upper Ordovician limestones from the Kirkfield Formation through to the Gull River Formation near the bottom of the borehole. Petroliferous odour was identified within and surrounding the Guelph Formation and Salina A units, as well as throughout the succession of Upper Ordovician limestones. Trace to abundant visible oil was identified in the Coboconk and Gull River formations. The UV log generally captures the same overall distribution of hydrocarbon occurrences along the borehole.

Overall, two main hydrocarbon horizons can be distinguished based on the distribution of hydrocarbon occurrences in SB_BH02. An upper horizon, throughout rocks of Silurian age and stratigraphically above the Cabot Head Formation, which is dominated by bituminous layering and locally petroliferous odour. A lower horizon, from the Kirkfield, Coboconk, and Gull River formations, where visible oil degassing and intense petroliferous odour were logged, associated with increased porosity found in some coarser limestone beds.

3.2.4 Structural Terminology

The following section provides definitions for structural terms used and identified in SB_BH02.

Vein (VN)- A fracture containing a mineral infilling. The definition is applied to features with mineral infill thickness less than 5 cm and greater than 1 mm.

Vein Zone (VNZ)- An interval of veining/infilled-fracturing where individual veins/fractures are not discernable.

Joint (JN)- A fracture along which there is no measurable displacement parallel to the plane of the fracture.

Fault (FLT)- a fracture or a zone of fractures that occur as a result of brittle deformation and within which there is relative displacement parallel to the fracture surfaces.

Broken Core Zone (BCZ)- Naturally occurring or mechanically induced feature characterized by core pieces that do not form full circumferential segments (e.g., not disks or cylinders).

Intact Fracture Zone (IFZ)- A brittle zone composed of a network of cohesive, natural fractures.

Lost Core Zone (LCZ)- Missing blocks or intervals of core where the pieces recovered do not fit together cleanly. Lost core can occur in zones of unconsolidated material (i.e., sand seams, clay beds), highly broken zones, fault zones, and zones where the core has been mechanically degraded from the drilling process (i.e., drill bit change zones, re-drilled core, etc.). Intervals of 'lost core' may also occur due to natural voids in the subsurface encountered during drilling.

Broken Fracture- Term used in geological and geotechnical core logging to describe a natural fracture that is non-cohesive and breaks the core into separate pieces. There is no implied association to other fracture characteristics, such as aperture. The 'broken' characteristic is also applied to other logged geological structures that are visibly non-cohesive, such as contacts.

Intact Fracture- A completely or partially cohesive, natural fracture.

Geological Aperture- An estimated measurement of the open space between two adjacent surfaces of a fracture determined visually during geological core logging, during interpretation of downhole televiewer logs, or during the integration of data from these two sources.

3.2.5 Structural Summary

This section describes the bedrock structural features measured along SB_BH02 based on the findings of the geological and geotechnical logging activity completed as part of WP03 (Geofirma 2022a). The step of integration with WP05 to assign true dip and dip direction to each logged structure is still to be completed and, for this reason, no stereographic plots have been included. Photographs of typical structures and structure intervals encountered in SB_BH02 are presented in pages B-49 to B-58 of Appendix B. A conservative approach was used when measuring structures/fractures during core logging as a result, the number of recorded structures/fractures may be over represented. The majority of the logged fractures are at high angle to the core axis and nearly parallel to bedding planes (see Appendix B for WP03 Report SB_BH02, Geofirma 2022a) Further analysis and integration of the structural data set from geophysical logs (WP05), including orientation information for the logged structures, will be reported in full in the South Bruce DGSM report.

A summary log is shown in Figure 15 indicating the position along the borehole of logged structures including joints (JN), veins (VN), vein zones (VNZ), intact fracture zones (IFZ), faults (FLT), broken core zones (BCZ) and lost core zones (LCZ). The summary log also presents logged geological aperture, and cumulative frequency curves for both broken and broken plus intact structures.

Approximately 93% of broken structures, including primarily joints and broken core zones, occur within the shallow bedrock above the Salina Formations. Three percent of broken structures occur in the Salina Group, with another 3 % of broken structures distributed sparsely across Lower Silurian and Upper Ordovician strata. The remaining approximately 1 % of broken structures occur in the Precambrian basement rocks. The summary structure log highlights the overall observation that the majority of logged features were identified in the Devonian and Silurian formations, as well as within the Precambrian bedrock. Similar to the findings at the Bruce Nuclear Site (Intera 2011), the intensity of fracturing within the Upper Ordovician formations is very low. In SB_BH02, some Devonian and Upper Ordovician structures had millimetre-centimetre scale bedding offset (Appendix B).

Joints were the most common natural structure logged, composing 58% of all logged natural structures in SB_BH02. A total of 402 joints were logged, including 325 broken and 77 intact or partially intact. The vertical distribution of joints was concentrated in the shallow bedrock (Devonian formations) (<155 m), the Upper Silurian limestones, dolostones and evaporites (157-386 m), and in the Precambrian basement rocks (>887 m).

Intact fracture zones (IFZ) represent intervals with an observable network of intact fractures. The distribution of this type of structure overlaps with that of the Devonian and Silurian joints. Broken Core Zones (BCZ) and Lost Core Zones (LCZ) were generally associated with highly fractured or karstic/paleokarstic core intervals and were concentrated in the shallow bedrock (<187 m).

Several fault structures logged in the shallow bedrock (<187m) were identified by millimetre- to centimetre-scale displacement of sedimentary bedding. Additionally, small-scale faulting occurs in the shale beds (with carbonate interbeds) of the Upper Ordovician with millimetre scale displacement of sedimentary bedding; these Upper Ordovician fault structures have anhydrite/salt infill (Appendix B-55, at 636.70-637.60 m). No major fault structures with greater than centimetre-scale offset were identified in core from SB_BH02. However, the vertical orientation of the borehole is not favourable to intersect steeply-dipping structures and, for this reason, steeply dipping fault (or faults) may be present inside the volume around the South Bruce Site would not have been intersected by the borehole

Any discontinuities or interpreted natural fractures with infill thickness less than 5 cm and greater than 1 mm were logged as veins, while vein zones were logged in intervals where multiple veins are present, and individual structures are not discernible. Logged veins were predominantly intact or partially intact with gypsum and anhydrite infill. These veins are generally parallel to bedding and occasionally cross-cut bedding or occur as brecciated intervals with anhydrite/gypsum containing cm-mm scale angular dolomitic shale fragments. A total of 158 veins were logged, including two broken (BR) and 156 intact or partially intact. One vein zone was logged as partially intact and the remainder 49 vein zones were logged as intact.

Calcite, gypsum and anhydrite are the most common secondary minerals logged throughout the Paleozoic rocks, while iron stain, chlorite and calcite are the most common secondary minerals logged in the Precambrian basement. The Upper Silurian Salina Group above the A-2 Unit Carbonate, in particular, hosts abundant, intact or partially intact, bedding-parallel, gypsum and anhydrite veins and vein zones. The prevalence of sub-horizontal veins within and above the Silurian Salina B Unit up to the base of the Bass Islands Formation (Figure 15) is likely related to subsidence after dissolution of salt in the Salina B Unit (Carter 2023). The salt dissolution is now represented by a breccia zone in the Salina B and Salina B Equivalent units with veins throughout.

Geological aperture was estimated during logging, and the results shown in Figure 15 represent the sum of logged aperture for every two metres of borehole length. The distribution of logged geological aperture follows closely the distribution of logged joints throughout the Devonian and Silurian formations.

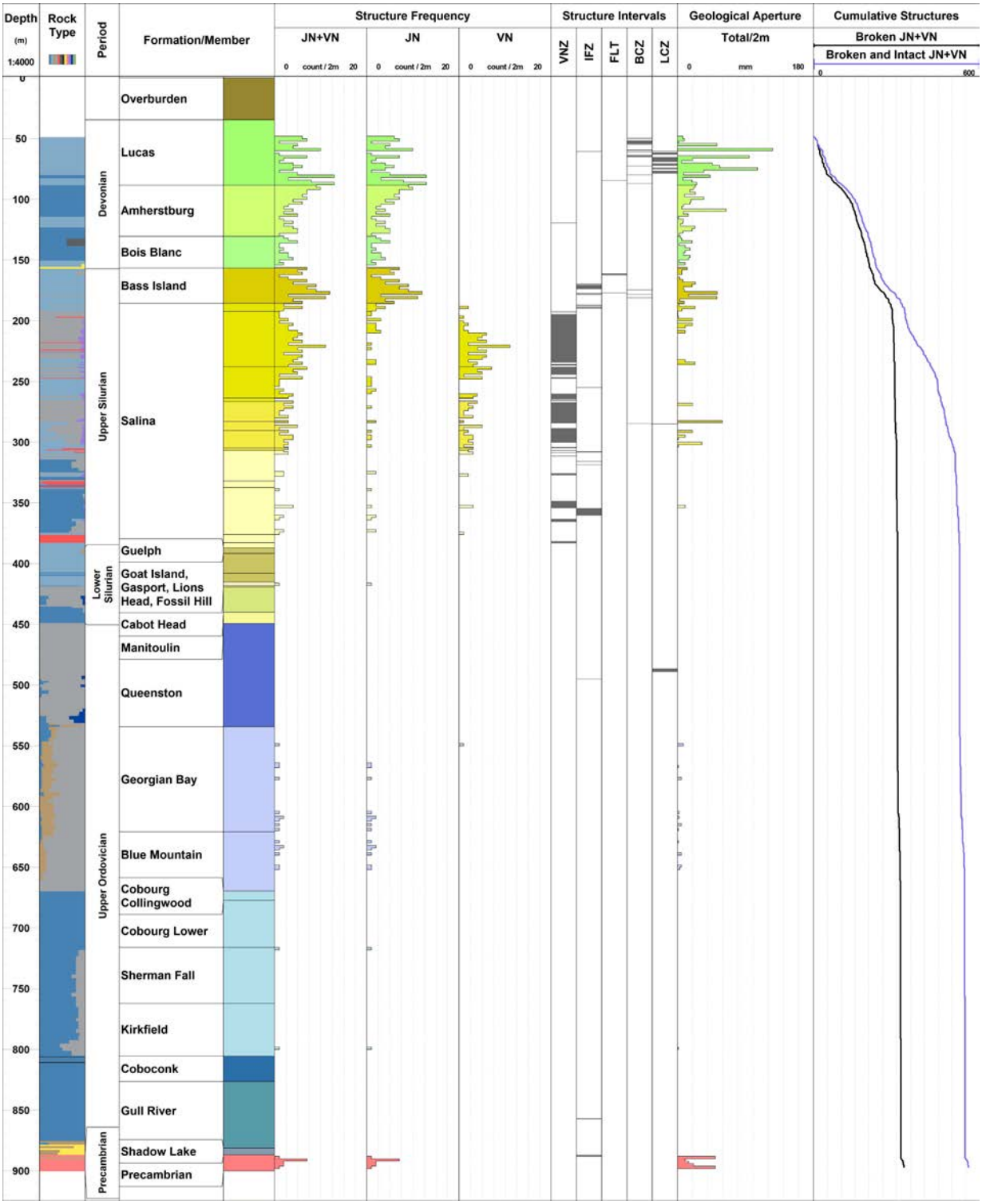


Figure 15: Summary of Logged Structures in SB_BH02, including fracture frequency and occurrence logs for joints (JN), veins (VN), vein zones (VNZ), intact fracture zones (IFZ), faults (FLT), broken core zones (BCZ) and lost core zones (LCZ). Geological aperture (total aperture), and fracture frequency logs are presented per 2 metre interval.

3.3 Discussion

Developing a geological understanding of the South Bruce Site is aided by the wealth of available information from the surrounding region in the form of historic hydrocarbon exploration boreholes, and the detailed site characterization activities undertaken at the Bruce Nuclear Site, which also included deep borehole drilling. The sum of this available information was also integrated into the recently updated 3D geological model for southern Ontario (Carter et al., 2021), providing a high-resolution framework within which to understand the South Bruce Site. The 3D model, in particular, highlights the high degree of lateral traceability of the Paleozoic formations across the entire region.

Overall, the drilled thickness of each Paleozoic stratigraphic package by geological period in SB_BH02 is as follows:

- Devonian – 122.31 m
- Silurian – 292.34 m
- Upper Ordovician – 437.68 m

The Upper Ordovician bedrock can be further subdivided into a shale-dominated upper package that includes the Queenston, Georgian Bay and Blue Mountain formations, which is 220.44 m thick, and a limestone-dominated lower package that includes all deeper formations above the Precambrian basement, which is 217.24 m thick.

While the Devonian bedrock is truncated by an erosional surface and therefore there is no clear basis for a regional comparison, the deeper bedrock thicknesses can be compared to those predicted by the 3D geological model of Carter et al. (2021). The thickness of Silurian bedrock predicted by the model is 307.52 m representing 5 % thickness difference between predicted and actual values. The thickness of the Upper Ordovician bedrock predicted by the model is 436.31 m representing a 1.37 m (less than 1 %) difference between predicted and actual thicknesses. Considering the shale and limestone subdivisions separately, predicted thicknesses and differences from actual are 237 m and 7 % for the shale formations, and 199.31 m and 8 % for the limestone formations. Although the separate packages differ slightly from the predicted, the overall thickness of the Upper Ordovician is consistent with the predicted model (Carter et al. 2021) and this highlights the exceptionally high degree of lateral consistency and predictability, which is a key geological attribute of the Upper Ordovician formations, in particular, across southern Ontario.

Below the Paleozoic bedrock, the top of the Precambrian basement was predicted to be encountered at 889.15 mBGS, while the actual drilled distance to the top of Precambrian was 886.93 m, representing a less than 3 m or less than 1 % discrepancy.

Overall, these results indicate a high degree of similarity between predicted and actual stratigraphic thicknesses encountered in SB_BH02.

3.3.1 Upper and Lower Silurian Formations/Units

Overall, the sequence and conditions of the Upper Silurian rocks encountered in SB_BH02 were as predicted in the 3D model (Carter al. 2021) and similar to Bruce Nuclear Site findings, from a lithological and thickness perspective (Intera 2021). The uppermost formation of the Upper Silurian is the Bass Islands Formation which is a very finely crystalline, laminated dolostone underlain by the Salina Group, which comprises a thick sequence of evaporite-dominated lithologies deposited in a restricted marine environment in the Michigan Basin including limestones, dolostones, anhydrite, halite and locally sylvite (Sonnenfeld and Al-Aasm 1991, Carter 2023). The Salina Group was formally divided into seven formations by Landes (1945), named Units A through G sequentially from oldest to youngest conformably overlain by the Bass Islands Formation. In current usage in Ontario, the Salina A Unit has been subdivided into a basal A-0 Carbonate, A-1 Evaporite, A-1 Carbonate, A-2 Anhydrite, and A-2 Carbonate in ascending order. Where halite beds are present, they are recognized by informal designation as A-2 Salt, B Salt, D Salt and F Salt to facilitate resource mapping (Carter 2023).

The Salina Group thins eastward into Ontario, principally due to thinning and pinch-out of the halite beds, with a maximum thickness of 420 m in the Sarnia area (Lambton County). Halite beds thin and pinch-out or have been removed by dissolution approaching the Algonquin Arch in southern Ontario, with lateral facies change to a much thinner sequence of interbedded anhydrite, dolostone and shales over the arch (Armstrong and Carter 2010). In southern Ontario, dissolution is most pronounced in the B Salt Unit (of the Salina B Unit), the thickest and most widespread of the salt beds in southern Ontario, with up to 90 metres of halite in the Sarnia area. Collapse of younger strata into the dissolution voids has locally fractured and brecciated the overlying strata (Armstrong and Carter 2010) and has had a controlling influence on thickness, distribution and structure of the overlying bedrock.

In southern Ontario, a major episode of dissolution of the B Salt and collapse of the overlying Salina Group formations occurred immediately after deposition of the Salina G Unit as evidenced by thickening of the Bass Islands Formation over areas of salt dissolution (Bailey Geological Services and Cochrane 1985). Salt dissolution has also occurred above pinnacle structures in the underlying Guelph Formation, along sub-regional faults in the Chatham Sag, and was the controlling mechanism in formation of large structural domes hosting oil reservoirs in the Lucas and Dundee formations (Bailey Geological Services 1985; Carter et al 2016). In SB_BH02, the rocks of the Salina Group above the A-2 Unit Carbonate are generally brecciated, indicative of a salt dissolution feature characterized by brecciated and fractured bedrock. Additionally, the fractures are infilled with finely crystalline fibrous gypsum veins with dimensions oriented to the fracture walls. It is important to note also that no halite beds were encountered in SB_BH02.

A geological cross-section from the regional 3D geological model (Carter et al. 2021) in the vicinity of the South Bruce Site shows collapse of all Salina Group formations above the B Unit and thickening of the Bass Islands Formation (Figure 16). Combining the findings from the Bruce Nuclear Site (Intera 2011) and drill core characteristics (brecciation and fracturing) observed in SB_BH02, this cross section supports the current understanding of depositional patterns and lateral predictability of the Upper Silurian strata. Devonian bedrock shows only limited structural effects from salt dissolution, indicating that dissolution occurred before deposition of the Bass Islands Formation (Carter 2023).

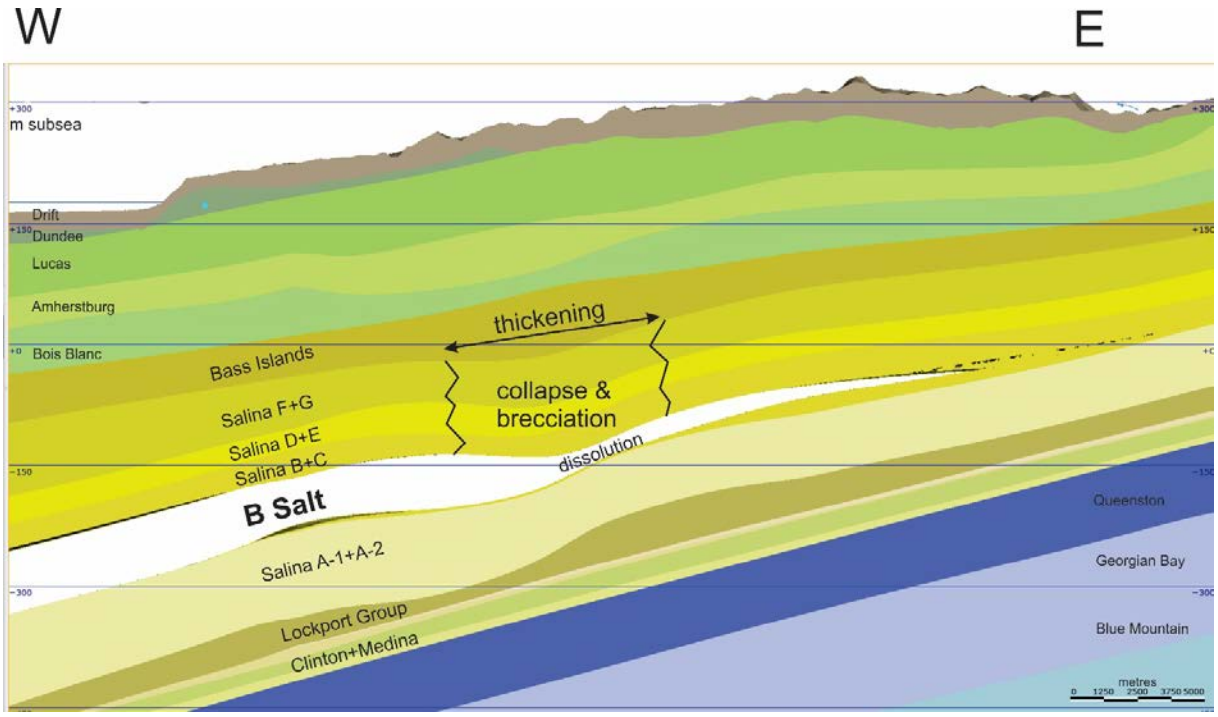


Figure 16 . Modified and adapted from Carter (2023). West to east cross-section immediately north of the South Bruce Site, constructed from a regional 3-D geological model (Carter et al. 2021) showing dissolution edge of the Salina B Salt with associated subsidence/collapse of the overlying Salina B, C, D, E, F, and G units, and thickening of the Bass Islands Formation. Younger strata appear to be unaffected, suggesting dissolution and subsidence occurred before deposition of the Bass Islands Formation.

The Guelph Formation intersected in SB_BH02 is the uppermost formation of the Lower Silurian Lockport Group. The Lockport Group is a series of carbonate deposits (limestones and dolostones) that with the exception of the Eramosa Formation, underlies all of southern Ontario south and west of the Niagara Escarpment. The Lockport Group consists of the Gasport, Goat Island, Eramosa and Guelph formations in ascending order. In our study area (South Bruce Site), the Lockport Group is capped by the lower Salina units of late Silurian age, which are described in previous sections of this report as a succession of carbonate and evaporites deposited in hypersaline, restricted marine settings (Armstrong and Carter 2010), and underlain by the limestones of the Lions Head Formation, the uppermost formation of the early Silurian Clinton Group at the South Bruce Site.

A new and unconventional paleogeographic interpretation (Brintnell 2012; Brunton et al 2012; Brunton and Brintnell 2020) is that the Lockport Group was deposited on an eastward-dipping carbonate ramp during the early Silurian, with water depths deepening from central Michigan into Ontario and further east, and the Algonquin Arch did not exist at that time. In this view, the central Michigan Basin is interpreted to have been a paleotopographic high during deposition of the Guelph Formation, with subaerial exposure post-dating Guelph deposition, resulting in intensive and extensive karstification of the Guelph dolostones and limestones soon after deposition. This is consistent with observations of Smith (1990) and Carter et al. (1994) who document a distinctive porous dark brown dolostone breccia with dolomudstone and wackestone occupying the stratigraphic position of the Guelph Formation, between pinnacles, which they interpreted as a paleosol karst rubble. This regional and interpinnacle paleokarst ranges from 2 to 6 m in thickness in Lambton County and extends northerly at least as far as the Bruce Nuclear Site in Bruce County where it is 4.1 to 5.4 m thick (Sterling and Melaney 2011). The Guelph Formation intersected in SB_BH02 is 5.02 m thick (Table 3), described as a brown-grey brecciated, karstic/vuggy medium-grained dolostone with heavy karstification, similar to the Bruce Nuclear Site findings (Intera 2011).

Figure 17 shows a distinctive series of lithofacies belts preserved in the Guelph Formation which resulted from complex depositional, erosional and diagenetic history (Brunton and Brintnell 2020, Carter 2023). In the area west of the carbonate platform (Figure 17), the Guelph Formation was subject to severe karstic weathering during a prolonged period of subaerial exposure that reduced the Guelph to a paleosol rubble/breccia, extending downward into the upper Goat Island Formation (Smith 1990; Carter et al. 1994; Brunton and Brintnell 2020; Carter 2023). Figure 17 shows that within the eastern extent of the regional Guelph Karst (paleokarst) there is a 50 km wide belt of pinnacles separated by paleokarst breccia. Brunton and Brintnell (2020) have interpreted these pinnacles as karst towers, while most previous workers considered them to be pinnacle reefs. SB_BH02 is located in a region susceptible to both karstification and pinnacle structures.

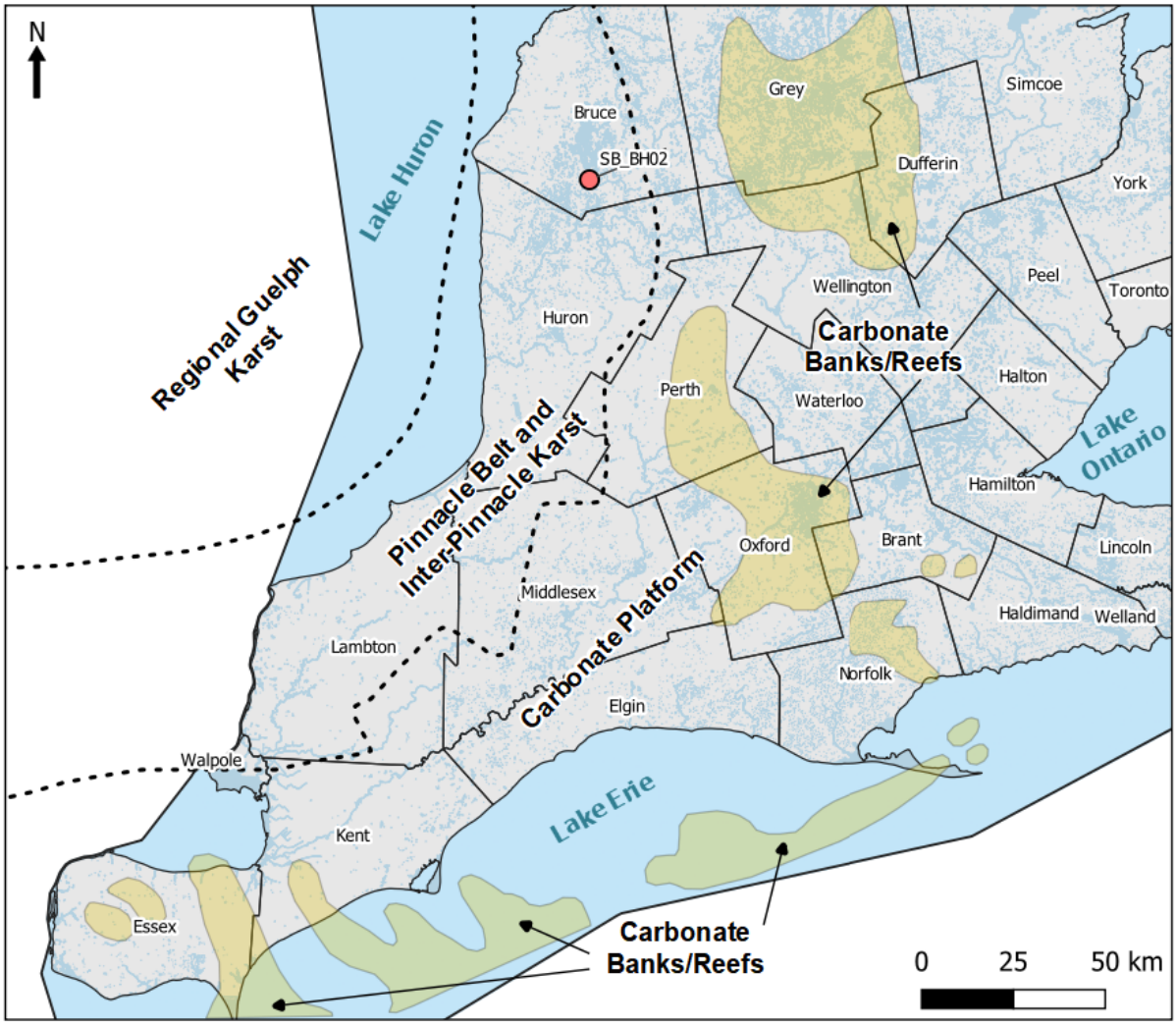


Figure 17. Facies belts in the Lockport Group, modified from Sanford (1969), Bailey (1986) and Carter et al. (1994) showing thickened carbonate banks on a slowly subsiding carbonate platform in the east and a regional karst horizon, pinnacle belt and inter-pinnacle karst belt developed on a paleotopographic high in what is now the Michigan Basin in the west (Brintnell, 2012; Brunton et al. 2020), Carter (2023). Geographic regions are presented as counties.

Pinnacle reefs are described as geological features with local relief above the regional Lockport surface of up to 128 m (McMurray 1985; Carter et al. 2016a). In Ontario, much smaller “incipient reefs”, with relief generally less than 30 m, have been discovered in Lambton County interspersed between the pinnacles. Pinnacle reefs are comprised of a stacked sequence of limestones and/or

dolostones of the Gasport, Goat Island and Guelph formations, capped by laminated dolostones/limestones of the Salina A-1 Unit Carbonate and massive, nodular and laminated anhydrite of the Salina A-2 Unit Anhydrite (Figure 18). In Lambton County, halite of the A-2 Salt (not present in SB_BH02) surrounds the pinnacles, pinching out on the flanks. Additionally, laminated dolostones of the A-0 Unit Carbonate are expected to occur on the flanks of reefs. Dolostone of the A-2 Unit Carbonate completely envelopes the pinnacles, thinning over the crests and exhibiting structural drape of up to 30 m, interpreted to be a result of compaction over the pinnacle structures prior to lithification. Dissolution of halite (salt) of the overlying B Unit has occurred over many of the pinnacles in Ontario, interpreted to be the result of upward flow of formation water within the pinnacle during burial compaction of the regional Lockport Group and lower Salina Group (Bailey 2000).

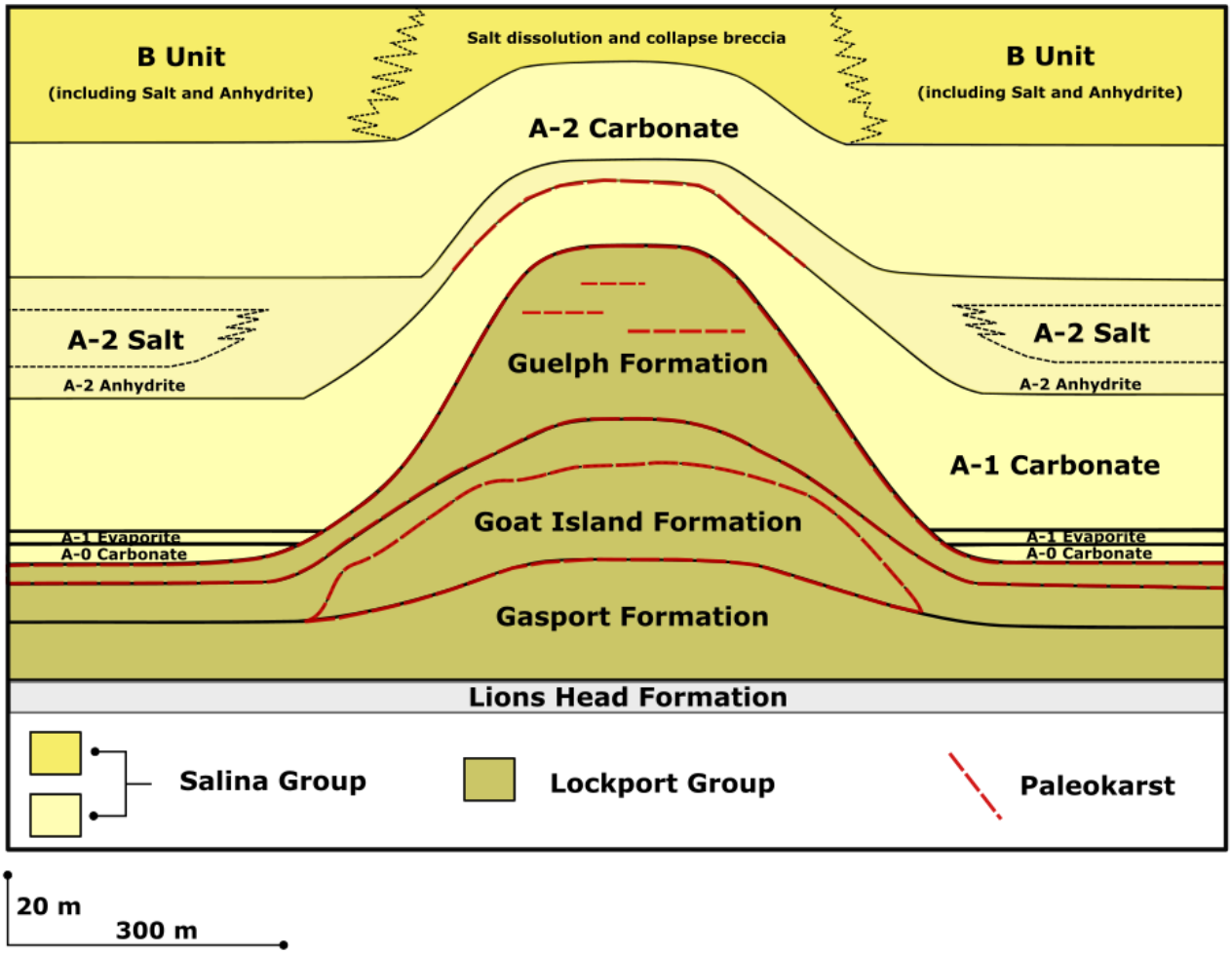


Figure 18. Conceptual model of a Guelph pinnacle reef showing stratigraphic, lithological and structural relationships with regional strata of the Lockport Group and lower Salina Group, within the Pinnacle and Interpinnacle Karst Belt of southern Ontario. Modified and adapted from Brintnell (2012), Brunton and Brintnell (2020), Carter et al. (2021) and Carter (2023). A-0 Unit Carbonate is interpreted to occur on flanks of reefs or in non reefal areas, which is supported by drill core findings from SB_BH02.

The interpreted overall thickness of the Lockport Group in SB_BH02 is 28.46 m. The Guelph, Goat Island and Gasport formations have an interpreted thickness of 5.02 m, 16.14 m and 7.30 m

respectively (Table 3). When compared to the nearby petroleum (OGSRL) wells T004881, F01262 and the regional 3D model predicted depths (Carter et al. 2021), there is an exceptionally high correlation and consistency in thicknesses in these formations. The difference between predicted and actual thickness of the Lockport Group in SB_BH02 (28.46m) is 2.11 m.

Table 3. Summary of Lockport Group tops from SB_BH02, T004881 and F012062.

Formation	SB_BH02	T004881	F012062	3-D Model (Carter et al. 2021)
Guelph	5.02 m	11.24 m	10.64 m	8.99[1]
Goat Island	16.14 m	18.00 m	15.24 m	13.31
Gasport	7.30 m	7.33 m	3.94 m	4.05
Total Lockport Thickness	28.46 m	36.57 m	29.82 m	26.35

Notes:

1. Model thickness of the Guelph Formation is combined with Salina A-0 Unit Carbonate in 3 D model (Carter et al. 2021) and represented as a single layer. Reason for this is A-0 Unit Carbonate does not have a good enough spatial distribution in the OGSRL database to provide/produce a reliable modelled layer, as it cannot be reliably picked without geophysical logs. The A-0 Unit Carbonate is also not picked in the T004881 or F012062 wells.

This difference in thickness is further illustrated by Table 4 that shows the thicknesses of the overlying lower Salina Units. When compared to SB_BH02, the thicknesses of lower Salina formations have 2-3 meters difference from the formations in nearby petroleum wells (T004881 and F012062). Furthermore, when taking a closer look at the actual SB_BH02 versus the predicted 3D model (Carter et al.2021) thickness, all formations in the lower Salina are within 2-3 m of actual vs predicted thickness except for the Salina A-2 Unit Carbonate that has a 12.35 m difference in actual versus predicted. This difference may be attributed to a few factors such as: local variation in formation thickness and/or regional scale resolution in model versus borehole scale. All of these observations support the current understanding of the conceptual model (Figure 18) for pinnacle and inter-pinnacle wells in southern Ontario.

Table 4. Summary of Salina Group tops from SB_BH02, T004881 and F012062 overlying the Lockport Group.

Formation	SB_BH02	T004881	F012062	Carter et al. 2021
Salina A-2 Carbonate	25.27 m	21.30 m	30.18 m	37.62 m
Salina A-2 Anhydrite	5.34 m	3.09 m	3.66 m	3.78 m
Salina A-1 Carbonate	38.52 m	40.55 m	38.40 m	31.19 m
Salina A-1 Evaporite	7.08 m	3.96 m	4.60 m	6.04 m
Salina A-0 Carbonate	3.66 m	Not Picked	Not Picked	Not Modelled

Overall, formations in the Lower Silurian intersected in SB_BH02 are laterally continuous and very consistent in thickness as predicted in the 3D regional model (Carter et al 2021). This includes the

limestones, dolostones and shales of the Medina and Clinton groups underlying the Lockport Group.

3.3.2 Upper Ordovician Formations

The Cobourg Formation has a total interpreted thickness in SB_BH02 of 46.68 m, including 7.85 m of the Upper Collingwood Member and 38.83 m of the Lower Member. The distinction between these subdivisions is based, as noted above, on placing the top of the lower Member of the Cobourg Formation below the lowermost significant (>10cm) dark grey-black shale bed of the Upper Collingwood Member and is supported by the change in signature in geophysical logs. The dominant rock type encountered throughout the lower Cobourg Formation is a very hard argillaceous and fossiliferous limestone.

The predicted thickness of the entire Cobourg Formation, based on the 3D model from Carter et al. (2021), is 28.03 m, indicating nearly a 20 m difference between predicted and actual SB_BH02 values. The 3D model from Carter et al. (2021) does not subdivide the Upper and Lower members of the Cobourg Formation due to sparsity of formation top picks in the Collingwood Member, therefore, representing the Cobourg Formation as a single layer in the regional model. However, when looking at nearby petroleum wells from the OGSRL database and considering the Cobourg Formation subdivisions separately, Geofirma (2022b) predicted a thickness of 16 m for the Collingwood Member and 40 m for the Lower Member. While these differences between predicted (regional 3D model) and actual (SB_BH02) are relatively large, this is likely more a function of the low degree of resolution of this subdivision pick in the regional 3D model versus the high degree of resolution in making this pick in fresh core with accompanying high-resolution geophysical logs. Overall, the total actual thickness of the Cobourg Formation is close to the predicted value, further highlighting the exceptionally high degree of lateral consistency and predictability of the Upper Ordovician formations at the regional scale.

3.3.3 Cambrian Sandstone

Based on the recent regional 3D modelling of Carter et al. (2021), the South Bruce Site is proximal to the zero-thickness edge of the Cambrian Sandstone unit (Figure 19). The position of SB_BH02 is located outside the interpreted, southeastern finger-like extension of this zero-thickness edge. Based on the model, Cambrian Sandstone was not expected to be encountered above the Precambrian basement in SB_BH02. Given that no evidence of a Cambrian unit was encountered in the borehole, it has been confirmed that no Cambrian Sandstone exists in the area based on available data to date.

For comparison, 40 km northwest at the Bruce Nuclear Site, the deep boreholes intersected approximately 17 m of Cambrian orthoquartzitic sandstone. At this site, anomalous hydraulic overpressures were also encountered in the Cambrian unit resulting in artesian flow conditions (Intera, 2011). Based on the experience of the drilling of SB_BH02, the lack of a Cambrian unit also resulted in the absence of such anomalous hydraulic conditions.

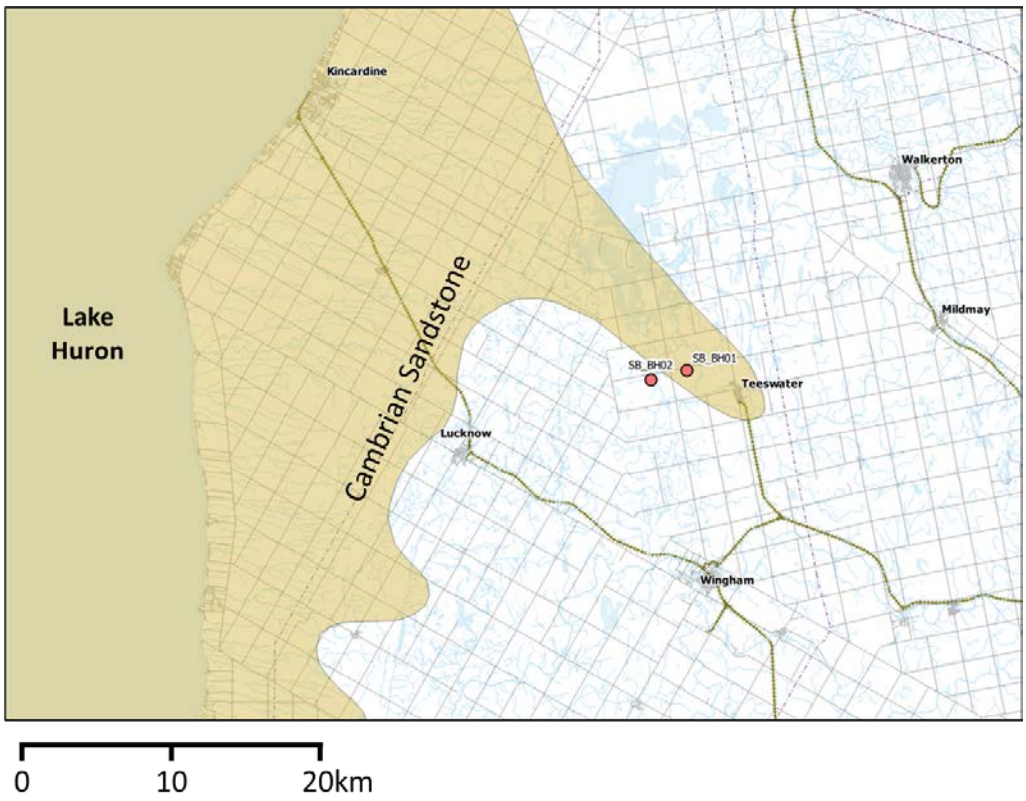


Figure 19. The shaded region represents the area of Southern Ontario in proximity to SB_BH01 and SB_BH02 underlain by Cambrian Sandstone as per the Carter et al. (2021) regional model.

4 SUMMARY OF FINDINGS AND UNCERTAINTIES

4.1 Findings

A total of 35 formations and members including the Pleistocene overburden were interpreted in SB_BH02 based on the integration of rock core observations (WP03 – Geofirma 2022a) with variable responses observed in geophysical well log data (WP05 – Geofirma 2023b). Natural and spectral gamma, gamma-gamma density and neutron geophysical logs provided evidence to distinguish each stratigraphic interval by rock type and internal character. As a result, the outcome of the stratigraphic picks are consistent with the framework presented by Carter et al. (2021). Guidance from Armstrong and Carter (2006, 2010) as well as criteria described in previous detailed reports from site characterization activities at the Bruce Nuclear Site (Intera 2011) also supported the development of the final stratigraphic log presented here.

Overall, the interpreted stratigraphic sequence encountered was comparable to that predicted to occur at the location of SB_BH02 based on a recently completed regional-scale 3D geological model (Carter et al., 2021). Apart from the Cobourg Formation that has thicker than predicted thickness, no other significant differences were found between predicted 3D geological model and actual SB_BH02 Paleozoic sequence.

A total of 12 different types of rock were identified, dominated by limestone, shale, and dolostone. Overall alteration was minor, and there is evidence of karstic conditions in the Lucas and Amherstburg formations indicating that recent weathering impacted the stratigraphic sequence

(mainly in shallow formations). Paleo-erosional surfaces have experienced paleo-weathering and paleo-karstification, in particular the A-1 Unit Carbonate and Guelph Formation. The types and distribution of hydrocarbon occurrences suggest that distinct hydrocarbon zones can be distinguished, consistent with the recognition that the shale units, in particular, represent cap (barrier) rocks that greatly inhibit cross-formational vertical connections.

The distribution and intensity of fracturing in SB_BH02 is similar to the conditions encountered at the Bruce Nuclear Site (Intera 2011). An increased fracture intensity occurs in the shallow subsurface and down to the base of the Guelph Formation. Below this formation, the fracture intensity decreases markedly through the entire Upper Ordovician succession. An increase in fracture intensity is again observed in the Precambrian bedrock intersected at the bottom of the borehole.

Faults with millimetre- to centimetre-scale displacement of bedding were identified in the shallow bedrock and with millimetre displacement in the Upper Ordovician shale beds (with carbonate interbeds). No major fault structures with greater than centimetre-scale offset were identified in core from SB_BH02. It can be stated that the very low intensity of logged fractures supports a statement that there is no regionally important fault structure close to the borehole. However, the presence of such a structure inside the South Bruce area and borehole site can absolutely not be ruled out on the basis of the results from SB_BH02. However due to the near-vertical orientation of the borehole, it is not possible to rule out steeply dipping or vertical faults.

Stratigraphic comparison between SB_BH01 and SB_BH02 and thickness variation in the different stratigraphic units are presented in the newly developed 3D Site Scale Geological Model for the South Bruce Site (DesRoches et al. 2022).

4.2 Uncertainties

It is acknowledged that findings presented in this report are based on available information from a single, near-vertical borehole. Whether or not the characteristics of the bedrock interpreted in this report will be representative of characteristics across the South Bruce Site remains uncertain. However, the level of uncertainty related to the overall understanding of the bedrock across the study area will decrease as information from other subdisciplines are integrated with the information presented above. It is also important to note that there is high degree of similarity between predicted stratigraphic thicknesses from the regional 3-D model from Carter et al. (2021) and the actual thicknesses encountered in SB_BH02, and this similarity addresses some of the uncertainty by highlighting the lateral continuity and predictability of formations in the area. Furthermore, findings from the Bruce Nuclear Site provide a natural analogue and complimentary dataset to support the characterization and understanding of the South Bruce Site.

The possibility for intersecting outliers of Cambrian Sandstone across the site remains uncertain. It also remains uncertain, at the time of writing this report, how or if the lack of Cambrian bedrock impacts the hydrogeological character of the Ordovician limestones. However, as noted above, artesian conditions were not encountered at the base of SB_BH02 whereas, at the Bruce Nuclear Site, both the Cambrian Sandstone and anomalous hydraulic conditions (overpressures) were encountered.

The types and frequency of especially steeply dipping fractures logged in SB_BH02 will be limited by the vertical orientation of the borehole, and it is likely that the orientation and intensity of fractures are underestimated due to borehole orientation bias (Terzaghi 1965). The stage of integration of WP03 and WP05 datasets is on-going and will be completed in order to define the true occurrence and structural orientation of each natural logged fracture and, particularly, the small-scale fault structures identified in the Devonian and Upper Ordovician with mm-cm scale sedimentary bedding offset. However, it is also important to understand that the type and

distribution of fractures, as well as their role in flow and transport, is radically different in this sedimentary environment compared to that in crystalline rock. In this sedimentary environment, and in the Upper Ordovician succession specifically, the very low frequency of logged fractures and the absence of flowing fractures in the Upper Ordovician, indicate that natural fractures are not likely to play a role in flow and transport modelling.

5 REFERENCES

Al-Aasm, I.S., and Crowe, R., 2018. Fluid compartmentalization and dolomitization in the Cambrian and Ordovician successions of the Huron Domain, Michigan Basin. Marine and Petroleum Geology, 92, p.160-178.

Al-Aasm, I.S., Crowe, R., Tortola, M. 2021. Dolomitization of Paleozoic successions, Huron Domain of southern Ontario, Canada: Fluid Flow and Dolomite Evolution. Water 2021, 13, 2449. https://doi.org/10.3390/w13172449.

Armstrong, D.K. and Carter T.R., 2006. An Updated Guide to the Subsurface Paleozoic Stratigraphy of Southern Ontario. Open File Report 6191. Ontario Geological Survey.

Armstrong, D.K. and T. R. Carter, 2010. The Subsurface Paleozoic Stratigraphy of Southern Ontario, Ontario Geological Survey, Special Volume 7, 301 p.

Armstrong, D.K. 2017. Paleozoic geology of the Welland–Fort Erie area, southern Ontario; Ontario Geological Survey, Preliminary Map P.3811, scale 1:50 000.

Armstrong, D.K 2018. Paleozoic geology of the Dunnville area, southern Ontario; Ontario Geological Survey, Preliminary Map P.3810, scale 1:50 000.

Bailey Geological Services Ltd. and Cochrane, R.O., 1984a. Evaluation of the conventional and potential oil and gas reserves of the Cambrian of Ontario. Ontario Geological Survey, Open File Report 5499, 72p.

Bailey Geological Services Ltd. and Cochrane, R.O.,1986. Evaluation of the conventional and potential oil and gas reserves of the Silurian sandstone reservoirs of Ontario; Ontario Geological Survey, Open File Report 5578, 275p.

Bailey, S.M.B. 2000. The Extremely Complicated, ‘Simple’ Pinnacle Reef Reservoirs of Ontario. Ontario Petroleum Institute, 39th annual conference. Technical Paper 3. London, Canada, 33 p.

Birchard, M.C., 1990. Stratigraphy and facies of the Middle Devonian Dundee Formation, southwestern Ontario, *in* Carter, T.R., (*ed.*), Subsurface Geology of Southwestern Ontario: A Core Workshop. American Association of Petroleum Geologists, 1990 Eastern Section Meeting, hosted by the Ontario Petroleum Institute, London, Ontario, p.131-146.

Birchard, M.C., Rutka, M.A. and Brunton, F.R., 2004. Lithofacies and geochemistry of the Lucas Formation in the subsurface of southwestern Ontario: A high-purity limestone and potential high-purity dolostone resource; Ontario Geological Survey, Open File Report 6137, 180p.

Brintnell, C., 2012. Architecture and stratigraphy of the Lower Silurian Guelph Formation, Lockport Group, southern Ontario and Michigan. The University of Western Ontario, London, Ontario, Canada, MSc thesis, 242 p.

Brunton, F.R., and Brintnell, C., 2020. Early Silurian sequence stratigraphy and geological controls on karstic bedrock groundwater-flow zones, Niagara Escarpment region and the subsurface of southwestern Ontario. Ontario Geological Survey, Groundwater Resources Study 13.

Brunton, F.R., Carter, T.R., Logan, C., Clark, J., Yeung, K., Fortner, L., Freckelton, C., Sutherland, L. and Russell, H.A.J. 2017. Lithostratigraphic compilation of Phanerozoic bedrock units and 3D geological model of southern Ontario; in H.A.J Russell, D. Ford and E.H. Priebe (compilers), Regional-Scale Groundwater Geoscience in Southern Ontario: An Ontario Geological Survey, Geological Survey of Canada, and Conservation Ontario Open House, Geological Survey of Canada, Open File 8212, p.3.

Budai, J.M. and J.L. Wilson. 1991. Diagenetic history of the Trenton and Black River Formations in the Michigan Basin. Geological Society of America Special Paper 256, 73-88.

Carter, T.R., Trevail, R.A., and Smith, L. 1994. Core workshop: Niagaran reef and inter-reef relationships in the subsurface of southwestern Ontario; Geological Association of Canada–Mineralogical Association of Canada, Annual Meeting, Waterloo 1994, Field Trip A5 Guidebook, 38p.

Carter, T.R., Brunton, F.R., Clark, J., Fortner, L., Freckelton, C.N., Logan, C.E., Russell, H.A.J., Somers, M., Sutherland L. and Yeung, K.H. 2017. Status report on three-dimensional geological and hydrogeological modelling of the Paleozoic bedrock of southern Ontario; in Summary of Field Work and Other Activities, 2017, Ontario Geological Survey, Open File Report 6333, p.28-1 to 28-15.

Carter, T.R., Brunton, F.R., Clark, J.K., Fortner, L., Freckelton, C., Logan, C.E., Russell, H.A.J., Somers, M., Sutherland, L. and Yeung, K.H. 2019. A three-dimensional geological model of the Paleozoic bedrock of southern Ontario. Ontario Geological Survey, Groundwater Resources Study 19 / Geological Survey of Canada, Open File 8618. https://doi.org/10.4095/315045

Carter, T.R., Clark, J., Colquhoun, I, Dorland, M., Phillips, A., 2016a. Ontario oil and gas plays 1 – exploration, production and geology. Canadian Society of Petroleum Geologists, Reservoir v.43, (08), p.19-25.

Carter, T.R., Logan, C.E., Clark, J.K., Russell, H.A.J., Brunton, F.R., Cachunjua, A., D'Arienzo, M., Freckelton, C., Rzyszczak, H., Sun, S., Yeung, K.H., 2021. A three-dimensional geological model of the Paleozoic bedrock of southern Ontario – Version 2. Geological Survey of Canada, Open File 8795, 103 p.

Carter,T.R., 2023. Regional Geology of Southern Ontario. NWMO Report number APM-REP-01332-0380. 154 p.

Cercone, K.R. 1984. Thermal history of Michigan basin; American Association of Petroleum Geologists Bulletin 68, 130-136.

Coniglio, M., and Williams-Jones, A.E., 1992. Diagenesis of Ordovician carbonates from the northeastern Michigan Basin, Ontario: evidence from petrography, stable isotopes and fluid inclusions. Sedimentology, v.39, p.813-836.

Coniglio, M., Sherlock, R., Williams-Jones, A.E., Middleton, K., Frape, S.K., 1994.Burial and hydrothermal diagenesis of Ordovician carbonates from the Michigan Basin, Ontario, Canada. in: Purser, B., Tucker, M., Zenger, D. (Eds.), Dolomites a Volume in Honour of Dolomieu. Special Publications of the International Association of Sedimentologists, v. 21, pp. p.231-254.

Coogan, A.H., and Maki, M.U., 1987. Knox Unconformity in the subsurface of northern Ohio. American Association of Petroleum Geologists, Search and Discovery article #91041.

Davies, G.R., and Smith, L.B., 2006. Structurally controlled hydrothermal dolomite facies: An overview. American Association of Petroleum Geologists Bulletin, v. 90, p. 1641-1690.

Davis, D., 2013, Application of U-Pb geochronology methods to the absolute age of determination of secondary calcite: Nuclear Waste Management Organization Open File Report TR-2013-21, 31 p.

Davis, D.W. 2016. Continued application of U–Pb geochronology methods to the absolute age determination of secondary calcite: 2014–2016. Nuclear Waste Management Organization Report NWMO-TR-2016-07, 72p.

Davis, D.W., Sutcliffe, C.N., Thibodeau, A.M., Spalding, J., Schneider, D., Cruden, A., Adams, J., Parmenter, A., Jensen, M., and Zajasz, Z., 2020. Hydrochronology of a proposed deep geological repository for low- and intermediate-level nuclear waste in southern Ontario from U–Pb dating of secondary minerals: response to Silurian and Cretaceous events. Canadian Journal of Earth Sciences, 57, p.464-476

Dickinson, W.R., G.E. Gehrels and J.E. Marzolf. 2010. Detrital zircons from fluvial Jurassic strata of the Michigan basin: Implications for the transcontinental Jurassic paleoriver hypothesis. Geology 38, 499-502.

Desrochers, A., and James, N.P., 1988. Early Paleozoic surface and subsurface paleokarst: Middle Ordovician carbonates, Mingan Islands, Quebec, *in* James, N.P., and Choquette, P.W. (*eds*), Paleokarst. Springer Science+Business, New York, p.2188-215, https://doi.org/10.1007/978-1-4612-3748-8

Diamond, L.W., Aschwanden, L., and Caldas, R., 2015. Fluid inclusion study of drill core and outcrop samples from the Bruce nuclear site, southern Ontario. Nuclear Waste Management Organization, NWMO-TR-2015-24, 126 p.

Engelder, T. 2011. Analogue Study of Shale Cap Rock Barrier Integrity. Nuclear Waste Management Organization Report NWMO DGR-TR-2011-23 R000. Toronto, Canada.

Ettensohn, F. R., 2008. The Appalachian foreland basin in eastern United States. Sedimentary basins of the world, 5, 105-179.

Gao, C., Shirota, J., Kelly, R.I., Brunton, F.R., and Van Haaften, S. 2006. Bedrock topography and overburden thickness mapping, southern Ontario. Ontario Geological Survey, Miscellaneous Release—Data 207.

Gao, C. 2011. Buried bedrock valleys and glacial and subglacial meltwater erosion in southern Ontario, Canada. Canadian Journal of Earth Sciences, 48, 801-818.

Geofirma Engineering Ltd., 2014. Phase 1 Geoscientific Desktop Preliminary Assessment, Processing and Interpretation of Borehole Geophysical Log and 2D Seismic Data, Municipalities of Arran-Elderslie, Brockton and South Bruce, Township of Huron-Kinloss and Town of Saugeen Shores, Report NWMO APM-REP-06144-0110 prepared for the Nuclear Waste Management Organization, Toronto, Canada.

Geofirma Engineering Ltd., 2022a. Phase 2 Initial Borehole Drilling and Testing, South Bruce: WP03 Data Report- Geological and Geotechnical Core Lore Logging, Photography and Sampling for SB-BH02 (No. APM-REP-01332-0335). Nuclear Waste Management Organization.

Geofirma Engineering Ltd., 2022b. Phase 2 Initial Borehole Drilling and Testing, South Bruce: WP02 Test Plan: Borehole Drilling and Coring for SB_BH02 (No. APM-REP-01332-0354). Nuclear Waste Management Organization.

Geofirma Engineering Ltd., 2023a. Phase 2 Initial Borehole Drilling and Testing, South Bruce: WP02 Data Report-Borehole Drilling and Coring for SB_BH02 (No. APM-REP-01332-0329). Nuclear Waste Management Organization.

Geofirma Engineering Ltd., 2023b. Phase 2 Initial Borehole Drilling and Testing, South Bruce. WP05 Data Report- Geophysical Well Logging and Interpretation for SB_BH02 (No. APM-REP-01322-03335). Nuclear Waste Management Organization.

Geosynthesis (2011). Nuclear Waste Management Organization. NWMO-DGR-TR-20-11-11.pp 420

Haeri-Ardakani, O., Al-Aasm, I., and Coniglio, M., 2013a. Petrologic and geochemical attributes of fracture-related dolomitization in Ordovician carbonates and their spatial distribution in southwestern Ontario, Canada. Marine and Petroleum Geology, 43, p.409-422.

Haeri-Ardakani, O., Al-Aasm, I., and Coniglio, M., 2013b. Fracture mineralization and fluid flow evolution: an example from Ordovician–Devonian carbonates, southwestern Ontario, Canada. Geofluids, 13, p.1-20.

Haeri-Ardakani, O., Al-Aasm, I., and Coniglio, M., and Samson, I.2013c. Diagenetic evolution and associated mineralization in Middle Devonian carbonates, southwestern Ontario, Canada. Bulletin of Canadian Petroleum Geology, 61, no.1, p.41-58.

Hamblin, A.P. 1999. Lower Silurian Medina Group of Southwestern Ontario: Summary of Literature and Concepts. Geological Survey of Canada Open File 3468.

Heaman, L.M. and B.A. Kjarsgaard. 2000. Timing of eastern North American kimberlite magmatism. Continental extension of the Great Meteor Hotspot Track? Earth and Planetary Science Letters Journal 178, 253-268

Hogarth, C.G. and D.F Sibley. 1985. Thermal history of the Michigan Basin: evidence from conodont coloration index. In: K.R. Cercone and J.M. Budai (Eds.) Ordovician and Silurian Rocks of the Michigan Basin. Michigan Basin Geological Society Symposium, Special Paper 4, 45-58.

Howell, P.D. and van der Pluijm, B.A., 1999. Structural sequences and styles of subsidence in the Michigan Basin. Geological Society of America Bulletin, v. 111, p. 974-991.

Huff, W.D., S.M. Bergstrom and D.R. Kolata. 1992. Gigantic Ordovician volcanic ash fall in North America and Europe: biological, tectonomagmatic, and event-stratigraphic significance. Geology 20, 875-878.

Hurley, N.F., and R. Budros, 1990. Albion-Scipio and Stoney Point fields-U.S.A., Michigan Basin, in, Beaumont, E.A., and Foster N.H. eds., Treatise of Petroleum Geology Atlas of Oil & Gas Fields, Stratigraphic Traps I. American Association of Petroleum Geologists, p. 1-32.

Intera Engineering Ltd., 2011. Descriptive Geosphere Site Model. Nuclear Waste Management Organization Report NWMO DGR-TR-2011-24 R000, Toronto, Canada.

International Subcommission on Stratigraphic Classification (ISSC), 1994. International Stratigraphic Guide -A guide to stratigraphic classification, terminology, and procedure (Amos Salvador, ed.). 2nd edition: The International Union of Geological Sciences and The Geological Society of America, Inc., 214 p.

International Subcommission on Stratigraphic Classification (ISSC), 1999. International Stratigraphic Guide - An abridged edition (Michael A. Murphy and Amos Salvador, eds.).: Episodes, v. 22, no. 4, pp. 255-271.

Jautzy, J.J., Petts, D.C., Clark, I.D., Al, T.A., Stern, R.A., and Jensen, M, 2020. Diagenetic evolution of a sedimentary system (Michigan Basin): Insights from petrography and S-isotope micro-analysis of pyrite. Chemical Geology, vol.541, p.1-14.

Johnson, M.D., Armstrong, D.K., Sanford, B.V., Telford, P.G. and Rutka, M.A. 1992. Paleozoic and Mesozoic geology of Ontario, in Thurston, P.C., Williams, H.R., Sutcliffe, R.H., and Stott, G.M., eds., Geology of Ontario. Ontario Geological Survey, Special Volume 4, Part 2, p.907-1008.

Kahle, O.F., 1988. Surface and subsurface paleokarst, Silurian Lockport and Peebles Dolomite, western Ohio, *in* James, N.P., and Choquette, P.W. (*eds*), Paleokarst. Springer Science+Business, New York, p.234-260, https://doi.org/10.1007/978-1-4612-3748-8

Kobluk, D.R., Pemberton, S.G., Karolyi, M. and Risk, M.J., 1977. The Silurian–Devonian disconformity in southern Ontario. Bulletin of Canadian Petroleum Geology, v.25, p.1157-1186.

Kolata, R., W.D. Huff and S.M. Bergstrom. 1998. Nature and regional significance of unconformities associated with Middle Ordovician Hagan K-bentonite complex in the North American midcontinent. Geological Society of America Bulletin 110, 723-739.

Legall, F.D., Barnes, C.R. and Macqueen, R.W. 1981., Thermal maturation, burial history, and hotspot development, Paleozoic strata of southern Ontario–Quebec, from conodont and acritarch colour alteration studies. Bulletin of Canadian Petroleum Geology, v.29, p.492-539.

Leighton, M.W. 1996. Interior cratonic basins: a record of regional tectonic influences, in vander Pluijm, B.A. and P.A. Catacosinos eds., Basement and Basins of North America.Geological Society of America Special Paper 308, p.77-93.

McMurray, M., 1985. Geology and organic geochemistry of Salina A-1 Carbonate oil source-rock lithofacies (Upper Silurian), southwestern Ontario. University of Waterloo, MSc thesis, Waterloo, ON, 236 p.

Morel, P. and E. Irving. 1978. Tentative paleocontinental maps for the early Phanerozoic and Proterozoic, Journal of Geology 86, 535–561.

Morrow, D. (1998). Regional subsurface dolomitization: models and constraints. Geoscience Canada.

Mussman, W.J., and Read, J.F., 1986. Sedimentology and development of a passive- to convergent-margin unconformity: Middle Ordovician Knox unconformity, Virginia Appalachians: Geological Society of America Bulletin, v. 97, p. 282-295.

Mussman, W.J., Montanez, I.P., and Read, J.F., 1988. Ordovician Knox paleokarst unconformity, Appalachians, *in* James, N.P., and Choquette, P.W. (*eds*), Paleokarst. Springer Science+Business, New York, p.234-260, https://doi.org/10.1007/978-1-4612-3748-8

Percival, J.A., and R.M. Easton, 2007. Geology of the Canadian Shield in Ontario: an Update. Ontario Power Generation, Report No. 06819-REP-01200-10158-R00, OGS Open File Report 6196, GSC Open File Report 5511.

Petts, D.C., Saso, J.K., Diamond, L.W., Aschwanden, L., Al, T.A., and Jensen, M., 2017. The source and evolution of paleofluids responsible for secondary minerals in low-permeability Ordovician limestones of the Michigan Basin. Applied Geochemistry, 86: p.121–137, doi:10.1016/j.apgeochem.2017.09.011.

Powell, T.G., R.W. MacQueen, J.F. Barker and D.G. Bree. 1984. Geochemical Character and Origin of Ontario Oils. Bulletin of Canadian Petroleum Geology 32, 289-312.

Prouty, C.E. 1988. Trenton exploration and wrench tectonics; Michigan Basin and environs. In: B.D. Keith (Ed.), The Trenton Group (Upper Ordovician series) of eastern North America, American Society of Petroleum Geologists Studies in Geology 29, 207-236.

Sanford, B.V., 1969. Silurian of southwestern Ontario. Ontario Petroleum Institute, Proceedings 8th Annual Conference, Toronto, Ontario, v.8, Technical Paper 5, 44p

Sanford, B.V., Thompson, F.J., and McFall, G.H., 1985. Plate tectonics – A possible controlling mechanism in the development of hydrocarbon traps in southwestern Ontario. Bulletin of Canadian Petroleum Geology v.33, p. 52-71

Sanford, B.V. 1993. St. Lawrence Platform: economic geology, in: Stott, D.F. and J.D. Aitken (Eds.) Sedimentary Cover of the Craton in Canada, ch.10. Geological Survey of Canada, Geology of Canada Series 5, p.787-798.

Shier, D. E. (2004). Well log normalization: Methods and guidelines. Petrophysics, 45(3), 268–280.

Somers, M.R., 2017. Paleozoic bedrock geology of southern Ontario. Oil, Gas and Salt Resources Library, Open File Data Release 2017-2, pdf file, accessed at https://s3.amazonaws.com/downloads.ogsrlibrary.com/open/OFDR-2017-2-OGSR-Petroleum-Well-Subcrop-Revision.pdf

Smith, L., 1990. Karst episodes during cyclic development of Silurian reef reservoirs, southwestern Ontario, in Carter, T.R., (ed.), Subsurface geology of southwestern Ontario − a core workshop. Ontario Petroleum Institute, London, ON, p. 69−88.

Sloss, L.L. 1963. Sequences in the cratonic interior of North America. Geological Society of America Bulletin 74, 93-114.

Sloss, L. L., 1988. Tectonic evolution of the craton in Phanerozoic time. The Geology of North America, 2, 25-51.

Sterling, S. and Schieck, D. 2014. Phase 1 Geoscientific Desktop Preliminary Assessment, Processing and Interpretation of Borehole Geophysical Log and 2D Seismic Data, Municipalities of Arran-Elderslie, Brockton and South Bruce, Township of Huron-Kinloss and Town of Saugeen Shores, Report NWMO APM-REP-06144-0110 prepared for the Nuclear Waste Management Organization, June, Toronto, Canada.

Sun, S. 2018. Stratigraphy of the Upper Silurian to Middle Devonian, southwestern Ontario. University of Western Ontario, London, Ontario, Electronic Thesis and Dissertation Repository, article 5230.

Sutcliffe, C.N., Thibodeau, A.M., Davis, D.W., Al-Aasm, I., Parmenter, A., Zajacz, Z., and Jensen, M., 2020. Hydrochronology of a proposed deep geological repository for low- and intermediate-level nuclear waste in southern Ontario from U–Pb dating of secondary minerals: response to Alleghanian events. Canadian Journal of Earth Sciences, vol 57, number 4, p.494-505.

Sutcliffe, C.N., Davis, D.W., Parmenter, A., Crowe, R., 2020. The utility of geochronology in constraining hydrogeological models: the application of U-Pb absolute ages to resolve timing of fluid flow in the Michigan Basin in southern Ontario. Canadian Society of Petroleum Geologists, Geoconference 2020, abstract

Tortola, M., 2019. Petrographic and geochemical attributes of Silurian and Devonian dolomitized formations in the Huron Domain, Michigan Basin. University of Windsor, Electronic Theses and Dissertations. 7740. https://scholar.uwindsor.ca/etd/7740

Tortola, M., Al-Aasm, I.S., and Crowe, R., 2020. Diagenetic Pore Fluid Evolution and Dolomitization of the Silurian and Devonian Carbonates, Huron Domain of Southwestern Ontario: Petrographic, Geochemical and Fluid Inclusion Evidence. Minerals, 10, 140, 52 p.Terzaghi, R.D., 1965. Sources of Error in Joint Surveys. Géotechnique 15, 287–304. https://doi.org/10.1680/geot.1965.15.3.287

Wang, H.F., K.D. Crowley and G.C. Nadon. 1994. Thermal History of the Michigan Basin from Apatite Fission-Track Analysis and Vitrinite Reflectance. In Basin Compartments and Seals, P. J. Ortoleva (Ed.), AAPG Memoir 61, 167-178.

White, D.J., D.A. Forsyth, I. Asudeh, S.D. Carr, H. Wu, R.M. Easton, and R.F. Mereu, 2000. A seismic-based cross-section of the Grenville Origen in southern Ontario, and western Quebec, Canadian Journal of Earth Sciences, Vol. 37, pp. 183-192.

Wigston, A. and Heagle, D., 2010. Bedrock Formations in DGR-1, DGR-2.

Worthington, S.R.H. 2011. Karst assessment. Nuclear Waste Management Organization, Report NWMO DGR-TR-2011-22, Toronto, Canada, accessed June 11, 2013 at: http://www.nwmo.ca/uploads/DGR%20PDF/Geo/Karst-Assessment.pdf, 17 p.

Uyeno, T.T., Telford, P.G. and Sanford, B.V., 1982. Devonian conodonts and stratigraphy of southwestern Ontario. Geological Survey of Canada, Bulletin 332, 55p.

Ziegler, A.M., C.R. Scotese, W.S. McKerrow, M.E. Johnson and R.K. Bambach. 1977. Paleozoic biogeography of continents bordering the Iapetus (pre-Caledonian) and Rheic (pre-Hercynian) oceans. Contributions in Biology and Geology 2, 1-22.

Appendix A:

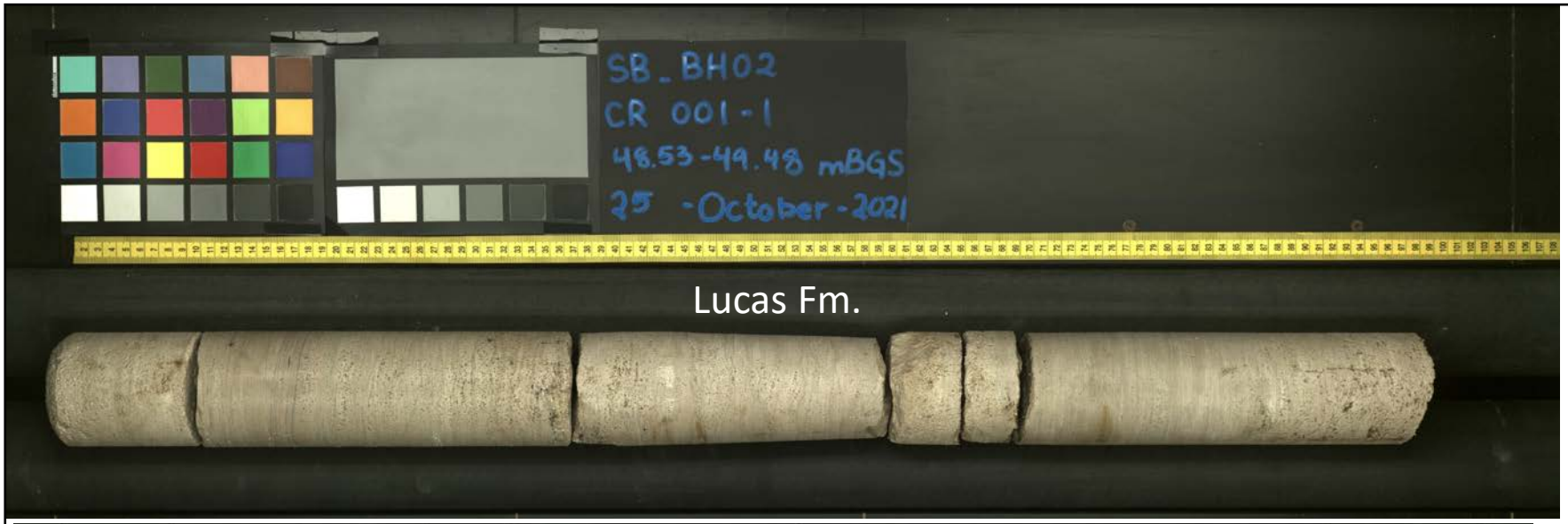
Summary List of Work Packages Completed for SB_BH02

Number	Work Package Name
WP01	Site Infrastructure and Access Road Construction
WP02	Borehole Drilling and Coring
WP03	Geological and Geotechnical Core Logging, Photography and Sampling
WP04A	Petrophysics Testing
WP04B	Geomechanical Testing of Core
WP04C	Porewater, Noble Gas, and Dissolved Gas Extraction and Analysis
WP04D	Mineralogy and Geochemical Analysis of Core
WP04E	Sorption Core Testing
WP04F	Measurement of Surface Area and Cation Exchange Capacity
WP04G	Organic Geochemistry and Clay Mineralogy
WP05	Geophysical Well Logging and Interpretation
WP06	Hydraulic Testing
WP07	Opportunistic Groundwater Sampling and Testing
WP08	Temporary Well Sealing
WP09	Instrumentation
WP10	Single Borehole Data Integration (Based on WP03 and WP05 Formation Top Data Only)

Appendix B:

Core Photo Compilation of Interpreted Formations and Structures for SB_BH02

Appendix B-Lithology and Structures





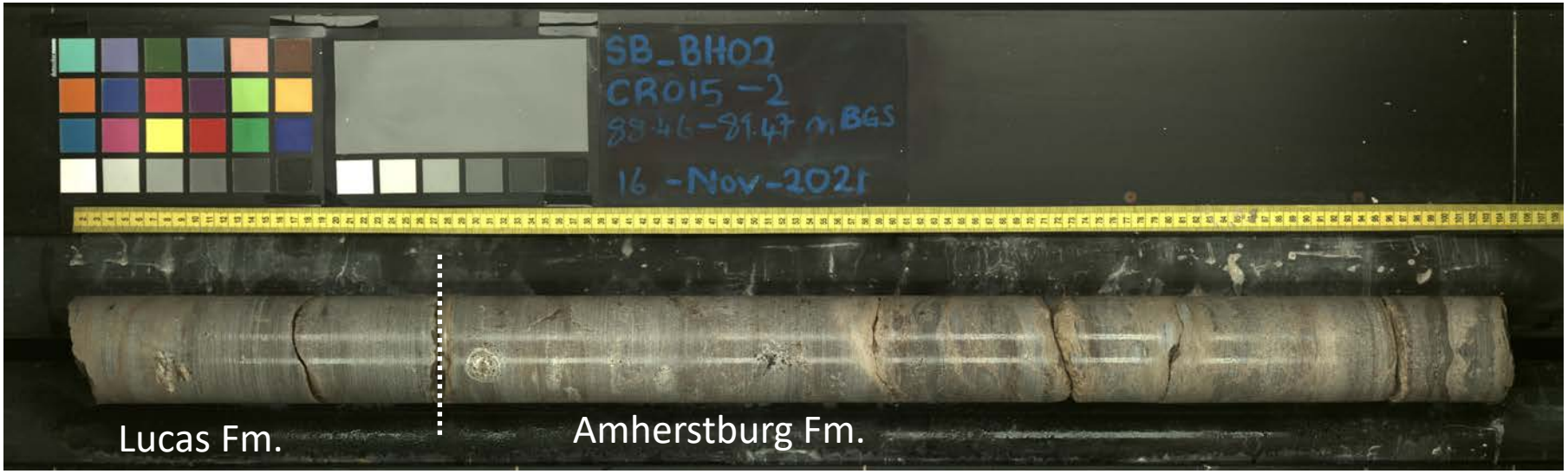
B1-Lucas Formation

SB_BH02 Representative Photos for Formations and Members

nwmo

NUCLEAR WASTE MANAGEMENT ORGANIZATION

SOCIÉTÉ DE GESTION DES DÉCHETS NUCLÉAIRES





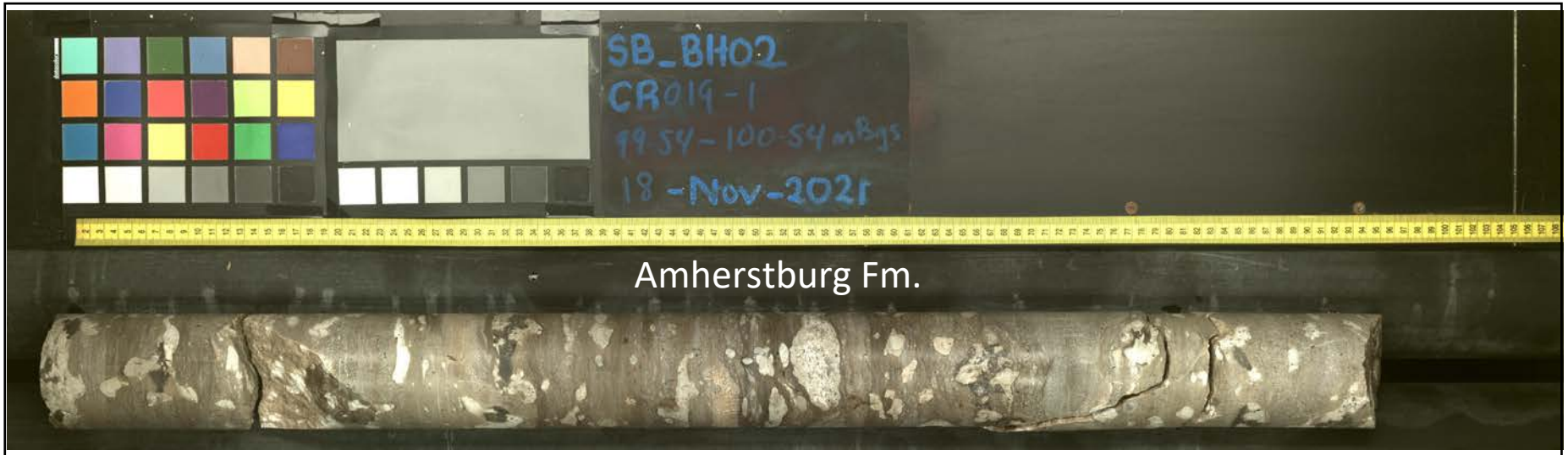
B2-Lucas-Amherstburg Formation

SB_BH02 Representative Photos for Formations and Members

nwmo

NUCLEAR WASTE MANAGEMENT ORGANIZATION

SOCIÉTÉ DE GESTION DES DÉCHETS NUCLÉAIRES

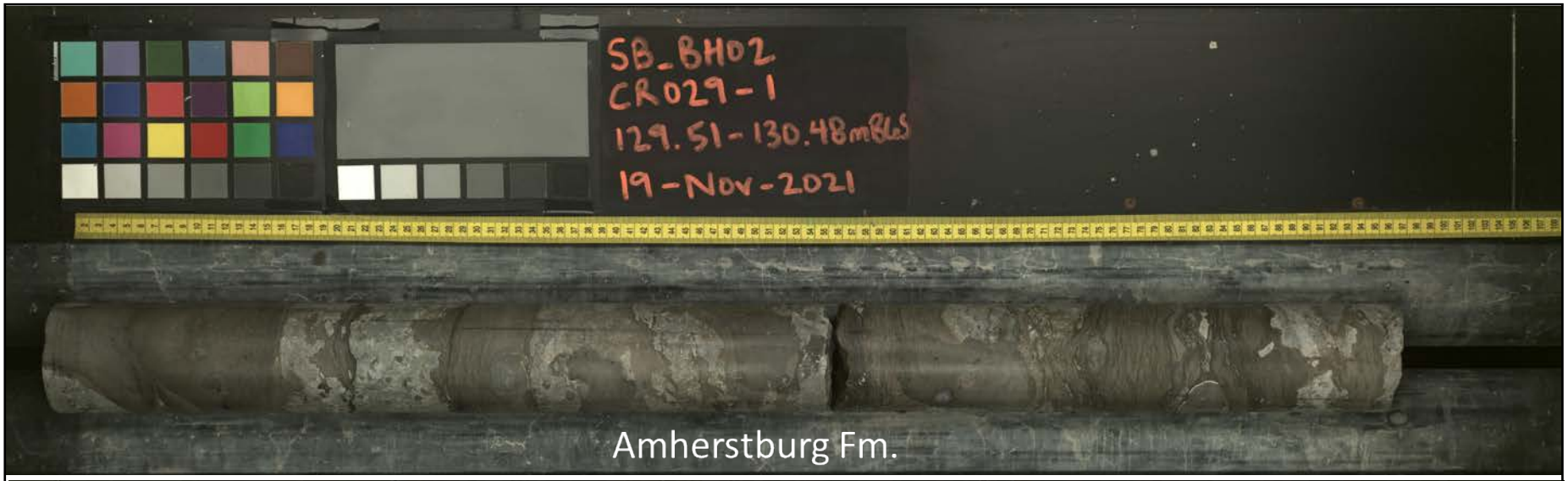




B-3 Amherstburg Formation

SB_BH02 Representative Photos for Formations and Members

NUCLEAR WASTE MANAGEMENT ORGANIZATION
SOCIÉTÉ DE GESTION DES DÉCHETS NUCLÉAIRES

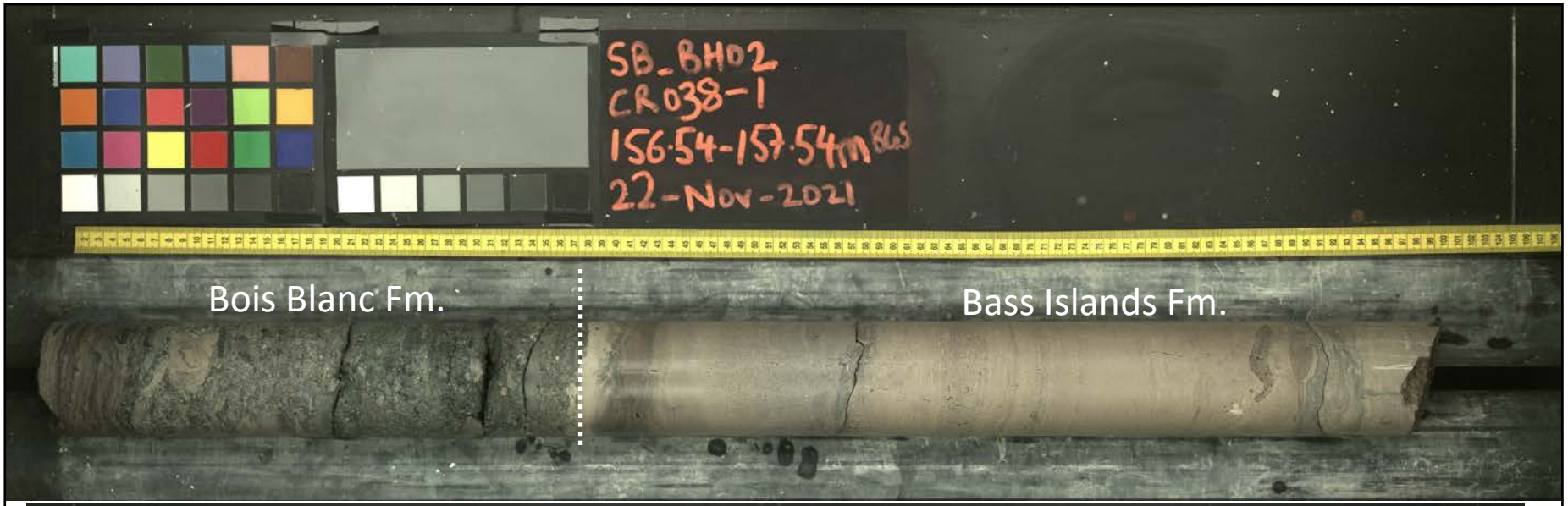




B-4 Amherstburg- Bois Blanc Formation

SB_BH01 Representative Photos for Formations and Members

NUCLEAR WASTE MANAGEMENT ORGANIZATION
SOCIÉTÉ DE GESTION DES DÉCHETS NUCLÉAIRES





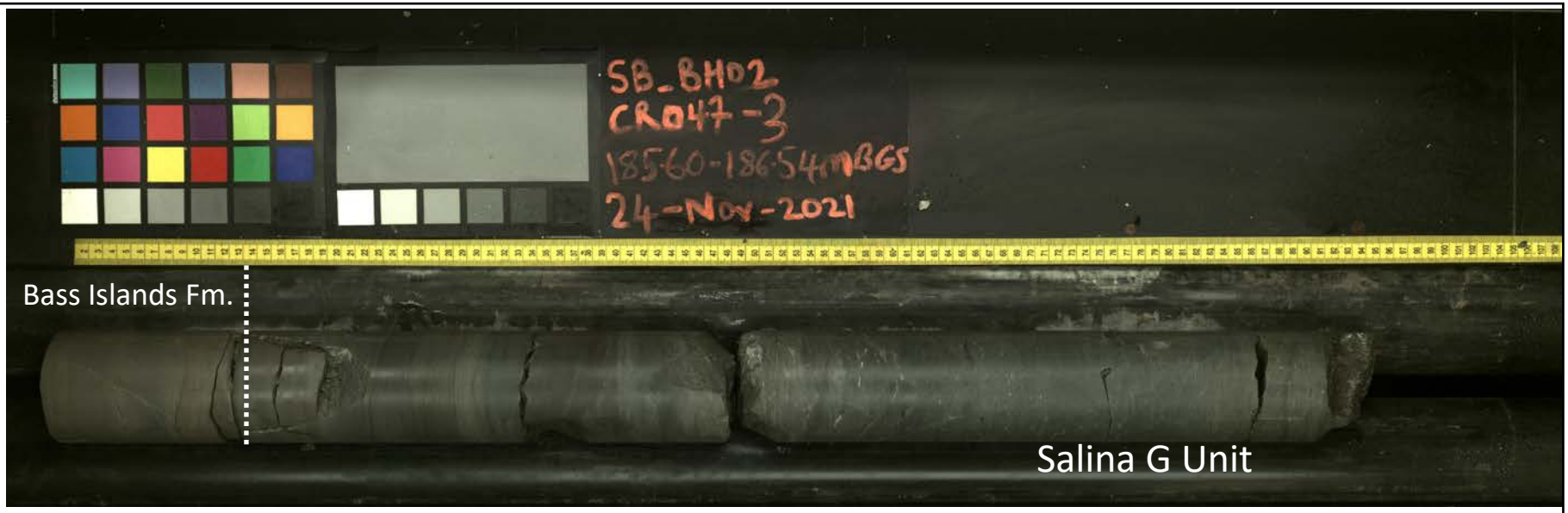
B-5 Bois Blanc-Bass Islands Formation

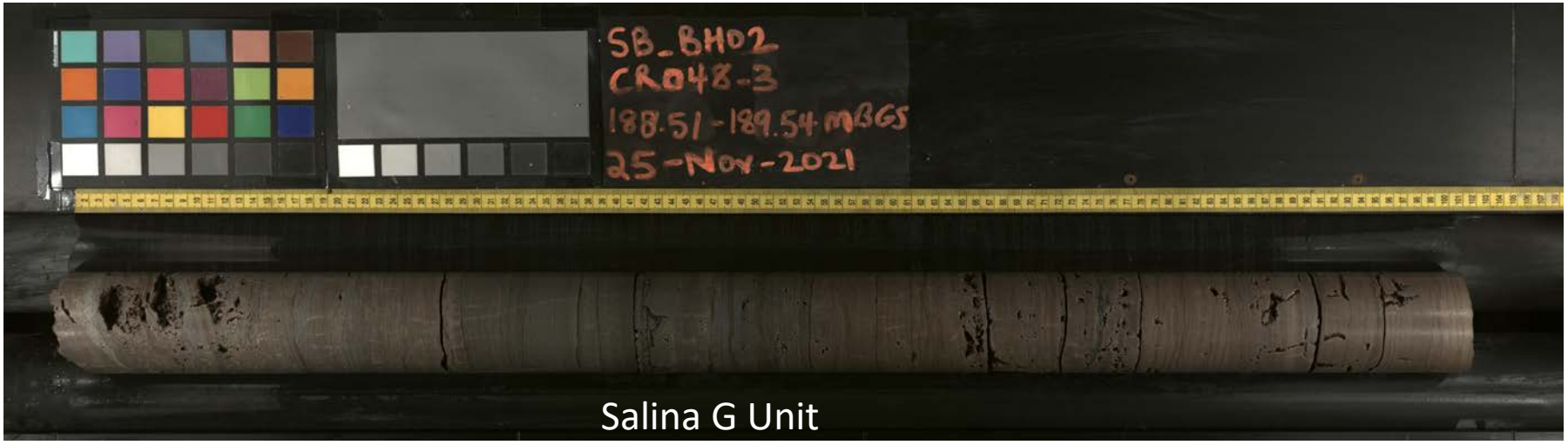
SB_BH02 Representative Photos for Formations and Members

nwmo

NUCLEAR WASTE MANAGEMENT ORGANIZATION

SOCIÉTÉ DE GESTION DES DÉCHETS NUCLÉAIRES





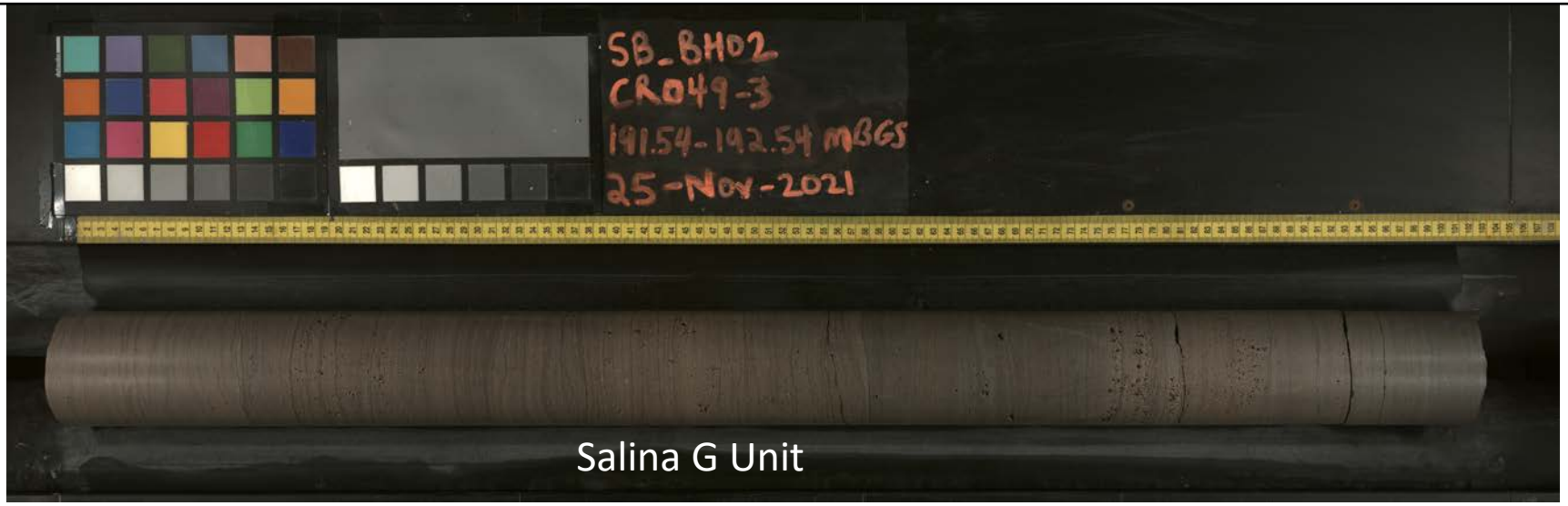
B-6 Bass Islands-Salina G Unit

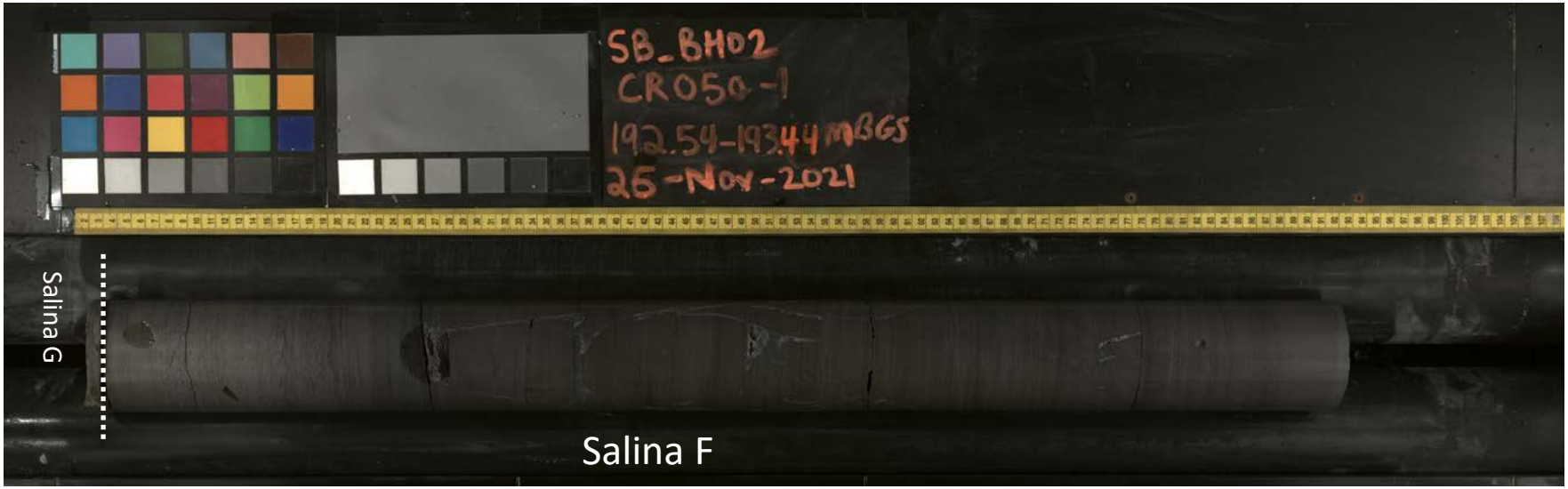
SB_BH02 Representative Photos for Formations and Members

nwmo

NUCLEAR WASTE MANAGEMENT ORGANIZATION

SOCIÉTÉ DE GESTION DES DÉCHETS NUCLÉAIRES





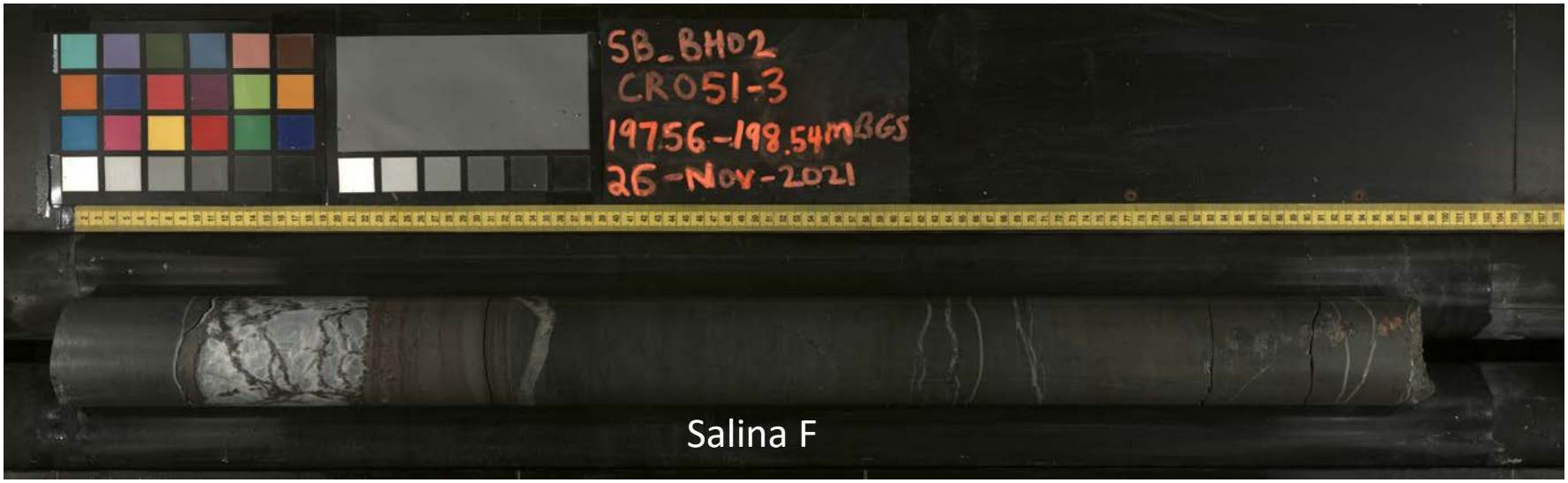
B-7 Salina G Unit-Salina F Unit

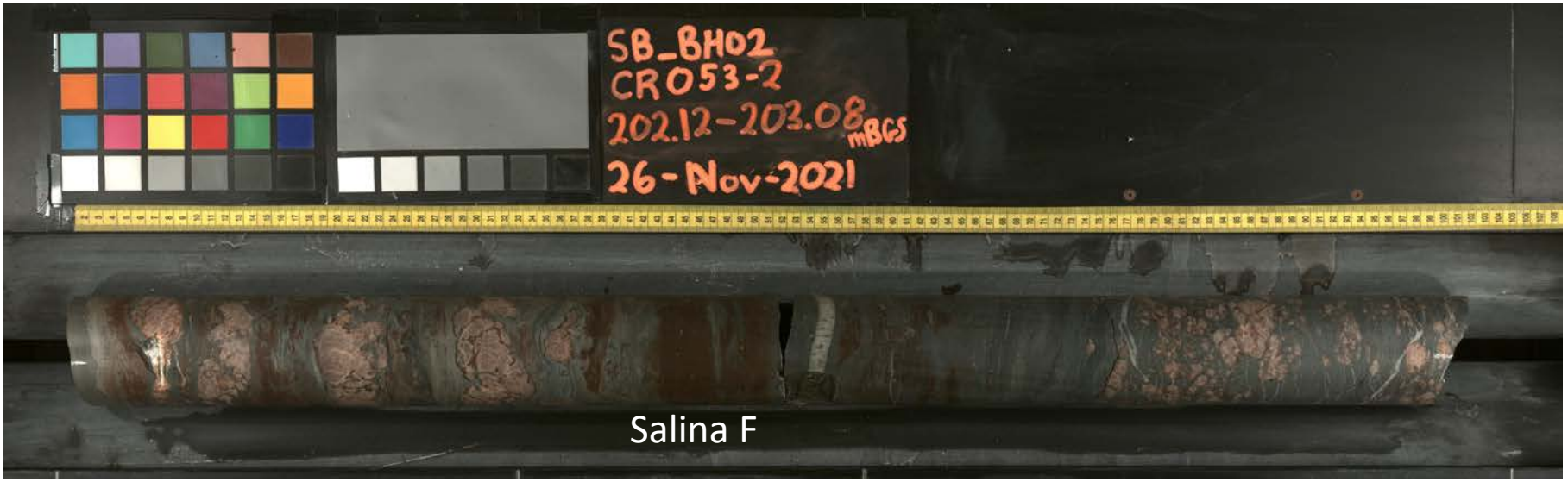
SB_BH02 Representative Photos for Formations and Members

nwmo

NUCLEAR WASTE MANAGEMENT ORGANIZATION

SOCIÉTÉ DE GESTION DES DÉCHETS NUCLÉAIRES





B-8 Salina F Unit

SB_BH02 Representative Photos for Formations and Members

nwmo

NUCLEAR WASTE MANAGEMENT ORGANIZATION

SOCIÉTÉ DE GESTION DES DÉCHETS NUCLÉAIRES





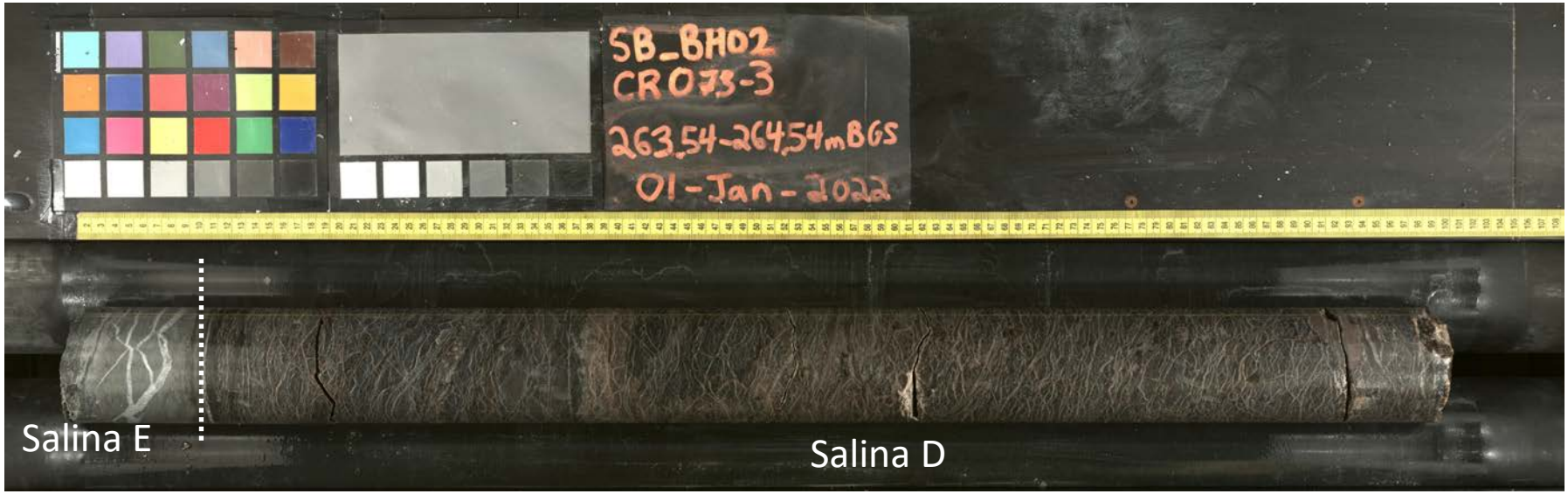
B-9 Salina F Unit- Salina E Unit

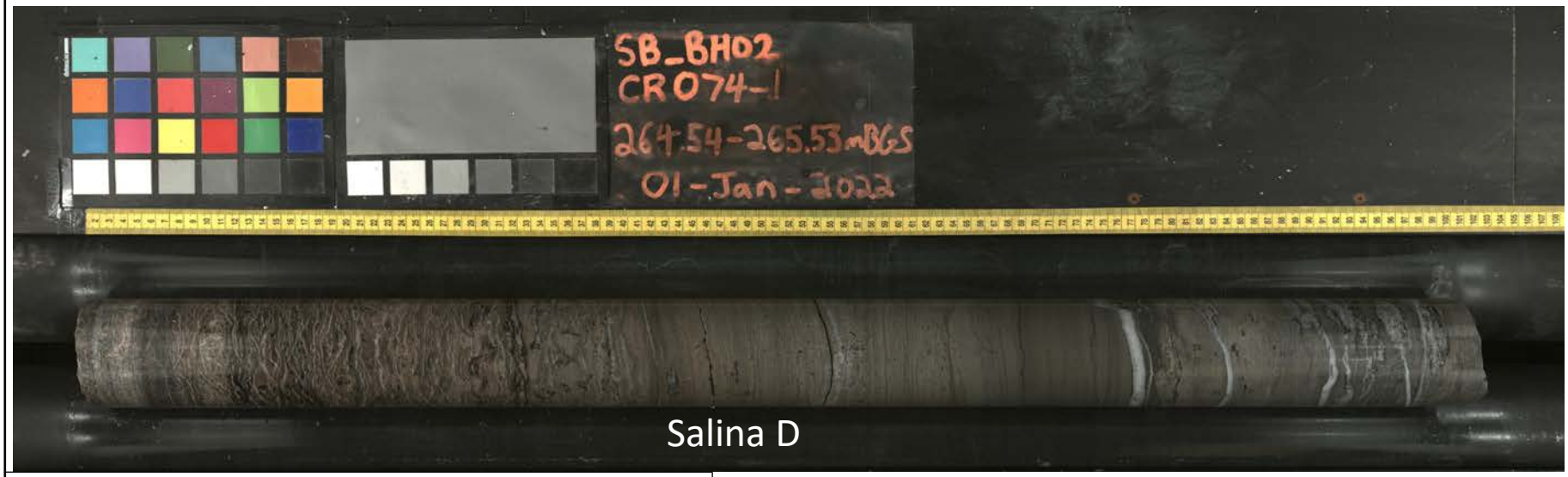
SB_BH02 Representative Photos for Formations and Members

nwmo

NUCLEAR WASTE MANAGEMENT ORGANIZATION

SOCIÉTÉ DE GESTION DES DÉCHETS NUCLÉAIRES





B-10 Salina E Unit-Salina D Unit

SB_BH02 Representative Photos for Formations and Members

nwmo

NUCLEAR WASTE MANAGEMENT ORGANIZATION

SOCIÉTÉ DE GESTION DES DÉCHETS NUCLÉAIRES





B-11 Salina D Unit- Salina C Unit

SB_BH02 Representative Photos for Formations and Members

nwmo

NUCLEAR WASTE MANAGEMENT ORGANIZATION

SOCIÉTÉ DE GESTION DES DÉCHETS NUCLÉAIRES





B-12 Salina C Unit-Salina B Unit

SB_BH02 Representative Photos for Formations and Members

nwmo
NUCLEAR WASTE MANAGEMENT ORGANIZATION
SOCIÉTÉ DE GESTION DES DÉCHETS NUCLÉAIRES





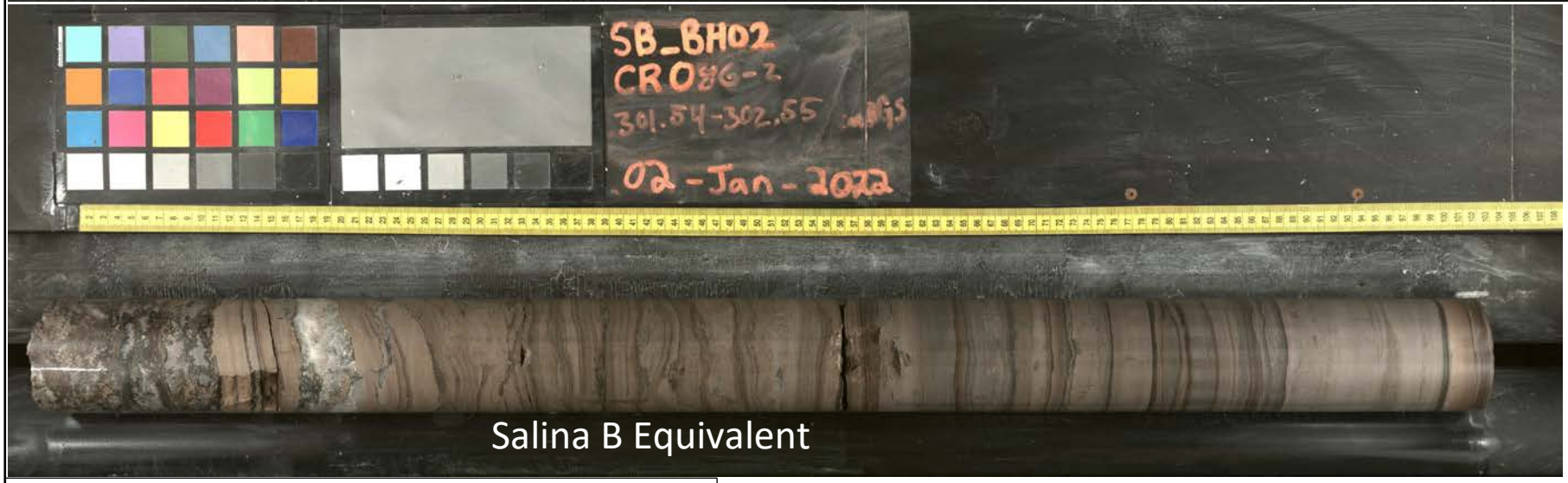
B-13 Salina B Unit- Salina B Equivalent

SB_BH02 Representative Photos for Formations and Members

NUCLEAR WASTE MANAGEMENT ORGANIZATION
SOCIÉTÉ DE GESTION DES DÉCHETS NUCLÉAIRES



Salina B Equivalent



Salina B Equivalent

B-14 Salina B Equivalent

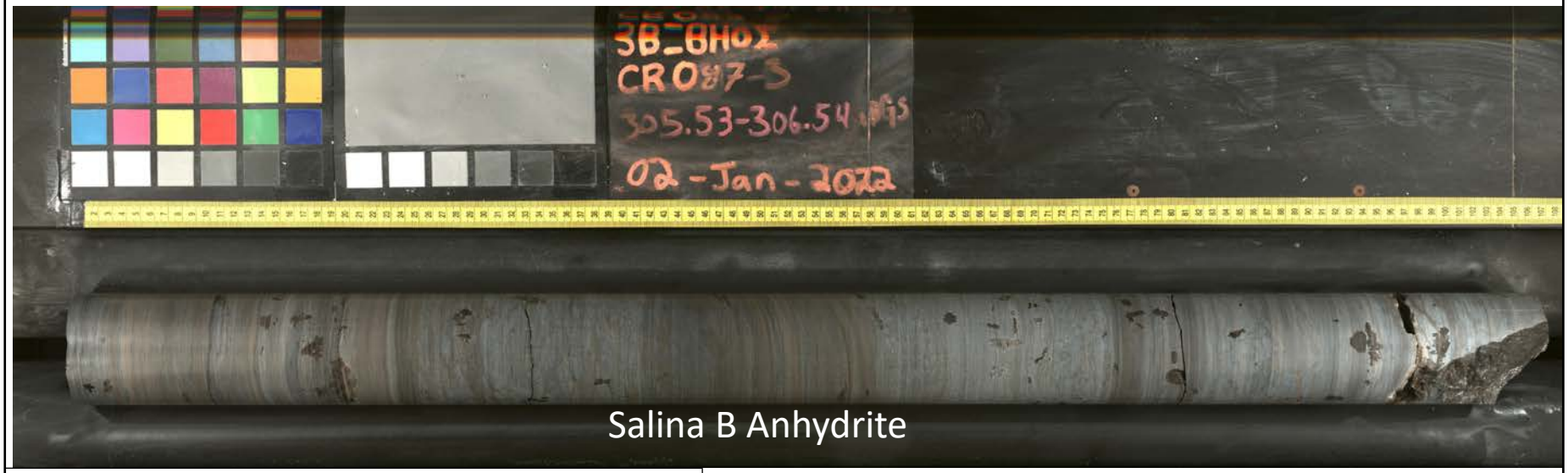
SB_BH02 Representative Photos for Formations and Members

nwmo

NUCLEAR WASTE MANAGEMENT ORGANIZATION

SOCIÉTÉ DE GESTION DES DÉCHETS NUCLÉAIRES





B-15 Salina B Equivalent-Salina B Anhydrite

SB_BH02 Representative Photos for Formations and Members

nwmo

NUCLEAR WASTE MANAGEMENT ORGANIZATION

SOCIÉTÉ DE GESTION DES DÉCHETS NUCLÉAIRES





B-16 Salina B Anhydrite-Salina A-2 Unit Carbonate

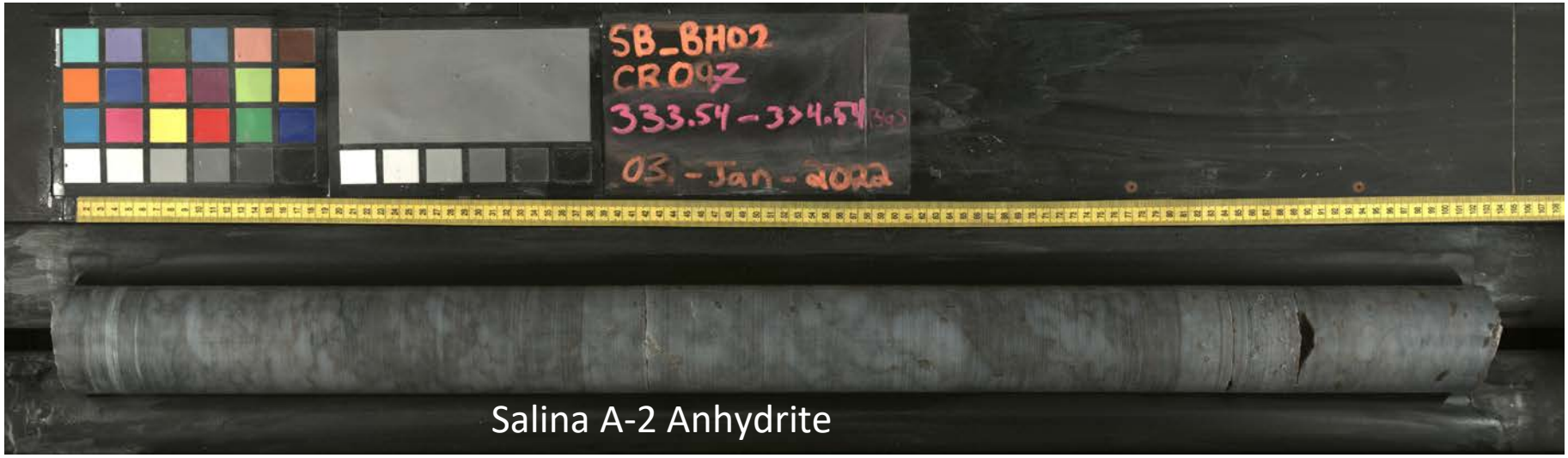
SB_BH02 Representative Photos for Formations and Members

nwmo

NUCLEAR WASTE MANAGEMENT ORGANIZATION

SOCIÉTÉ DE GESTION DES DÉCHETS NUCLÉAIRES





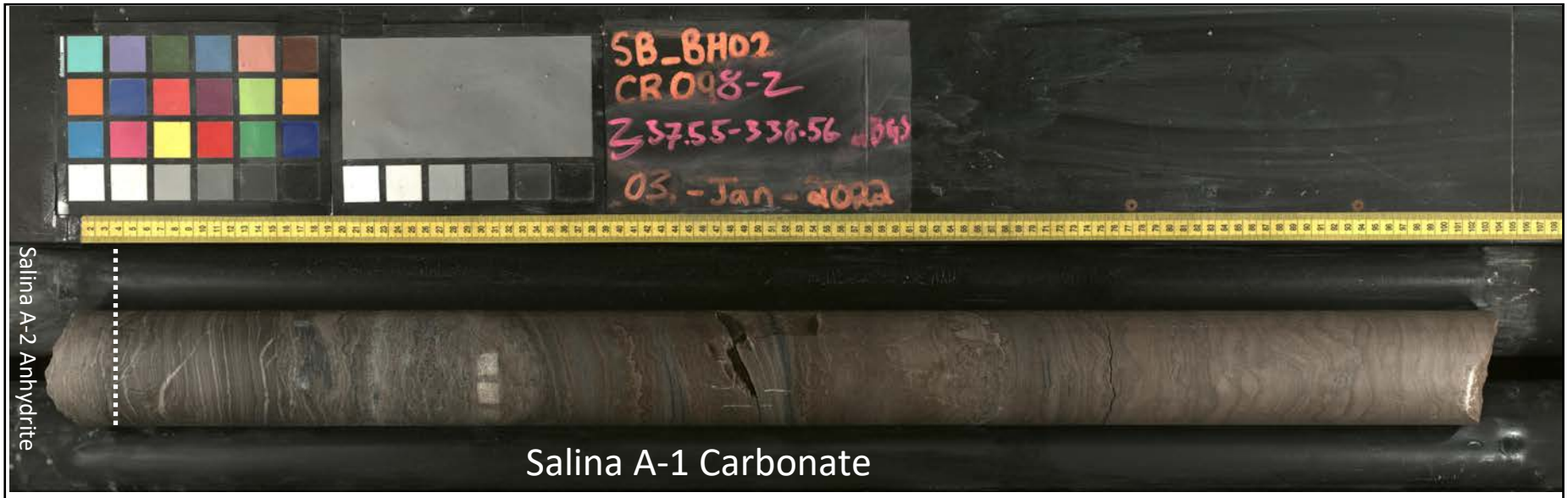
B-17 Salina A-2 Unit Carbonate-Salina A-2 Unit Anhydrite

SB_BH02 Representative Photos for Formations and Members

nwmo

NUCLEAR WASTE MANAGEMENT ORGANIZATION

SOCIÉTÉ DE GESTION DES DÉCHETS NUCLÉAIRES





B-18 Salina A-2 Unit Anhydrite-Salina A-1 Unit Carbonate

SB_BH02 Representative Photos for Formations and Members

nwmo

NUCLEAR WASTE MANAGEMENT ORGANIZATION

SOCIÉTÉ DE GESTION DES DÉCHETS NUCLÉAIRES



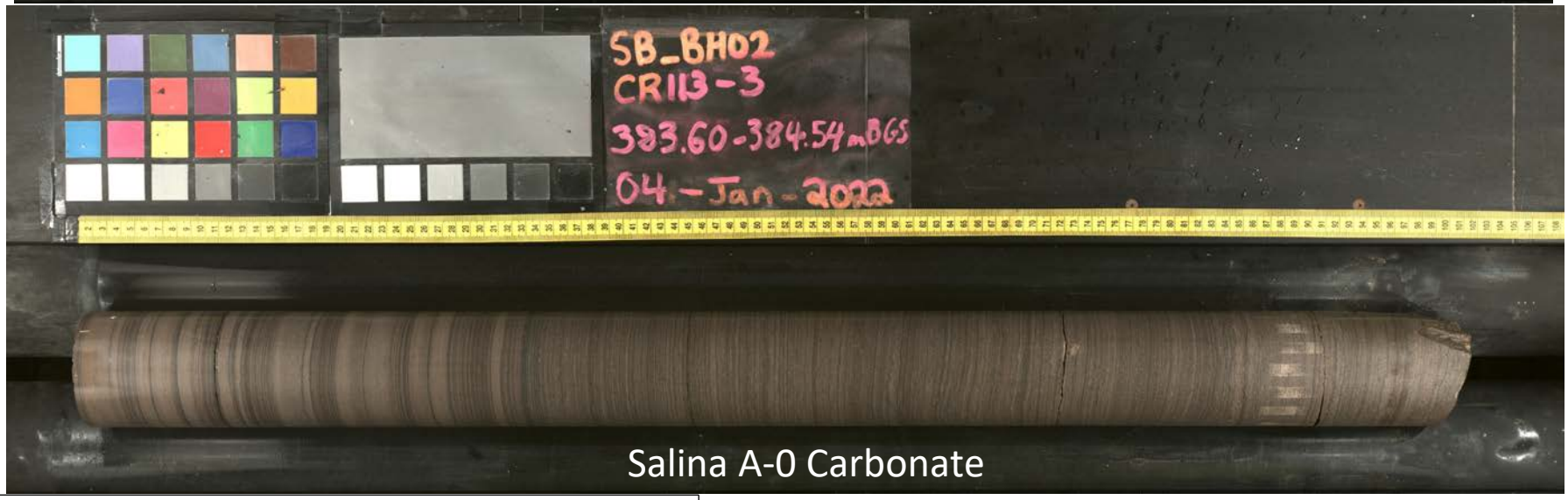


B-19 Salina A-1 Unit Carbonate- Salina A-1 Unit Evaporite

SB_BH02 Representative Photos for Formations and Members

NUCLEAR WASTE MANAGEMENT ORGANIZATION
SOCIÉTÉ DE GESTION DES DÉCHETS NUCLÉAIRES





B-20 Salina A-1 Evaporite and Salina A-0 Carbonate

SB_BH02 Representative Photos for Formations and Members

nwmo

NUCLEAR WASTE MANAGEMENT ORGANIZATION

SOCIÉTÉ DE GESTION DES DÉCHETS NUCLÉAIRES





B-21 Salina A-1 Carbonate,Guelph Formation

SB_BH02 Representative Photos for Formations and Members

nwmo
NUCLEAR WASTE MANAGEMENT ORGANIZATION
SOCIÉTÉ DE GESTION DES DÉCHETS NUCLÉAIRES





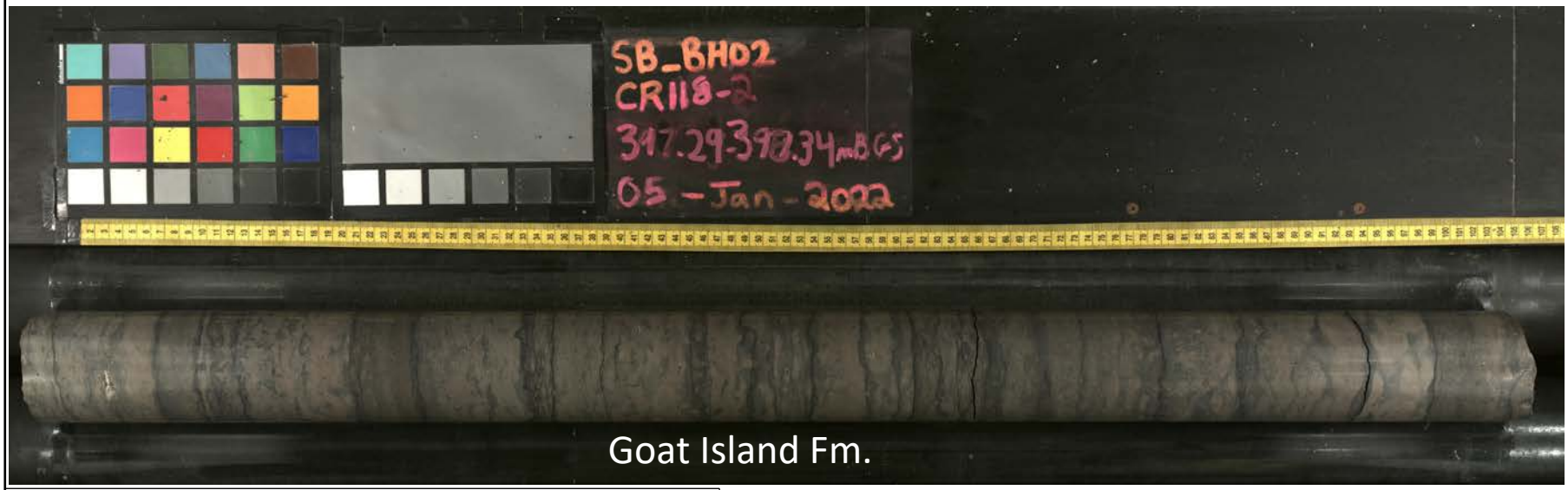
B-22 Guelph-Goat Island Formation

SB_BH02 Representative Photos for Formations and Members

nwmo
NUCLEAR WASTE MANAGEMENT ORGANIZATION
SOCIÉTÉ DE GESTION DES DÉCHETS NUCLÉAIRES



Goat Island Fm.



Goat Island Fm.

B-23 Goat Island Formation

SB_BH02 Representative Photos for Formations and Members

nwmo

NUCLEAR WASTE MANAGEMENT ORGANIZATION

SOCIÉTÉ DE GESTION DES DÉCHETS NUCLÉAIRES





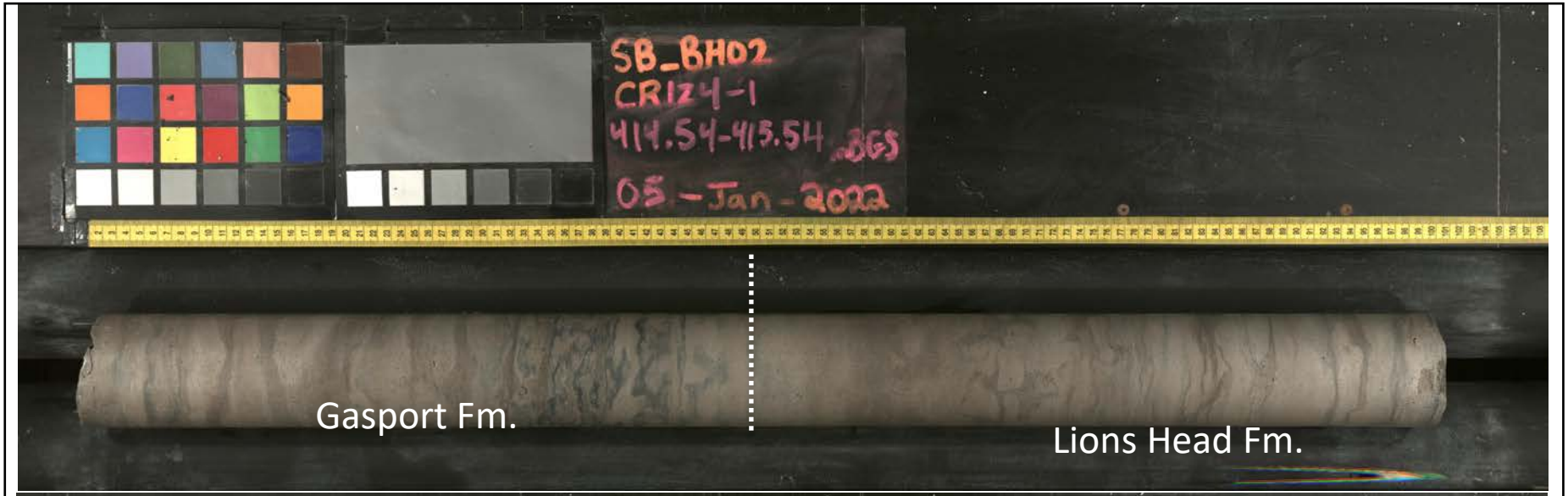
B-24 Goat Island-Gasport Formation

SB_BH02 Representative Photos for Formations and Members

nwmo

NUCLEAR WASTE MANAGEMENT ORGANIZATION

SOCIÉTÉ DE GESTION DES DÉCHETS NUCLÉAIRES





B-25 Gasport-Lions Head Formation

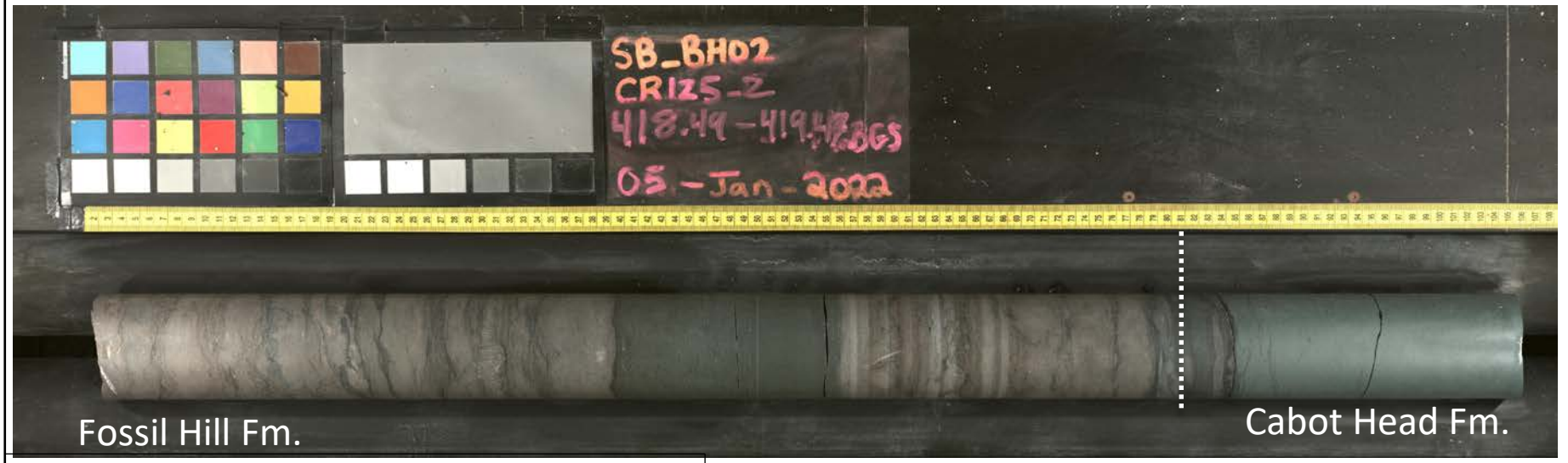
SB_BH02 Representative Photos for Formations and Members

nwmo

NUCLEAR WASTE MANAGEMENT ORGANIZATION

SOCIÉTÉ DE GESTION DES DÉCHETS NUCLÉAIRES





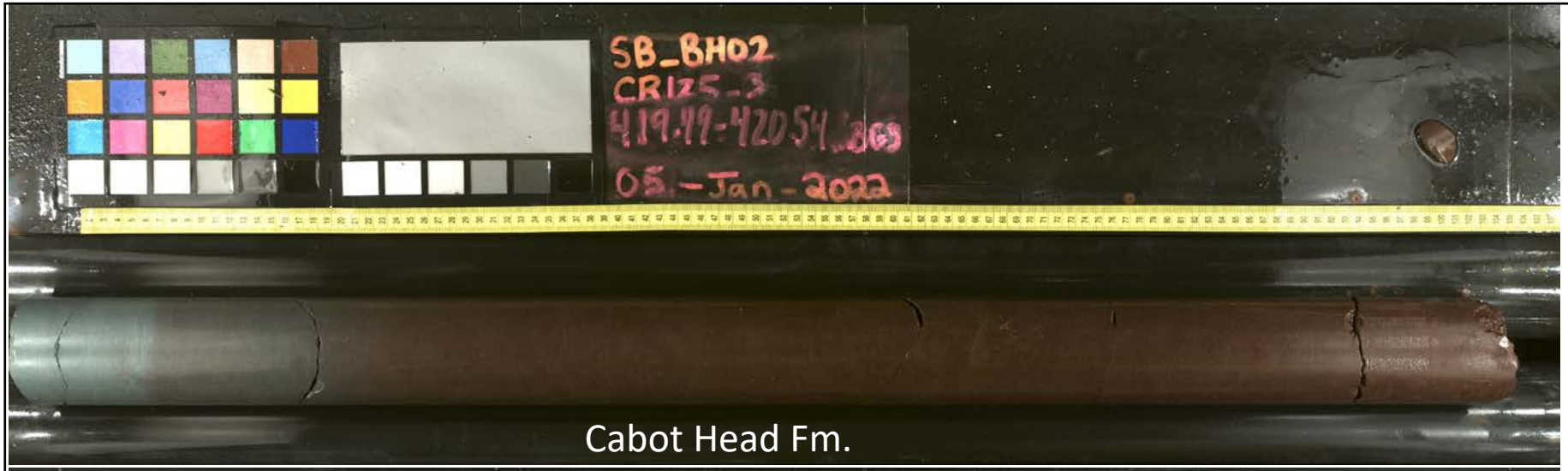
B-26 Lions Head-Fossil Hill Fm, Fossil Hill- Cabot Head Fm.

SB_BH02 Representative Photos for Formations and Members

nwmo

NUCLEAR WASTE MANAGEMENT ORGANIZATION

SOCIÉTÉ DE GESTION DES DÉCHETS NUCLÉAIRES



Cabot Head Fm.



Cabot Head Fm.

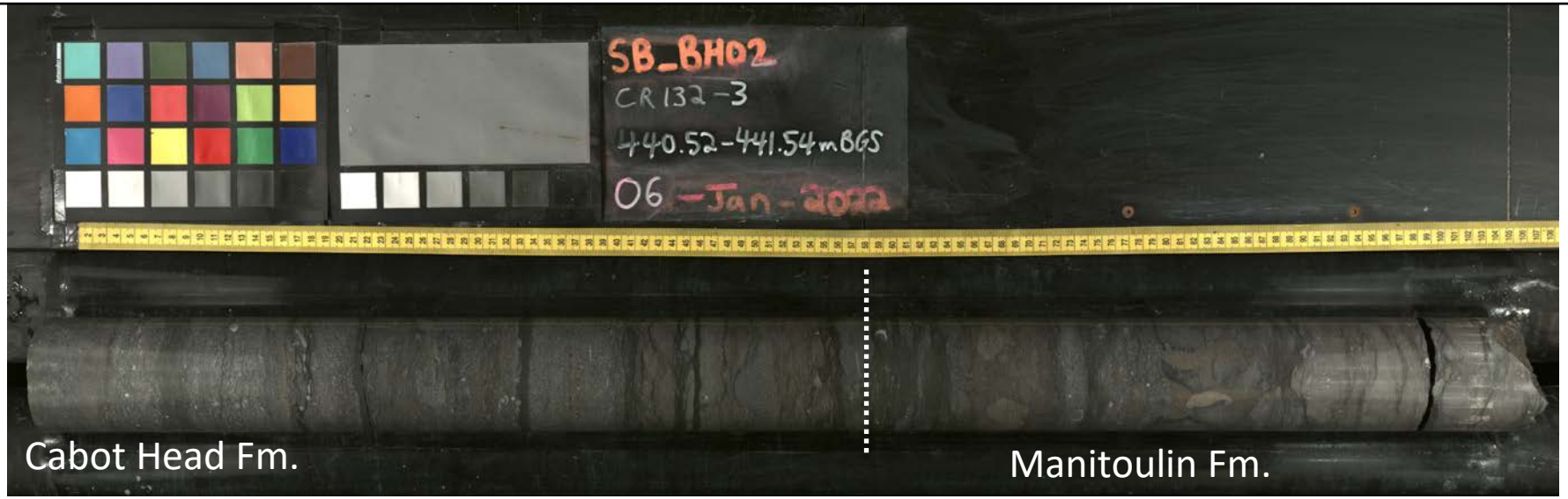
B-27 Cabot Head Formation

SB_BH02 Representative Photos for Formations and Members

nwmo

NUCLEAR WASTE MANAGEMENT ORGANIZATION

SOCIÉTÉ DE GESTION DES DÉCHETS NUCLÉAIRES





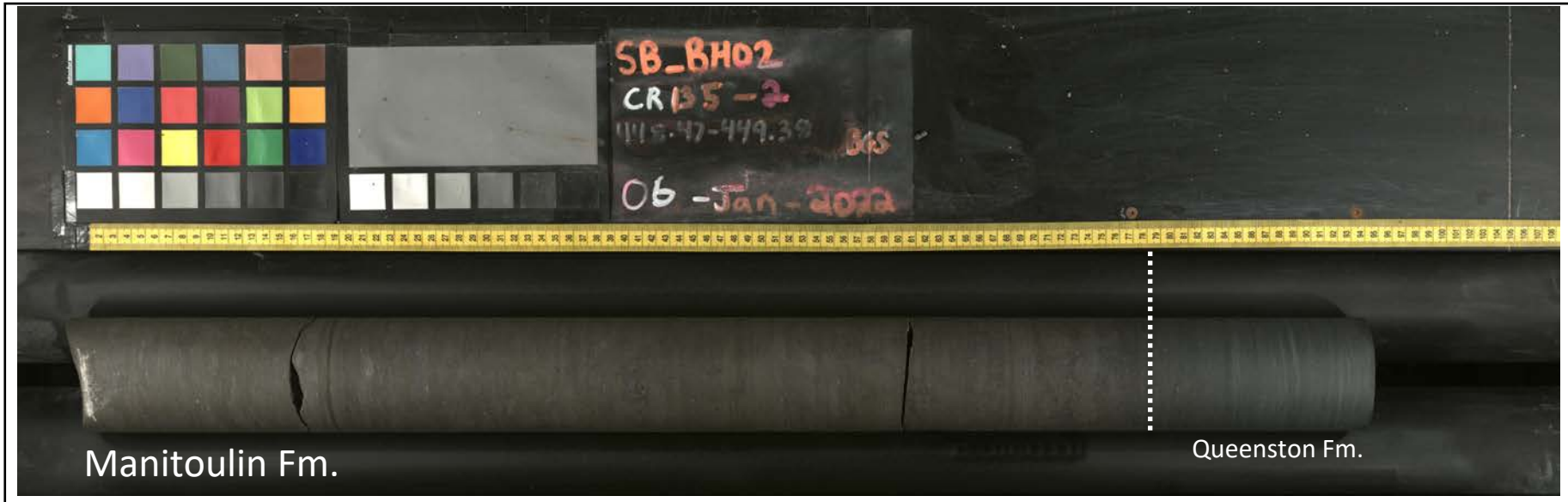
B-28 Cabot Head-Manitoulin Formation

SB_BH02 Representative Photos for Formations and Members

nwmo

NUCLEAR WASTE MANAGEMENT ORGANIZATION

SOCIÉTÉ DE GESTION DES DÉCHETS NUCLÉAIRES





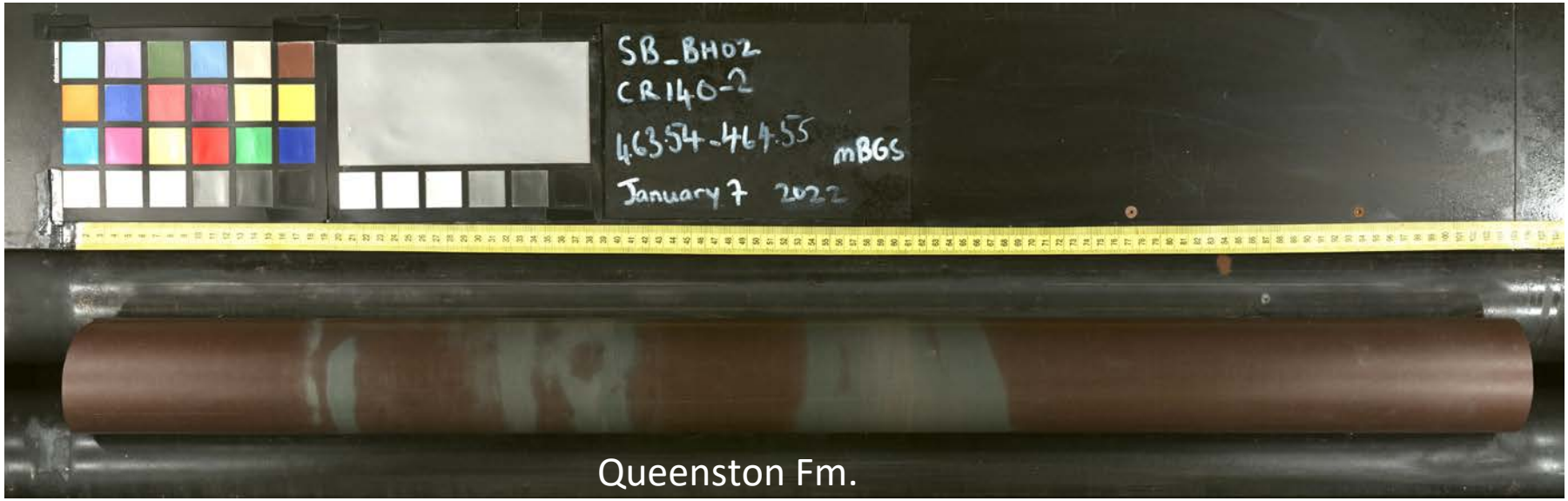
B-29 Manitoulin-Queenston Formation

SB_BH02 Representative Photos for Formations and Members

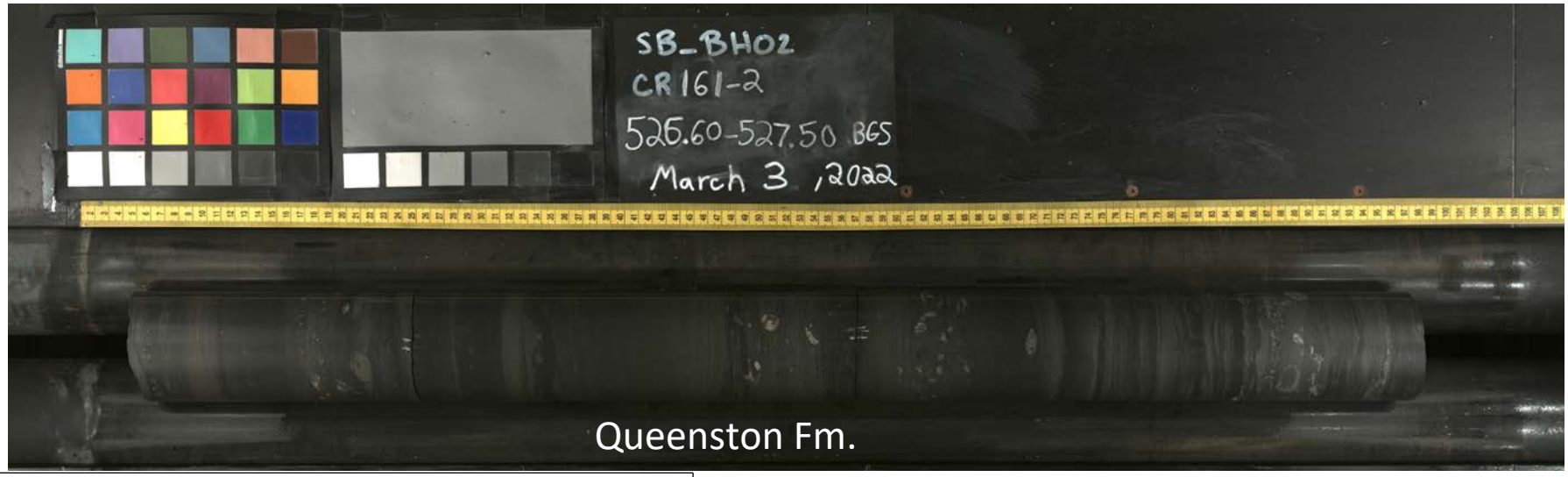
nwmo

NUCLEAR WASTE MANAGEMENT ORGANIZATION

SOCIÉTÉ DE GESTION DES DÉCHETS NUCLÉAIRES



Queenston Fm.



Queenston Fm.

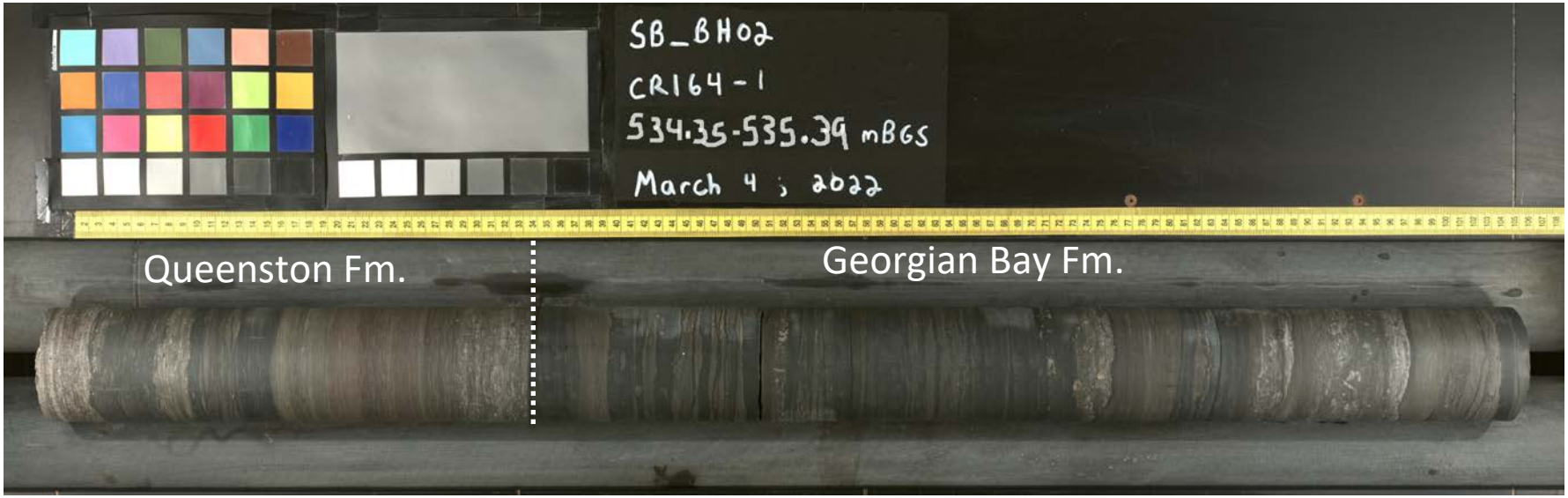
B-30 Queenston Formation

SB_BH02 Representative Photos for Formations and Members

nwmo

NUCLEAR WASTE MANAGEMENT ORGANIZATION

SOCIÉTÉ DE GESTION DES DÉCHETS NUCLÉAIRES

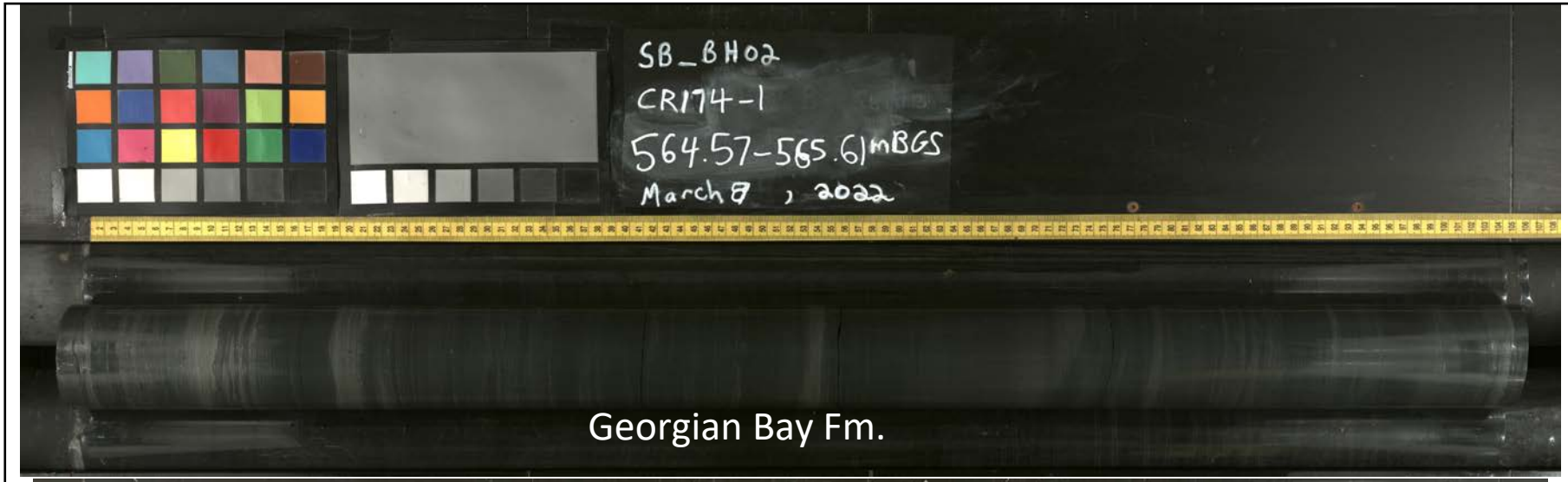




B-31 Queenston-Georgian Bay Formation

SB_BH02 Representative Photos for Formations and Members

NUCLEAR WASTE MANAGEMENT ORGANIZATION
SOCIÉTÉ DE GESTION DES DÉCHETS NUCLÉAIRES



Georgian Bay Fm.

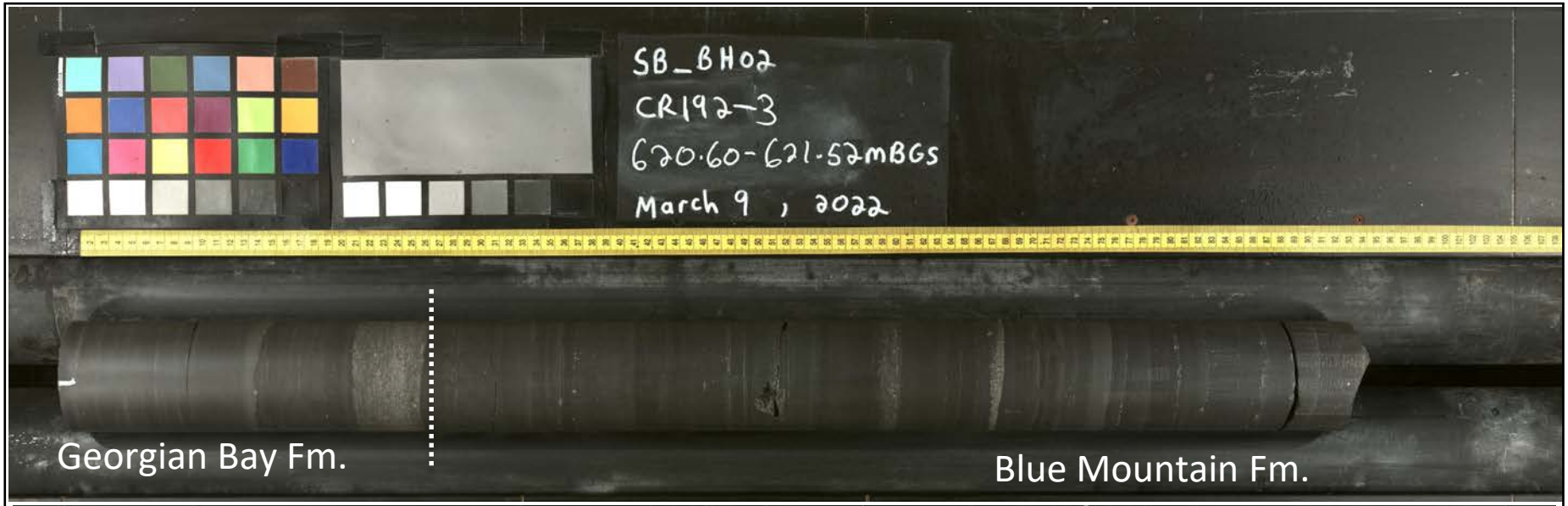


Georgian Bay Fm.

B-32 Georgian Bay Formation

SB_BH02 Representative Photos for Formations and Members

NUCLEAR WASTE MANAGEMENT ORGANIZATION
SOCIÉTÉ DE GESTION DES DÉCHETS NUCLÉAIRES





B-33 Georgian Bay-Blue Mountain Formation

SB_BH02 Representative Photos for Formations and Members

nwmo

NUCLEAR WASTE MANAGEMENT ORGANIZATION

SOCIÉTÉ DE GESTION DES DÉCHETS NUCLÉAIRES



Blue Mountain Fm.



Blue Mountain Fm.

B-34 Blue Mountain Formation

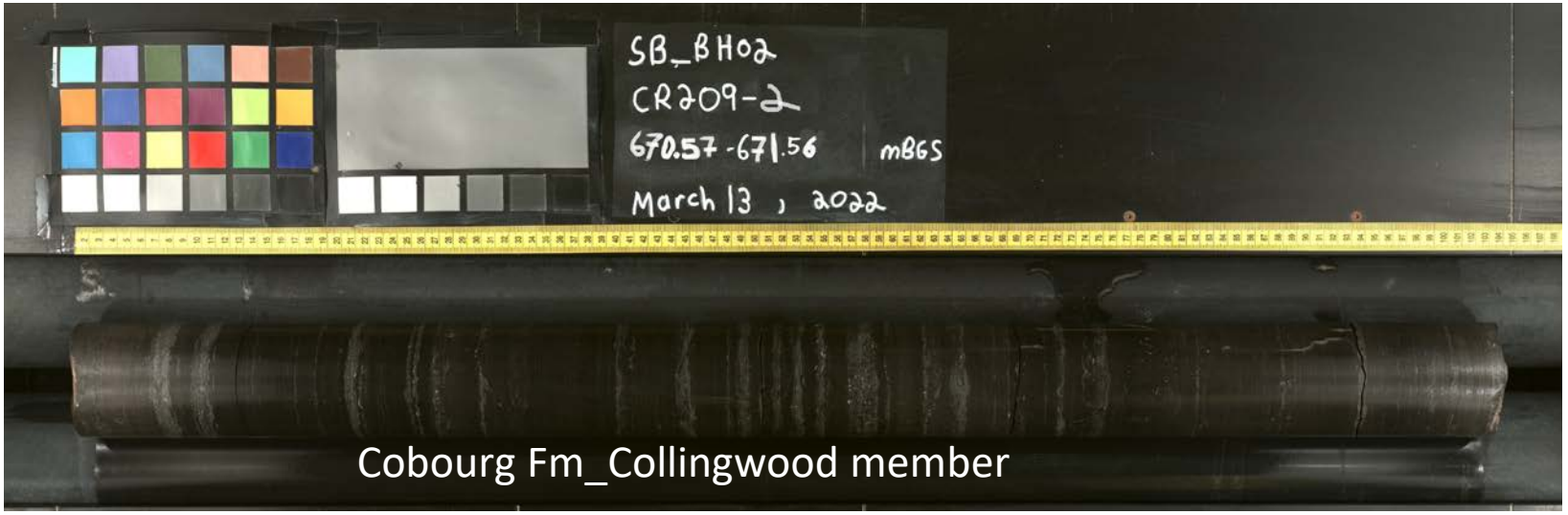
SB_BH02 Representative Photos for Formations and Members

nwmo

NUCLEAR WASTE MANAGEMENT ORGANIZATION

SOCIÉTÉ DE GESTION DES DÉCHETS NUCLÉAIRES





B-35 Blue Mountain-Cobourg Formation_Collingwood member

SB_BH02 Representative Photos for Formations and Members

nwmo

NUCLEAR WASTE MANAGEMENT ORGANIZATION

SOCIÉTÉ DE GESTION DES DÉCHETS NUCLÉAIRES



Cobourg Fm_Collingwood Member



Cobourg Fm_Collingwood Member

B-36 Cobourg Formation_Collingwood member

SB_BH02 Representative Photos for Formations and Members

nwmo

NUCLEAR WASTE MANAGEMENT ORGANIZATION

SOCIÉTÉ DE GESTION DES DÉCHETS NUCLÉAIRES



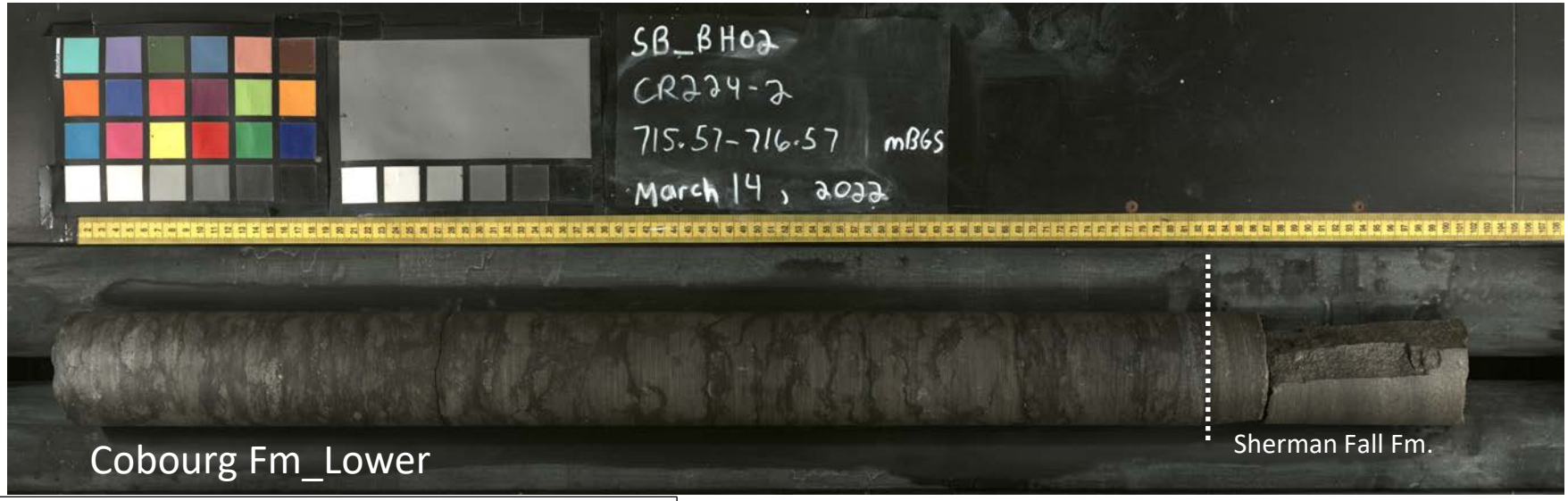


B-37 Cobourg_Collingwood member-CobourgFormation_Lower

SB_BH02 Representative Photos for Formations and Members

NUCLEAR WASTE MANAGEMENT ORGANIZATION
SOCIÉTÉ DE GESTION DES DÉCHETS NUCLÉAIRES





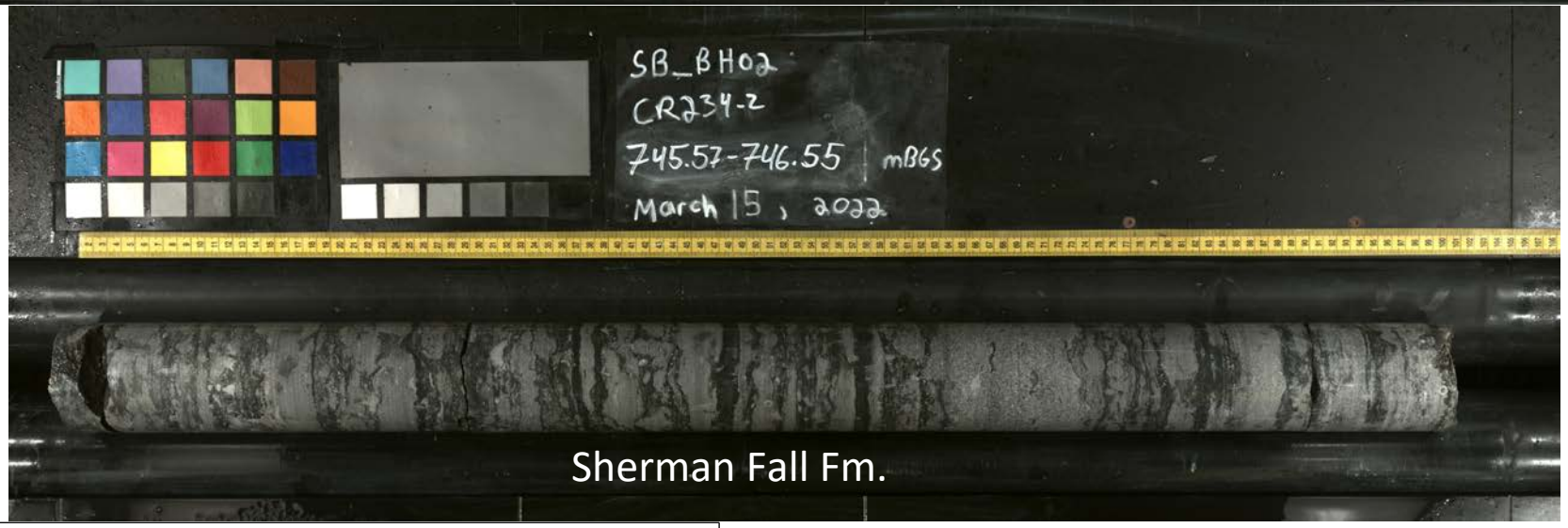
B-38 Cobourg Formation_lower member-Sherman Fall Formation

SB_BH02 Representative Photos for Formations and Members

NUCLEAR WASTE MANAGEMENT ORGANIZATION
SOCIÉTÉ DE GESTION DES DÉCHETS NUCLÉAIRES



Sherman Fall Fm.



Sherman Fall Fm.

B-39 Sherman Fall Formation

SB_BH02 Representative Photos for Formations and Members

nwmo

NUCLEAR WASTE MANAGEMENT ORGANIZATION

SOCIÉTÉ DE GESTION DES DÉCHETS NUCLÉAIRES

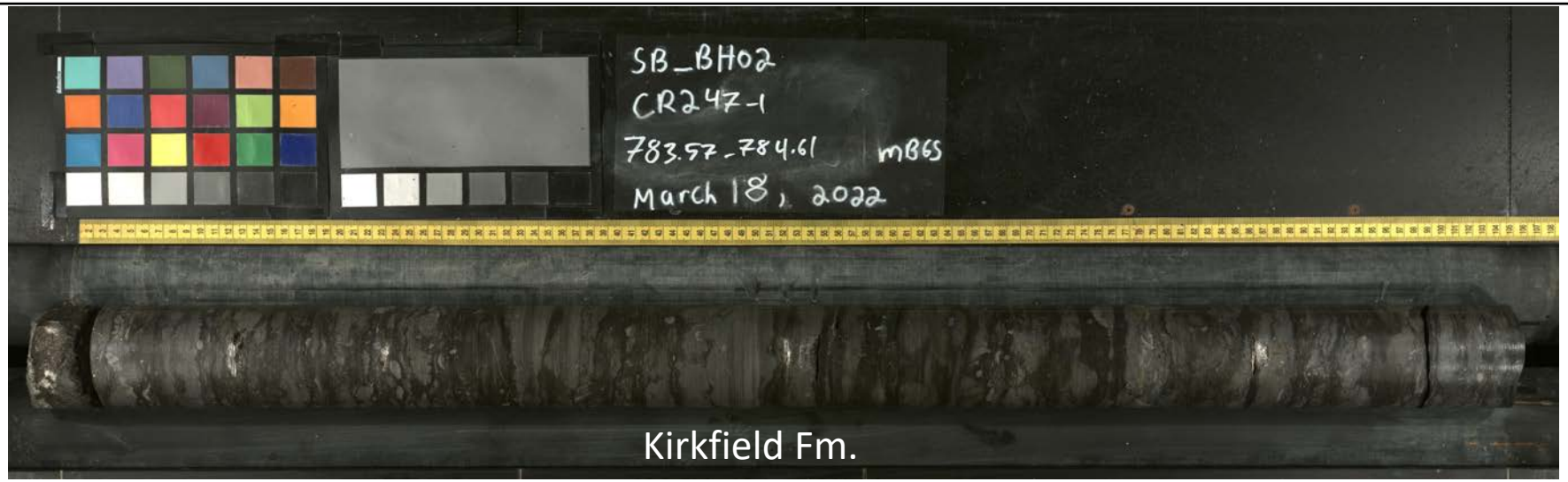




B-40 Sherman Fall-Kirkfield Formation

SB_BH02 Representative Photos for Formations and Members

NUCLEAR WASTE MANAGEMENT ORGANIZATION
SOCIÉTÉ DE GESTION DES DÉCHETS NUCLÉAIRES



Kirkfield Fm.



Kirkfield Fm.

B-41 Kirkfield Formation

SB_BH02 Representative Photos for Formations and Members

NUCLEAR WASTE MANAGEMENT ORGANIZATION
SOCIÉTÉ DE GESTION DES DÉCHETS NUCLÉAIRES





B-42 Kirkfield-Coboconk Formation

SB_BH02 Representative Photos for Formations and Members

nwmo
NUCLEAR WASTE MANAGEMENT ORGANIZATION
SOCIÉTÉ DE GESTION DES DÉCHETS NUCLÉAIRES



Coboconk Fm.



Coboconk Fm.

B-43 Coboconk Formation

SB_BH02 Representative Photos for Formations and Members

nwmo

NUCLEAR WASTE MANAGEMENT ORGANIZATION

SOCIÉTÉ DE GESTION DES DÉCHETS NUCLÉAIRES





B-44 Coboconk-Gull River Formation

SB_BH02 Representative Photos for Formations and Members

NUCLEAR WASTE MANAGEMENT ORGANIZATION
SOCIÉTÉ DE GESTION DES DÉCHETS NUCLÉAIRES





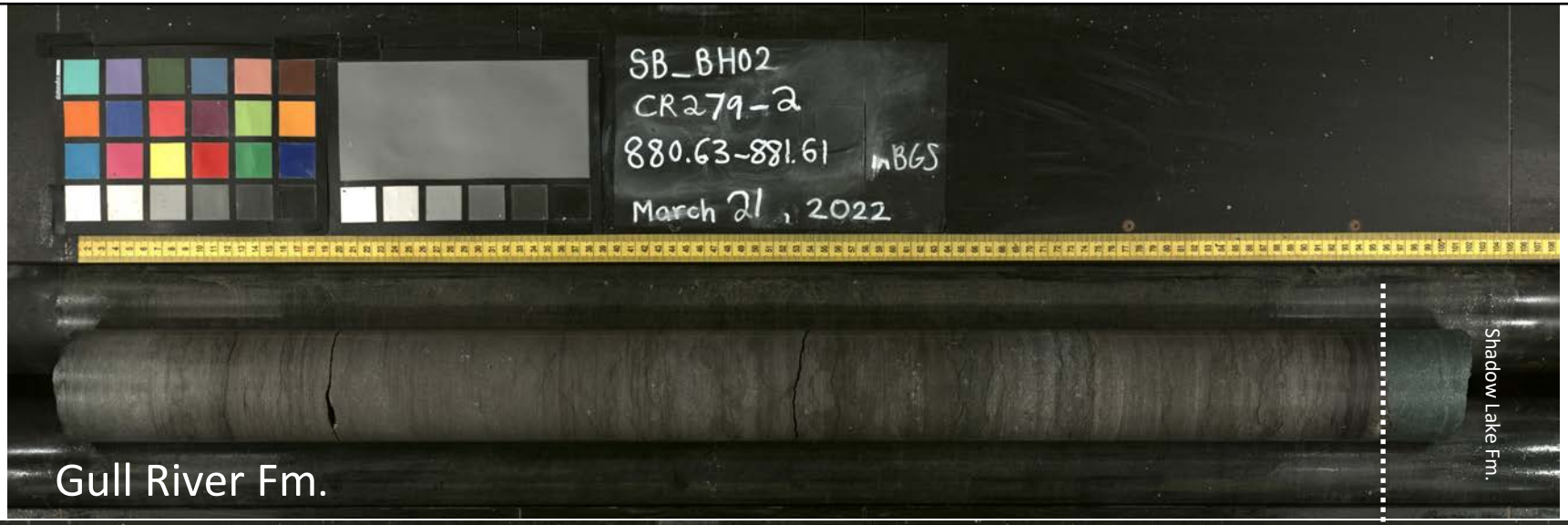
B-45 Gull River Formation

SB_BH02 Representative Photos for Formations and Members

nwmo

NUCLEAR WASTE MANAGEMENT ORGANIZATION

SOCIÉTÉ DE GESTION DES DÉCHETS NUCLÉAIRES





B-46 Gull River-Shadow Lake Formation

SB_BH02 Representative Photos for Formations and Members

nwmo

NUCLEAR WASTE MANAGEMENT ORGANIZATION

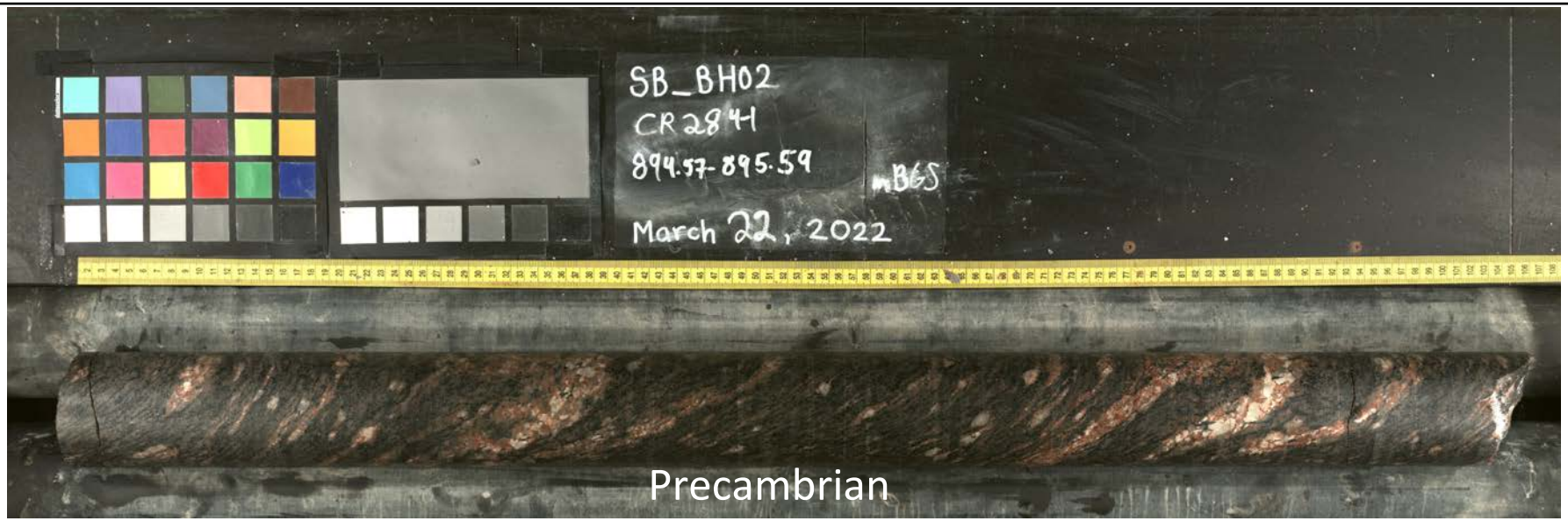
SOCIÉTÉ DE GESTION DES DÉCHETS NUCLÉAIRES



B-47 Shadow Lake Formation-Precambrian Basement

SB_BH02 Representative Photos for Formations and Members

NUCLEAR WASTE MANAGEMENT ORGANIZATION
SOCIÉTÉ DE GESTION DES DÉCHETS NUCLÉAIRES





B-48 Precambrian Basement

SB_BH02 Representative Photos for Formations and Members

NUCLEAR WASTE MANAGEMENT ORGANIZATION
SOCIÉTÉ DE GESTION DES DÉCHETS NUCLÉAIRES

Structures



B-49 Devonian Structures

SB_BH02 Representative Photos of Devonian Structures from 75.53-84.77mBGS (Lucas Formation)

nwmo
NUCLEAR WASTE MANAGEMENT ORGANIZATION
SOCIÉTÉ DE GESTION DES DÉCHETS NUCLÉAIRES



B-50 Devonian Structures

SB_BH02 Representative Photos of Devonian Structures from 91.69-98.16 mBGS (Amherstburg Formation)

nwmo
NUCLEAR WASTE MANAGEMENT ORGANIZATION
SOCIÉTÉ DE GESTION DES DÉCHETS NUCLÉAIRES



B-51 Devonian Structures

SB_BH02 Representative Photos of Upper Silurian Structures from 124.33-131.20 mBGS (Bois Blanc and Formation)

nwmo

NUCLEAR WASTE MANAGEMENT ORGANIZATION

SOCIÉTÉ DE GESTION DES DÉCHETS NUCLÉAIRES



B-52 Upper Silurian Structures

SB_BH02 Representative Photos of Upper Silurian Structures from 157.43-163.82 mBGS

NUCLEAR WASTE MANAGEMENT ORGANIZATION
SOCIÉTÉ DE GESTION DES DÉCHETS NUCLÉAIRES



B-53 Upper Silurian Structures

SB_BH02 Representative Photos of Upper Silurian Structures from 170.41-177.27 mBGS

nwmo

NUCLEAR WASTE MANAGEMENT ORGANIZATION

SOCIÉTÉ DE GESTION DES DÉCHETS NUCLÉAIRES



B-54 Upper Silurian Structures

SB_BH02 Representative Photos of Upper Silurian Structures from 177.27-185.23 mBGS

nwmo
NUCLEAR WASTE MANAGEMENT ORGANIZATION
SOCIÉTÉ DE GESTION DES DÉCHETS NUCLÉAIRES



B-55 Upper Ordovician Structures

SB_BH02 Representative Photos of Upper Ordovician Structures from 635.06-641.70 mBGS (Georgian Bay Formation)

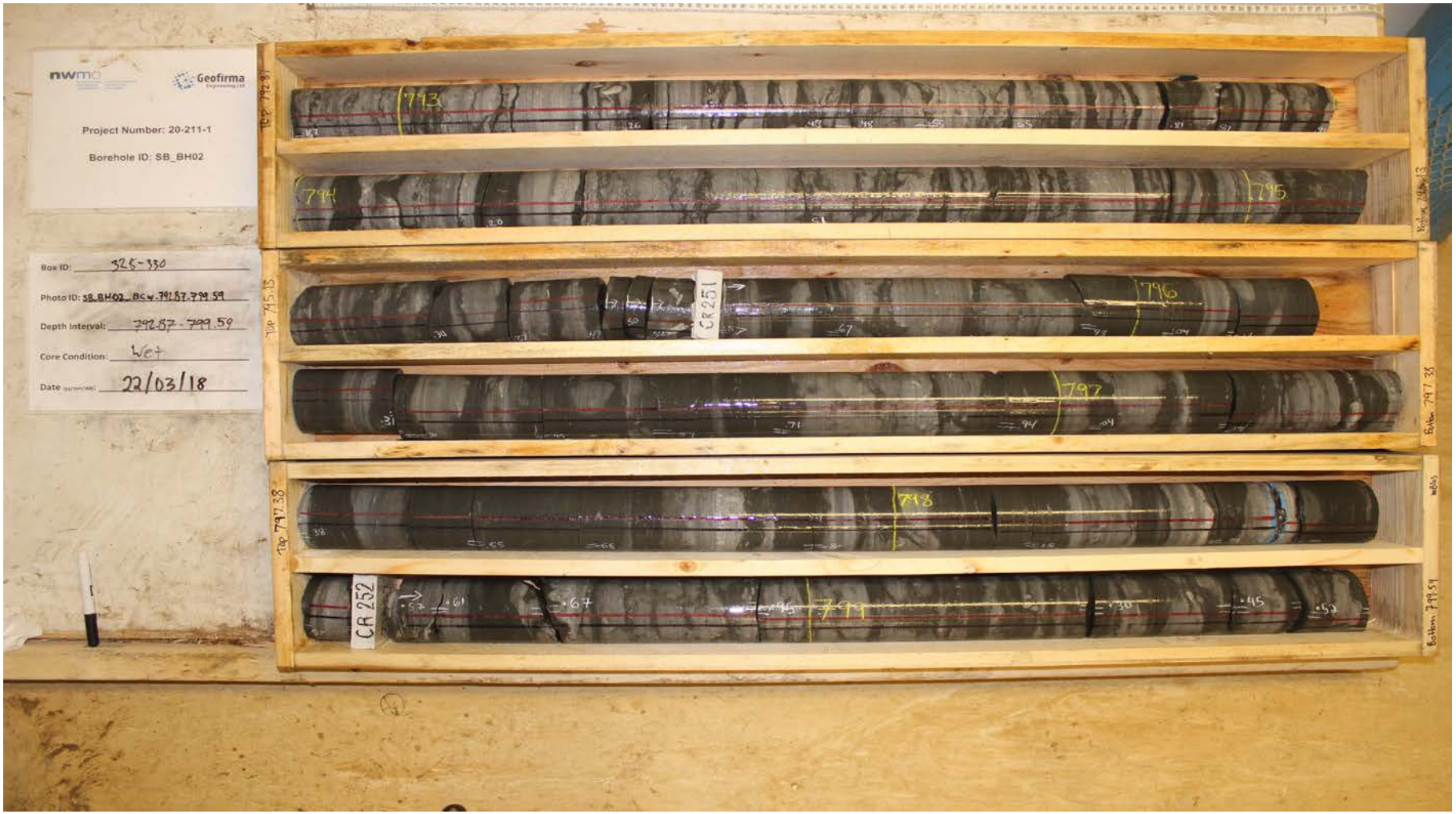
nwmo
NUCLEAR WASTE MANAGEMENT ORGANIZATION
SOCIÉTÉ DE GESTION DES DÉCHETS NUCLÉAIRES



B-56 Upper Ordovician Structures

SB_BH02 Representative Photos Upper Ordovician Structures from 648.19-654.79 mBGS

nwmo
NUCLEAR WASTE MANAGEMENT ORGANIZATION
SOCIÉTÉ DE GESTION DES DÉCHETS NUCLÉAIRES



B-57 Upper Ordovician Structures

SB_BH02 Representative Photos of Upper Ordovician Structures from 792.87-799.59 mBGS

nwmo
NUCLEAR WASTE MANAGEMENT ORGANIZATION
SOCIÉTÉ DE GESTION DES DÉCHETS NUCLÉAIRES



B-58 Precambrian Structures

SB_BH02 Representative Photos of Precambrian Structures from 886.58-893.26 mBGS (Precambrian)

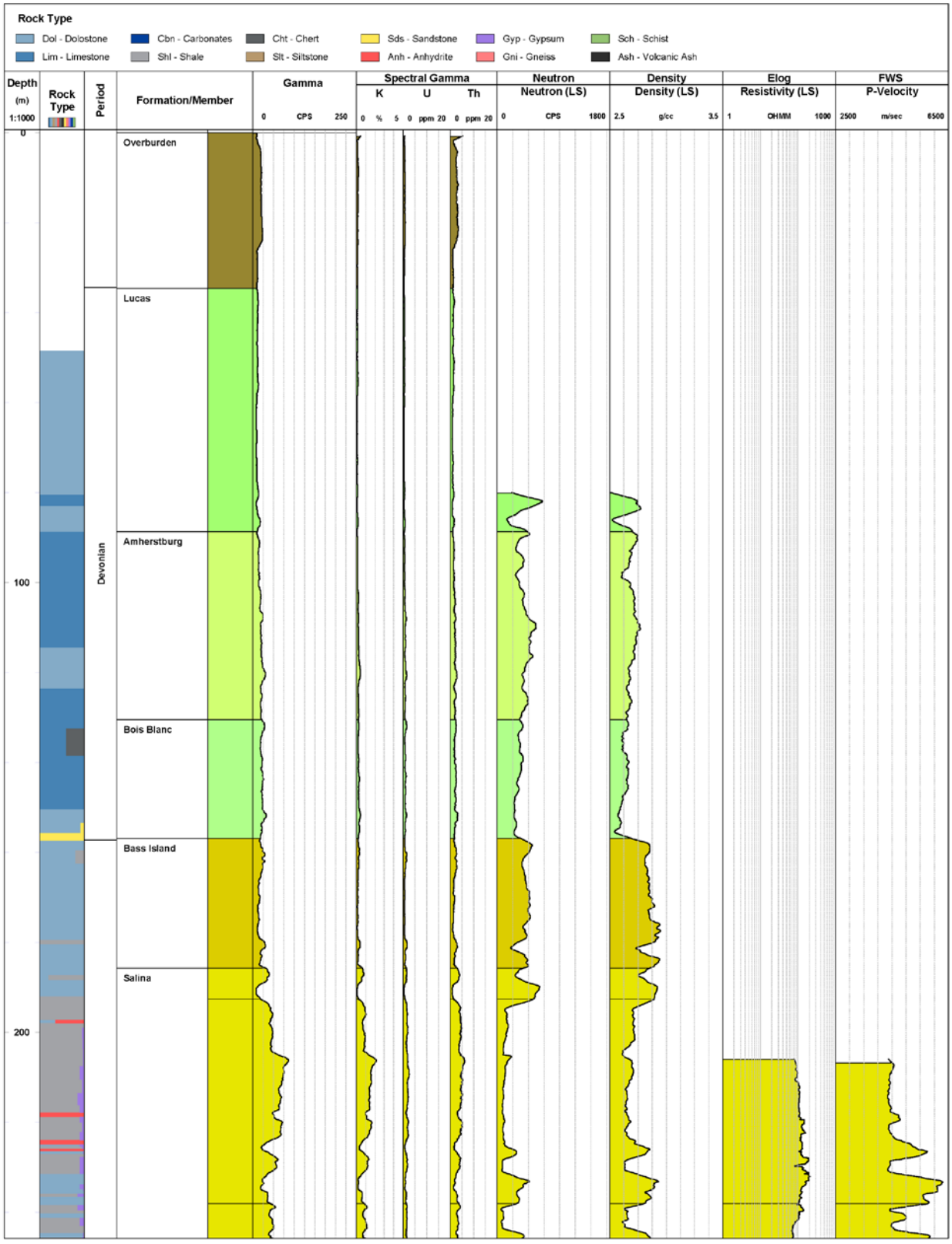
nwmo

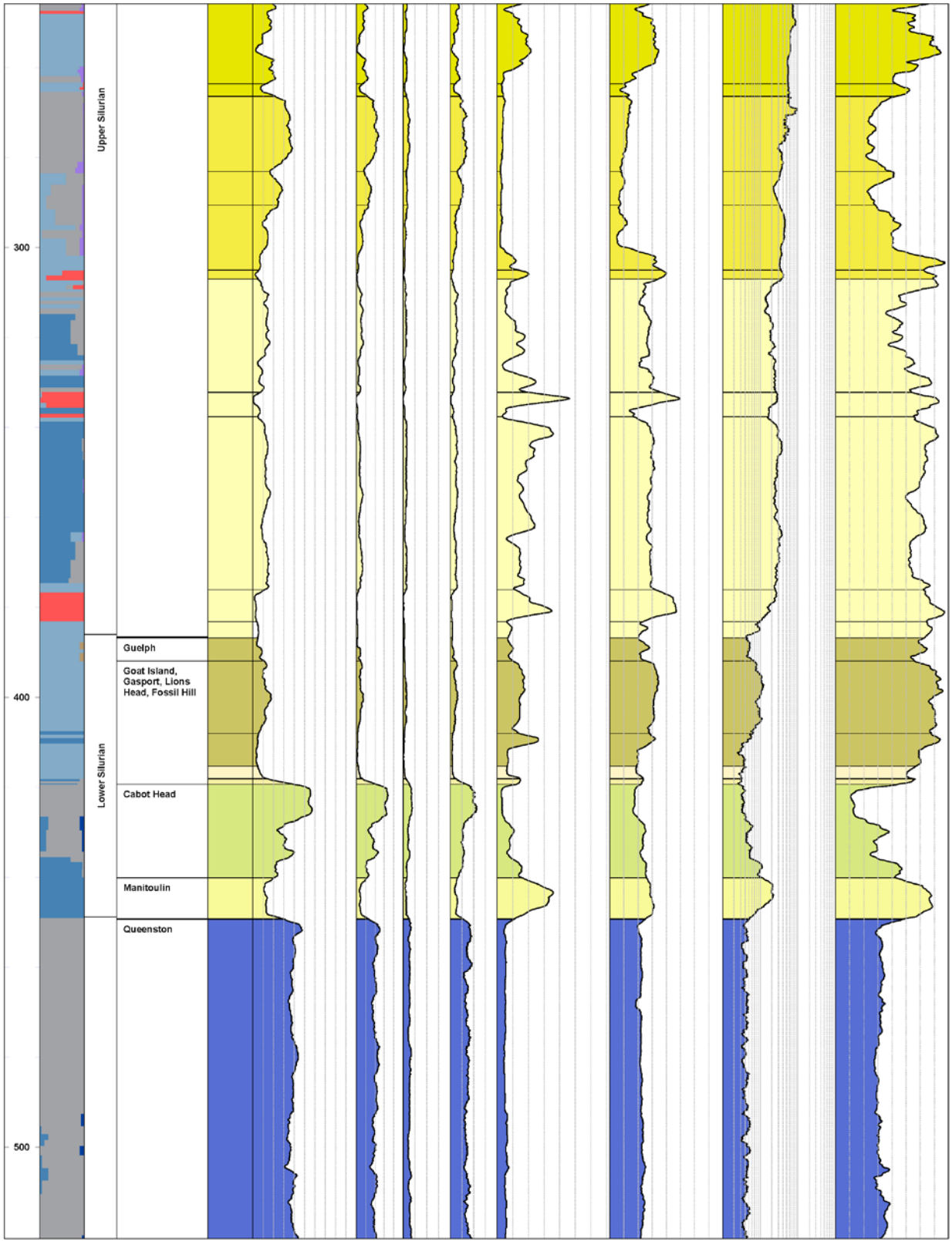
NUCLEAR WASTE MANAGEMENT ORGANIZATION

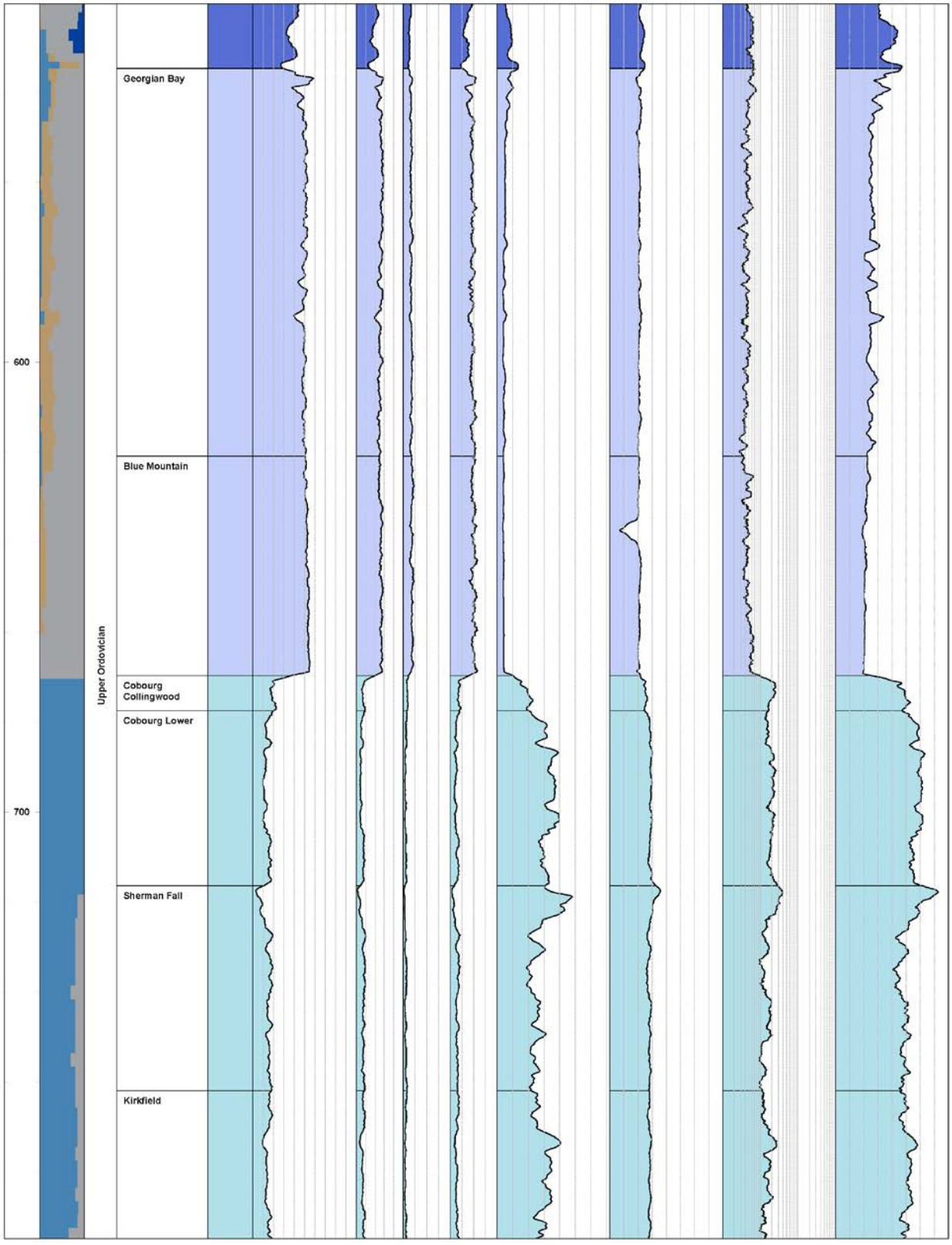
SOCIÉTÉ DE GESTION DES DÉCHETS NUCLÉAIRES

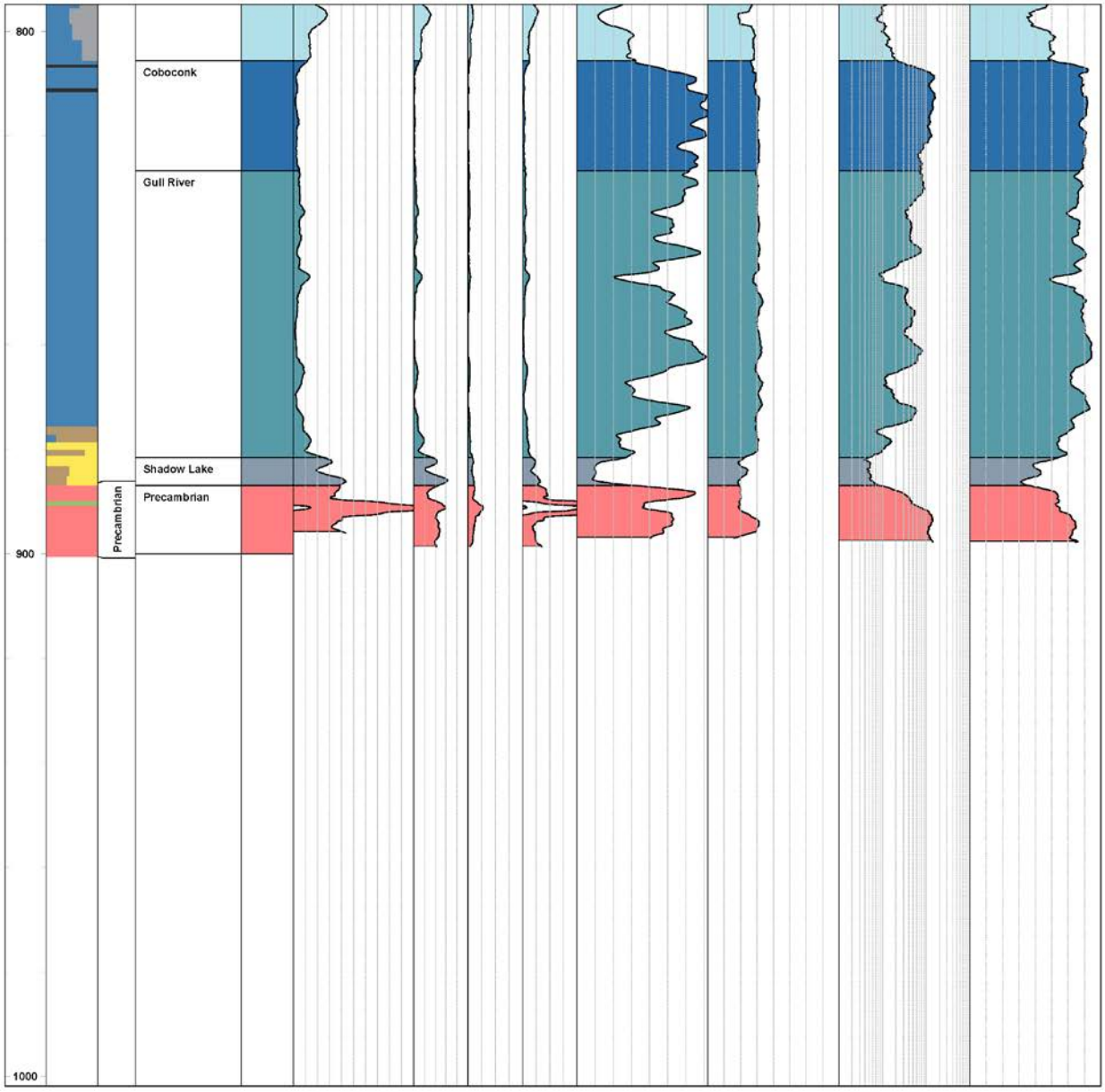
Appendix C:

Geophysical Well Log Compilation of Interpreted Formation and Member Tops for SB_BH02 (Scale 1:1000)


Rock Type
Dol - Dolostone
Lim - Limestone
Cbn - Carbonates
Shl - Shale
Cht - Chert
Slt - Siltstone
Sds - Sandstone
Anh - Anhydrite
Gyp - Gypsum
Gni - Gneiss
Sch - Schist
Ash - Volcanic Ash
Depth (m) 1:1000
Rock Type
Period
Formation/Member
Gamma
0 CPS 250
Spectral Gamma
K U Th
0 % 5 0 ppm 20 0 ppm 20
Neutron
Neutron (LS)
0 CPS 1800
Density
Density (LS)
2.5 g/cc 3.5
Elog
Resistivity (LS)
1 OHMM 1000
FWS
P-Velocity
2500 m/sec 6500
0
100
200
Devonian
Overburden
Lucas
Amherstburg
Bois Blanc
Bass Island
Salina


Upper Silurian
Lower Silurian
Guelph
Goat Island, Gasport, Lions Head, Fossil Hill
Cabot Head
Manitoulin
Queenston
300
400
500


600
700
Upper Ordovician
Georgian Bay
Blue Mountain
Cobourg Collingwood
Cobourg Lower
Sherman Fall
Kirkfield


800
900
1000
Coboconk
Gull River
Shadow Lake
Precambrian
Precambrian